Guidance cue integration in commissural axons

Tyler Sloan

Doctor of Philosophy

Department of Medicine, Division of Experimental Medicine

McGill University, Montreal, Canada

April 15th, 2016

A thesis submitted to McGill University in partial fulfillment of the requirements for the degree of Doctor of Philosophy

Page

Table of contents

Chapter II: Integration of Shallow Gradients of Shh and Netrin-1 Guides Commissural Axons

Appendix:

Abstract

During nervous system development, specific connections develop between discrete neurons, often spanning large distances. The growth cones of developing axons are influenced by attractive and repulsive chemical signals, which act in concert to help the growth cone navigate to its appropriate location. The developing commissural tract of the spinal cord has been considered by many to be an excellent model system for studying axon guidance, as their growth cones integrate several guidance cues to follow a complex trajectory that is remarkably consistent across evolutionary time.

Historically, advances in the field of axon guidance have benefited from theoretical, conceptual and technical advances in the related study of chemotaxis: the directed movement of cells in response to extracellular signals. Growth cones and other motile cells are capable of sensing spatial differences in the distribution of guidance molecules they encounter during their migration, and can infer direction using these gradients. Embryonic concentration gradients establish naturally by molecular diffusion, which is helped or hindered by many biochemical processes, while the contemporary laboratory techniques used to recreate these gradients range from simple to elaborate. While concentration gradients can provide directional information for growing cells, the information they provide is inherently limited by multiple sources of noise. The theoretical considerations of the biophysical processes which allow growth cones to correctly interpret the direction of biomolecular concentration gradients are considered in detail. Various mechanisms have been proposed to enable cells and growth cones to robustly interpret the direction of a concentration gradient when constrained by noise. Analogies are drawn between functionally distinct cell types, with a special consideration for the interpretation of morphogen gradients. Specifically, I focus on how the integration of multiple gradients can enhance chemotactic ability.

I hypothesize that a growth cone's ability to perceive a concentration gradient can be limited by the gradient steepness, and that a combination of chemoattractants can help the growth cone overcome this limitation by acting together synergistically; referred to as steepness-limited synergy. I support the hypothesis with data generated using a novel microfluidics-based

guidance assay, *le Massif*, and by quantitative analysis of the Sonic Hedgehog concentration gradient *in vivo*.

I demonstrate that commissural axons can be guided synergistically by a combined gradient of Sonic Hedgehog and Netrin-1, specifically in regions where a single cue gradient is insufficiently steep to guide axons. I also provide evidence that the phosphorylated form of Src-Family Kinase might act as an integration node for these distinct signaling pathways within the growth cone. The results are discussed in the context of theoretical predictions from the literature, and what is known regarding guidance cue integration by the growth cone. I discuss several potential mechanisms underlying this synergy, and finally I extend my results analytically to demonstrate that axons can be guided across a longer distance by combined concentration gradients than by a gradient of a single guidance cue. These conclusions suggest tangible applications for combined concentration gradients in the context of nerve regeneration, and more generally these findings elucidate fundamental biological mechanisms by which chemotactic ability can be enhanced *in vivo*.

Résumé

Au cours du développement du système nerveux, des connexions spécifiques se développent entre les neurones qui couvrent souvent de grandes distances. Les cônes de croissance d'axones en développement sont influencés par des signaux chimiques attractifs et répulsifs. Ces derniers agissent ensemble pour aider le cône de croissance à naviguer jusqu'à son emplacement approprié. Les axones commissuraux de la moelle épinière sont un excellent modèle pour étudier le guidage axonal. En effet, leurs cônes de croissance intègrent plusieurs signaux de guidage pour suivre une trajectoire complexe, qui est remarquablement similaire entre les espèces. Historiquement, les progrès dans le domaine du guidage axonal ont bénéficié des avancées théoriques, conceptuelles et techniques dans l'étude de la chimiotaxie. Les cônes de croissance, comme les cellules mobiles, sont capables de détecter des différences spatiales dans la distribution des molécules qu'ils rencontrent. En utilisant ces gradients ils peuvent en déduire la direction dans laquelle ils doivent se tourner. Les gradients embryonnaires s'établissent naturellement par la diffusion moléculaire, qui est aidée ou entravée par de nombreux processus biochimiques, tandis que les gradients créés par les techniques de laboratoire contemporaines vont de simples à complexes. Alors que les gradients de concentration peuvent fournir une information directionnelle pour les cellules en migration, celle-ci est intrinsèquement limitée par de multiples sources de bruit. Ainsi, divers mécanismes ont été proposés pour permettre à des cellules et des cônes de croissance d'interpréter la direction d'un gradient d'un signal de guidage.

Dans cette thèse, je fais des analogies entre les différents types de cellules, avec une attention particulière pour l'interprétation des gradients morphogènes. Plus précisément, je me concentre sur la façon dont l'intégration de multiples gradients peut améliorer la capacité chimiotactique. Mon hypothèse est que la capacité d'un cône de croissance à percevoir un gradient de concentration peut être limitée par la pente du gradient, et qu'une combinaison d'agents chimio-attractifs peut aider le cône de croissance à surmonter cette contrainte. Ainsi, j'ai quantifié la pente du gradient du morphogène Sonic Hedgehog (Shh) dans la moelle épinière et ai constaté qu'elle est très peu abrupte. J'ai ensuite développé un système

microfluidique in vitro pour reproduire de faibles gradients, démontrant que plus le gradient est abrupt, plus les axones réagissent aux signaux de guidage. Par ailleurs, le gradient d'un signal de guidage n'est pas toujours suffisant pour orienter les axones. Dans ce cas, j'ai montré qu'une combinaison de signaux de guidage peut agir en synergie afin d'aider l'axone à interpréter la direction du gradient. Lorsque Shh et la Nétrine-1 sont réunis, leurs faibles gradients combinés polarisent l'activité d'enzymes kinases de la famille des (SFK) dans le cône de croissance, indiquant que les SFKs peuvent intégrer les deux signaux de guidage. Ces résultats sont discutés dans le contexte des prédictions théoriques et de ce qui est déjà connu à propos de l'intégration des signaux de guidage par le cône de croissance. Je propose plusieurs mécanismes potentiels pour expliquer cette synergie, et enfin, je démontre par l'analyse que les axones pourraient être guidés à travers une plus grande distance par des gradients combinés que par un gradient d'un seul signal de guidage. Ces conclusions suggèrent des applications tangibles pour les gradients de concentration combinés dans le domaine de la régénération nerveuse. Plus généralement, ces résultats élucident les mécanismes biologiques fondamentaux par lesquels la capacité chimiotactique peut être améliorée *in vivo.*

Acknowledgements

First and foremost, I would like to thank my supervisor, Dr Frédéric Charron for giving me the opportunity to join the lab, and pursue such interesting questions. When I joined the lab, I didn't know how to use a spreadsheet effectively. Six years later, I can code in several languages to make complex measurements and explore data in more ways than I could ever have imagined possible. He constantly challenged me to try novel ways of measuring, and fostered an environment where learning new skills and coming up with creative solutions was encouraged. He allowed me the luxury of making of my PhD what I wanted from it, to explore interesting tangents that may eventually form a basis for further biological insights.
Fred has taught me how to think like a scientist, a skill that I can see influencing other facets of my life. I feel now as though I'm able to break down any complex problem into a series of smaller, simpler challenges. While I move on to the next stage of my life, it is not because I've exhausted everything there is to learn in the lab; I could certainly benefit from being here another 5 or more years.

I also want to acknowledge other lab members who have helped enormously in the completion of this work. I would also like to express my gratitude to Patricia Yam, who helped directly by editing and rewriting huge portions of the Plos Biology manuscript, while taking extra time to use this as a teaching experience for me to write better scientific articles. The current body of work have lack a foundation if she had not developed certain techniques in her time as a post-doc in the lab, which gave me a starting-off point to jump into asking such interesting biological questions. Beyond this, she contributed to my work intellectually through countless discussions relating to experimental design, data analysis, and theoretical analysis of potential models, so she has influenced just about every aspect of my thesis work.

Steves Morin was the technician in the Charron lab, and dissected around 95% of all spinal cords I have used for commissural preparations throughout my PhD. On the seldom occasion he was unavailable, I would also like to thank Julien Ferrent, Shirin Makihara, Lea Lepelletier, Chris Kent, and Jimmy Peng for technical assistance related to commissural preparations or spinal cord sections. I would also like to thank Chris Law, who while not a lab member, was a constant

source of feedback and ideas relating to coding and algorithmic problem solving, but he was also always prepared to answer my most naïve questions – the ones I was too embarrassed to ask my mentors. I would also like to thank Dominic Filion, the microscope and MATLAB guru, who helped this work greatly by helping me to take nice images, writing code to help me with analysis, and encouraging me to jump into the world of MATLAB. Jessica Barthe also deserves a notable mention, as she managed the animal facility, and although my interaction with her and the facility were minimal, I appreciate her patience and professionalism.

Furthermore, I want to acknowledge the members of my thesis committee, the all-star cast who made me the only student I know who actually looked forward to his committee meetings. David Juncker, gave me my first research opportunity as an undergraduate student, and despite me lacking any engineering background and having failed calculus, I was able to learn a cutting-edge field (microfluidics) that allowed me to leverage my skillset above the rest of the 2009 graduating class of McGill. Through my interactions with him, I also was forced to develop a thicker skin and take criticism, which might be the hardest thing I've learned to do so far. I want to also thank Mohammad Qasaimeh, who took me under his wing when I was an undergraduate student, and taught me how to use microfluidics. I express my gratitude to Tim Kennedy, firstly for generously providing essential reagents that were used throughout my studies. But more importantly, Tim's insightful comments at committee meetings and Neuroengineering seminars helped advance the work conceptually. I particularly appreciate his keen interest in my work, and the ease at which he can take complex cell-biological phenomena and explain them with vivid imagery. I would like to thank Claude Lazure, who served as the Experimental Medicine representative while I was still a masters student, and was extremely encouraging for me to pursue a PhD. After Dr Lazure began working full time at FRQ, David Hipfner took on this role, and has also been open to discuss whenever I've needed it. I would also like to acknowledge Artur Kania, who also served as a member of my committee and provided extremely useful feedback at shared lab meetings, along with Michel Cayouette, throughout my PhD. Together, I would like to thank the entire committee for being so enthusiastic and encouraging about my work, and giving me the yearly boost in confidence that

let me feel like the king of the world that would last for at least a few days after each meeting. I would like to thank the NSERC-CREATE program in Neuroengineering for funding my research, and Joseph Paulin for the scholarship I received for the year of 2011.

In my personal life, I would like to thank Patricia Banville, for supporting me throughout the many downs throughout the course of my Ph.D. This thesis is dedicated to my parents, Rosemary and Derrick Sloan. They both passed away while holding their breath for me to “write my damn thesis”. It is therefore a great shame that neither of them was able to see me defend and graduate. My father was supportive of my decision to continue graduate school indefinitely in the form of a PhD, but was on my ass at every opportunity to get out as soon as possible and get a real job, preferably government. My mother was supportive of everything, period.

Preface and Contribution of Authors

This thesis was written in accordance with McGill University's "Guideline for Thesis Preparation." It is presented in article-based format, in accordance with the guidelines of the National Library of Canada. The data presented in this thesis is the original work of the candidate, and has been published, in part in the following peer-reviewed articles:

Sloan TF, Qasaimeh MA, Juncker D, Yam PT, Charron F (2015) Integration of shallow gradients of shh and netrin-1 guides commissural axons. PLoS Biol 13: e1002119

The candidate was the lead investigator and author for the work described in this thesis, but would like to acknowledge the contributions of colleagues in the described work.

1. Dr. Patricia Yam and Dr. Frédéric Charron performed and quantified the dot blot in Figure II.S1D.
2. Dr. Frédéric Charron identified the range of commissural guidance errors, shown in Figure II.1B and Table II.S1.
3. Dr. Patricia Yam and Dr. Frédéric Charron contributed to the writing of the above publication, which forms the second chapter of this thesis.
4. Dr. Patricia Yam and Dr. Frédéric Charron contributed to the conception and design of experiments.
5. Dr. Mohammad Qasaimeh and David Juncker contributed to the design and fabrication of the microfluidic gradient generator used throughout this study.

All of the results in Chapter II are considered original scholarship, and provide unique contributions to knowledge. This includes:

1. The quantification of the concentration gradient of Sonic Hedgehog (Shh)
2. The geometry of the microfluidic device and the development of the high-throughput turning assay
3. Our discovery that the gradient steepness is critical for turning of commissural axons
4. Our discovery that Shh and Netrin-1 act together synergistically *in vitro*

List of Figures and Tables

Chapter I: General introduction

Chapter II: Integration of shallow gradients of Shh and Netrin-1 guides commissural axons

Appendix:

List of Abbreviations

BMP	Bone morphogenetic protein
BMPR	Bone morphogenetic protein receptor
Boc	Brother of Cdon
BSA	Bovine Serum Albumin
cAMP	cyclic adenosine monophosphate
CMA	Central moving average
CXCL2	Chemokine (C-X-C motif) ligand 2
DCC	Deleted in Colorectal Carcinoma
DRG	Dorsal Root Ganglion
e10.5	Embryonic day 10.5
ECM	Extracellular matrix
Eph	Ephrin receptor
FAK	Focal Adhesion Kinase
FGF	Fiboblast Growth Factor
Flk-1	Fetal Liver Kinase 1
fMLP	N-Formylmethionine-leucyl-phenylalanine
fp	Floor plate
F-actin	Filamentous actin
GABA	gamma-Aminobutyric acid
GAP	GTPase-activating protein
gc	Growth cone

GDNF	Glial cell line-derived neurotrophic factor
GEF	Guanine nucleotide exchange factor
GFP	Green fluorescent protein
GFRα1	GDNF family receptor alpha-1
GPCR	G protein-coupled receptor
Hh	Hedgehog (Drosophila)
HSPG	Heparan Sulfate Proteo-Glycan
K_d	Dissociation constant
LEGI	Local excitation, global inhibition
LMC_L	Lateral motor column-lateral
LTB4	Leukotriene B4
MW	Molecular Weight
nc	Notocord
NGF	Nerve Growth Factor
NSA	Netrin Synergizing Activity
NT-3	Neurotrophin-3
P75NTR	p75 neurotrophin receptor A.k.a. Low affinity nerve growth factor receptor
PBS	Phosphate buffered saline
PFA	Paraformaldehyde
PI3K	Phosphoinositide 3- kinase
pSFK	phosphorylated Src-Family Kinase
Ptch1	Patched 1

PTEN	Phosphatidylinositol-3,4,5-triphosphate 3-phosphatase
Robo	Roundabout
SCF	Stem Cell Factor
SFK	Src-Family Kinase
Shh	Sonic Hedgehog
Smo	Smoothened
SQ	Synergy Quotient
Trk	Tyrosine receptor kinase
Unc	Uncoordinated
VEGF	Vascular endothelial growth factor
Wnt	Wingless-related integration site
δ	ΔC/C = Fractional change in concentration = Gradient steepness
ΔC	Change in concentration across 10μm
δGC	Fractional change in signal intensity across the width of a growth cone

Chapter I: General Introduction

I.1. Axon Guidance

I.1.i. A brief history of axon guidance

During embryonic development, axons must be guided across long distances to make specific connections, and exactly how they do this is the central question of axon guidance. It is such a complex problem that late 19th century scientists went so far as to deny that there could be a solution, as the earliest formulations of reticular theory had denied that the problem was real. Proponents of reticular theory, most vocally lead by Camillo Golgi, held that the nervous system was composed of a reticulum of interconnected fibres, which could not be further subdivided into discrete components. Their principle argument was the lack of evidence for a physical gap between an axon and its target. Despite the fact that the cellular theory of life was widely accepted for all non-neural systems of the body, reticular theory was intuitive and convenient. Coincidentally, it entirely removed the need to explain the complex connectivity of the nervous system, which must have seemed like an impossible task to 19th century anatomists. The question of how the pieces fit together was rendered moot if all said pieces were and were always joined. The Spanish anatomist Santiago Ramon Y Cajal was a leading proponent of the neuron doctrine: the theory of discrete nerve elements. He performed a series of experiments using Golgi-impregnation (known as the 'black reaction'), and for the first time this allowed discrete neurons, with their axons and dendrites, to be imaged in their finite nature. However, the neuron doctrine wasn't unequivocally proven until the invention of the electron microscope, which undeniably showed the existence of a synapse, and vanquished reticular science to the annals of history. While this was a major conceptual breakthrough, it most certainly complicated things; scientists no longer debated *if* the nervous system is built from discrete units, the emphasis was placed on describing *how* such specific and orderly connections could be made over such long distances - and the century-old research program to be known as axon guidance was born.

Among his myriad writings, Cajal made some important predictions with respects to the basic principles by which such complex assembly could take place. He identified the growth cone in fixed specimens, and recognized similarities between the form of the growth cone and of

migrating Leukocytes, which had recently been observed to migrate in chemoattractant gradients. He thus postulated that the growth cone could be guided from a distance by chemical cues in the environment (Cajal, 1892). Unfortunately, technical limitations made his hypothesis impossible to test; he opined that "[as for the chemotaxic property, it is currently impossible to identify by direct observations or experiments]". It was several years after the discovery of the growth cone that Ross Granville Harrison developed the sterile tissue culture technique, and was the first to observe the growth cone moving in real-time. He lamented its continual and dynamic change in form, and wrote a textbook chapter in which he described the outgrowth of the growth cone as a mode of protoplasmic movement (Harrison, 1910). While this is now considered to be an obvious feature of the growth cone, these observations allowed neurobiologists to benefit from theoretical and experimental advances that were already accumulating regarding the directed movement of other migrating cell types.

Due to the technical limitations of the time, and the fact that tissue culture was still in its infancy, the concept of chemical guidance cues was not supported further by experimental evidence until over half a century later, when advances in tissue culture techniques allowed Roger Sperry to perform his now classical experiments in *Xenopus* tadpoles. He surgically removed one of the tadpoles' eyes, and replaced it in a different orientation. He observed that the axonal fibres grew back to their initial targets following the manipulation. This supported the chemo-affinity hypothesis, a model where cell-extrinsic guidance cues provide growth cones with the positional information necessary to guide axons to their correct targets (Sperry, 1963).

For the years which followed, researchers searched for target-derived guidance cues. The identification of Nerve Growth Factor (NGF) was a crucial step forward, as this protein could induce directed outgrowth of axons towards explant tissues co-cultured in a matrix of collagen (Chamley and Dowel, 1975). An eloquent experiment followed several years later, where it was demonstrated that a growing axon could reorient towards the tip of a micropipette containing soluble NGF (Gundersen and Barrett, 1979, 1980). Despite the excitement this generated among neurobiologists, it remained unclear whether NGF was a bona fide guidance cue, as it did not appear to guide developing axons in vivo (Tessier-Lavigne and Placzek, 1991). The

search for target-derived tropic cues was successful nearly a century after the hypothesis was initially proposed, when it was demonstrated that that sensory axons from trigeminal ganglion explants embedded in a collagen gel could grow specifically toward a source of a neurotropic factor secreted by tissue of the maxillary process (Lumsden and Davies, 1983, 1986). The discovery of a target-derived chemical cue with the ability to reorient axons of the central nervous system followed, when it was shown that the floor plate of the spinal cord released molecule(s) that could induce commissural axons to reorient and grow distances of several hundred micrometers towards a floorplate explant (Tessier-Lavigne et al., 1988), recapitulating the trajectory grown *in vivo*. These classical experiments conclusively demonstrated the potential for secreted molecules to induce directional change in developing axons, and consequently ushered the axon guidance research program into the modern era of in vitro experimental manipulation. The ever-elusive axon was finally well on its way to be described in terms of molecular biology. A genetic screen in *Caenorhabditis elegans* identified a series of related mutations that resulted in an 'uncoordinated' behavioural phenotype (Hedgecock et al., 1990). Further work identified the protein Unc-6 as a component of the extracellular matrix that is required for the guidance of pioneering axons (Ishii et al., 1992). The vertebrate homologues of Unc-6 (the Netrin family of guidance molecules) were discovered and sequenced several years later (Kennedy et al., 1994, Serafini et al., 1994), at which point the floodgates opened and the axon guidance research program came into full force (Figure I.1).

I.1.ii. The growth cone

To understand axon guidance, one must necessarily look in detail at the growth cone, as this temporary structure at the tip of the growing axon exquisitely controls the trajectory that a growing axon will take. There is no shortage of metaphors used to describe different aspects of the growth cone function: its' searching and pathfinding behaviour has been likened to a dog walking on a leash, and the mechanics of its' propulsion has been likened to the clutch of a car. I offer an additional metaphor that captures its complex functional role and its transient existence: The pioneer growth cone functions like the shanty-town on railhead of an expanding

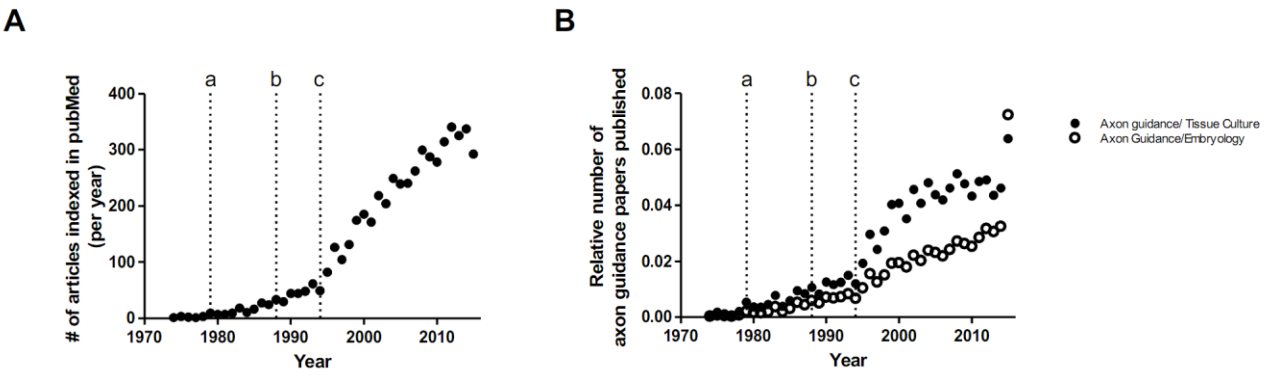

Figure I.1. Axon guidance publications. There was a steady rise in the number of axon guidance research articles published throughout the 1980`s, which was followed by a sharp increase in the mid-90`s. **A)** The total number of publications indexed in Pubmed (per year) is shown. To correct for the general increase in yearly publications, I calculated the guidance ratio as the ratio of number of axon guidance articles published, relative to the number of publications in **B)** Tissue Culture or Embryology. Dashed lines refer to landmark studies in the field: a) Gundersen and Barrett 1979 – discovery of growth cone turning towards a pipette containing soluble NGF, b) Tessier-Lavigne et al 1988 – Discovery of chemoattraction of axons in the central nervous system, c) Kennedy, Serafini et al 1994 – sequencing and isolation of the Netrin family of proteins responsible for the chemoattractive behaviour.

transcontinental railroad: it is here where instructive decisions are made, and tracks are laid, ultimately leaving behind it the railway's final, consolidated form. The railhead is guided around potentially dangerous terrain features or hostile native groups by a diverse and complementary team of surveyors, engineers and support workers, who instruct the laborers where to build. Their principal goal is to follow the overall plan, while remaining dynamic and adaptive when faced with uncertainty. Analogously, the growth cone contains a multitude unique molecular components that serve complementary and integratory roles, to ultimately control where the axonal structure is assembled.

The growth cone plays the role of a navigator that integrates cues from the environment, locally modulating the dynamics of the cytoskeletal machinery, and consequently altering the actin-based structure. It effectively repeats a cycle of protrusion, engorgement, and consolidation to advance the axon to its final target (Lowery and Van Vactor, 2009) (Figure I.2), at which point the growth cone is no longer necessary. Crucially, its forward movement must be capable of being influenced by spatial biases in the signals it receives. In this way, the assembly of the actin subunits into longer chains is influenced by local intracellular changes that are a response to features of the growth cones local environment, whether chemical or physical, and this allows for directed growth.

The growth cone consists of several distinct zones that differ in the composition and function. The periphery of the growth cone is made of lamellipodia, which contains a meshwork of branched actin filaments, and filopodia, which contain long, parallel branches of filamentous actin (F-actin). The central domain of the growth cone is enriched in cellular organelles and has a dense microtubule array. The transition zone links the central and peripheral zones, and is believed to contain contractile structures that play a strong role in regulating actin and microtubules. The filaments of actin are built through a balance of assembly at the barbed ends and disassembly at the pointed ends, while the rates of these processes are determined by

Figure I.2. Stages of growth cone motility. The motility of the growth cone can be described by three separate stages: Protrusion, Engorgement, and Consolidation. **A)** In its baseline or resting state, the growth cone contains anatomically distinct zones. The C-domain contains stable microtubules that act like the 'railhead' of the consolidated axon shaft. Exploratory dynamic microtubules extend into the filopodia of the P-domain, where each stray microtubule provides a possible future direction for the axon. **B)** Protrusion of the filopodia occurs when receptors on the growth cone surface are bound and form adhesions with the substrate. This results in molecular signaling cascades that act like a 'clutch' to couple the substrate with the actin cytoskeleton. The 'clutch' strengthens, causing local attenuation of retrograde F-actin flow, anchoring actin with respect to the substrate and allowing the P-domain to translocate forward. **C)** Engorgement occurs as actin is cleared from behind the 'clutch' site, and the C-domain microtubules invade this region, guided by actin arcs and bundles. **D)** Finally, consolidation occurs as the recently advanced C-domain compacts to form a new segment of the axon shaft, which involves compacting and stabilizing the microtubules of the newly-localized C-domain. Adapted from (Lowery and Van Vector 2009)

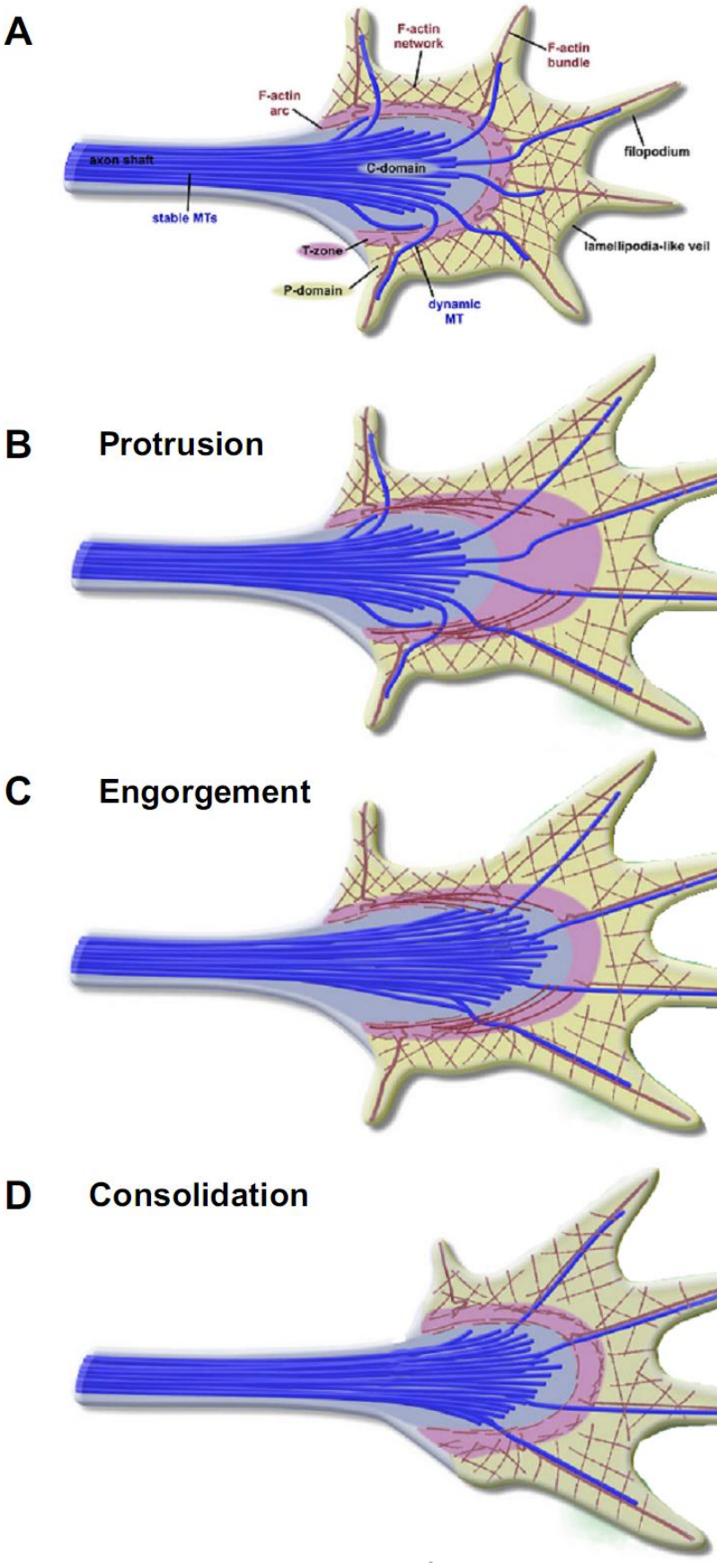
A
F-actin network
F-actin bundle
F-actin arc
filopodium
axon shaft
C-domain
stable MTs
T-zone
lamellipodia-like veil
P-domain
dynamic MT
B
Protrusion
C
Engorgement
D
Consolidation

many regulatory proteins. This tight regulation allows signaling pathways to locally influence the assembly process. The continuous assembly at the barbed end (at the growth cone periphery) and disassembly at the pointed end (in the central domain) allows the actin polymer to maintain a constant length while the subunits are constantly moving, a process called F-actin treadmilling (Lowery and Van Vactor, 2009).

The forward movement of the growth cone is driven by a combination of F-actin treadmilling and 'retrograde flow', the latter of which refers to the continuous movement of actin away from the leading edge towards the center of the growth cone. This is understood to be driven by both the contractility of Myosin II (Suter and Forscher, 2000) and the polymerization of actin in the growth cone periphery. The continuous retrograde flow has been likened to the idling of an engine, as the behaviour is repeated until the forces it generates are leveraged by a molecular clutch to propel the growth cone forward (Medeiros et al., 2006). The 'clutch hypothesis' (Mitchison and Kirschner, 1988) provides a mechanism by which the potential energy of the actin-dynamics can be leveraged to generate forward movement. The model couples the adhesions of the growth cone and the substratum to the dynamics of actin in a mechanism that resembles a clutch of an engine. The integrin receptors at the surface of the growth cone bind to the adhesive substrate, forming a receptor complex that mechanically couples the receptors to the F-actin flow. By anchoring the F-actin, retrograde flow is prevented, and the forces generated by the resistance of the actin network are transmitted back to the adhesions. This provides mechanical resistance, whereby the actin network overcomes the retrograde current, resulting in increased surface traction that causes the plasma membrane to translocate forward (Brown et al., 2006, Bard, 2008, Giannone et al., 2009, Aratyn-Schaus and Gardel, 2010).

Microtubules play an active role to bias and steer this machinery. Prior to the protrusion of the growth cone membrane, individual microtubules actively explore the P-domain of the growth cone by their property of dynamic instability (Letourneau, 1983, Cassimeris et al., 1987). This refers to a process by which their polymerization-based growth is interrupted by 'catastrophic' phases of rapid depolymerisation and microtubule shrinkage; the exploratory behaviour of the microtubules is largely determined by the extent of this instability. It is believed that dynamic

instability provides the microtubules with the ability to quickly remodel and selectively grow in response to extracellular cues (Vitriol and Zheng, 2012). After the protrusion occurs by F-actin flow, bundled microtubules move in to the area of new growth, consolidating the newly assembled axon shaft, thereby fixing the axons direction (Suter and Forscher, 2000, Buck and Zheng, 2002). Microtubule interactions with actin are critical, since actin acts as a barrier to premature microtubule invasion, and as a guide to microtubules during their advance (Zhou and Cohan, 2004, Burnette et al., 2007). It is thought that the microtubules act as a scaffold for localized recruitment of key signal components (Suter et al., 2004), which are linked to the actin assembly directly, or via adaptor proteins.

A principal role of the growth cone is to spatially bias this machinery in response to cues in the environment (Lowery and Van Vactor, 2009), a task that involves various types of molecules that include kinases (Meriane et al., 2004, Robles et al., 2005, Wolf et al., 2008, Yam et al., 2009), phosphatases (Ensslen-Craig and Brady-Kalnay, 2004), calcium ions (Gomez and Zheng, 2006) and the Rho family GTPases, which are downstream of virtually all guidance signalling receptors (Govek et al., 2005, Koh, 2006). Similar to how the team of surveyors and engineers guide the laborers around local topography, this compendium of molecules must act together, spatially and temporally, to control the interaction between microtubules and actin in response to asymmetric guidance cues, to help the axon navigate the extracellular mileu *en route* to its target.

At the molecular level, the growth cone must be able to perform a complex integration of multiple sources of information in order to make an informed 'decision' about the localization of an external cue. The surface of the growth cone is covered in receptors, which bind specifically to cues in the external environment. The interaction of a guidance cue ligand with its receptor on the growth cone leads to local intracellular changes in downstream signalling molecules, which ultimately lead to more actin polymerization locally. In this model, when there is an asymmetry in the amount of bound receptors on different sides of the growth cone, as in the presence of an external concentration gradient, then these tightly-regulated signaling cascades can reflect the direction of the gradient in the spatial distribution of downstream signaling events (Yam et al., 2009), thus providing an internal representation of the external

gradient. Precisely how the growth cone is able to integrate graded extrinsic information in the form of guidance cues, and generate an intrinsic representation in the form of asymmetric intracellular signaling molecules is a central question in axon guidance, and *the* central problem of chemotaxis.

I.1.iii. Commissural neurons: an exceptional model system for studying axon guidance

Of Cajal's numerous preparations, few have been etched into the minds of young researchers as the famous Golgi-stained commissural neurons of the spinal cord. The cell bodies of these neurons are located in the dorsal spinal cord, but their single axon extends along the boundary of the spinal cord and grows towards and across the floorplate in a single plane. It was by observing these iconic preparations and others that Cajal posed his chemotactic hypothesis. The observation of such seemingly intentional axonal behaviour was intriguing, as it was thought that being able to explain such behaviour in one type of cell would provide the tools to understand the complex wiring of the entire nervous system. This belief has been carried on in some form to the present day, as the commissural neurons of the spinal cord are still one of the most commonly studied model system for axon guidance, and findings made in commissural axons often generalize, at least in principle, to other model axons.

Spinal commissural neurons reside in the dorsal spinal cord, and their axons are initially repelled by a Bmp7:Gdf7 heterodimer via the BMPR1B receptor (Augsburger et al., 1999, Butler and Dodd, 2003, Phan et al., 2010, Yamauchi et al., 2013) which requires downstream PI3-Kinase activity (Perron and Dodd, 2011). They are also repelled by Draxin (Islam et al., 2009), which itself binds directly to DCC in reduce the outgrowth of these axons to the roofplate (Ahmed et al., 2011) and possibly by also antagonizing Netrin-1 directly (Gao et al., 2015). The growth cones are then attracted towards the ventral midline by Shh (Charron et al., 2003), Netrin-1 (Kennedy et al., 1994), and VEGF (Ruiz de Almodovar et al., 2011) via the receptors Boc (Okada et al., 2006), DCC (Keino-Masu et al., 1996), and Flk-1 (Ruiz de Almodovar et al., 2011), respectively. The attractive responses to Netrin-1, Shh and VEGF all require activation of Src-family Kinases (Li et al., 2004, Meriane et al., 2004, Yam et al., 2009, Ruiz de Almodovar et al.,

2011). Although it is not known whether the repellants work simultaneously with the attractants, guidance towards the floorplate requires the coordination of a minimum of five distinct guidance cues.

The behaviour of the growth cone as it approaches and crosses the floor plate involves even more coordination between signalling pathways, as the sensitivity of the growth cones to the midline repellants Slit and Sema are initially silent, but becomes active after encountering floorplate derived cues. After crossing the midline, they are repelled by Slit and Semaphorin-3B (Zou et al., 2000) via the Robo1/2 (Long et al., 2004) and Neuropilin-2 (Zou et al., 2000) receptors, respectively. The repulsion ensures that the axons do not re-enter the floorplate and re-cross the midline. Additionally, the correct and timely exit from the floorplate also requires Stem Cell Factor acting via the receptor Kit (Gore et al., 2008), which provides a growth impulse to these axons. Following floorplate exit, commissural axons subsequently switch their responsiveness to Shh in a time-dependent manner and make an anterior turn (Yam et al., 2012). They are guided by Shh and Wnt gradients in a longitudinal direction: The increasing anterior-posterior Shh gradient acts as a repellent (Bourikas et al., 2005, Yam et al., 2012), while the decreasing anterior-posterior Wnt4 gradient attracts post-crossing commissural axons via the receptor Frizzled-3 (Lyuksyutova et al., 2003). Because of the numerous instances where commissural axons are guided simultaneously by multiple cues, these axons are an excellent model to study guidance cue integration (Figure I.3).

Each of these signaling pathways must eventually converge onto a relatively small number of actin-binding proteins which directly modulate actin polymerization, thereby allowing the growth cone to advance and be steered by exploratory microtubules. Although the details of how each of these guidance cue/receptor combinations are linked to the assembly and disassembly of actin is not fully understood, the Netrin-1 signaling pathway provides a nice example, as many of the molecular components have been described, and there appears to be a near-complete explanatory link between the ligand and the actin cytoskeleton. Netrin-1 binding to DCC is known to cause DCC to dimerize, leading to the formation of a complex

Figure I.3. Multiple cues guide commissural axons towards and across the floorplate. **A)** Commissural axons are initially repelled away from the roofplate by Bmp7:Bmp1Rb and Draxin-DCC mediated repulsion. **B)** Growth cones require the presence of Netrin-1 in order to grow into the ventral half of the spinal cord. The axons are simultaneously attracted by gradients of Shh (via Boc), Netrin-1 (via DCC) and VEGF (via Flk-1). Disruption of any of these signaling pathways is sufficient to cause misguidance phenotypes in commissural axons. **C)** As the growth cones approach the floorplate, they remain guided by the attractants, and are temporarily insensitive to the midline repellents Slit and Semaphorin-3B. The insensitivity to the repellants allows the commissal axons to enter the floorplate. **D)** When Slit binds to the Robo receptors on the growth cone, there is a direct interaction between Robo and DCC, which represses the attraction to Netrin-1. At the same time, exposure of the growth cones to Shh leads to an upregulation of Neuropilin-2, which makes the growth cones sensitive to the repellant semaphorin-3B. Concurrently, Stem Cell Factor acts via the receptor Kit to induce a growth impulse, which allows the commissural growth cones to exit the contralateral floorplate.

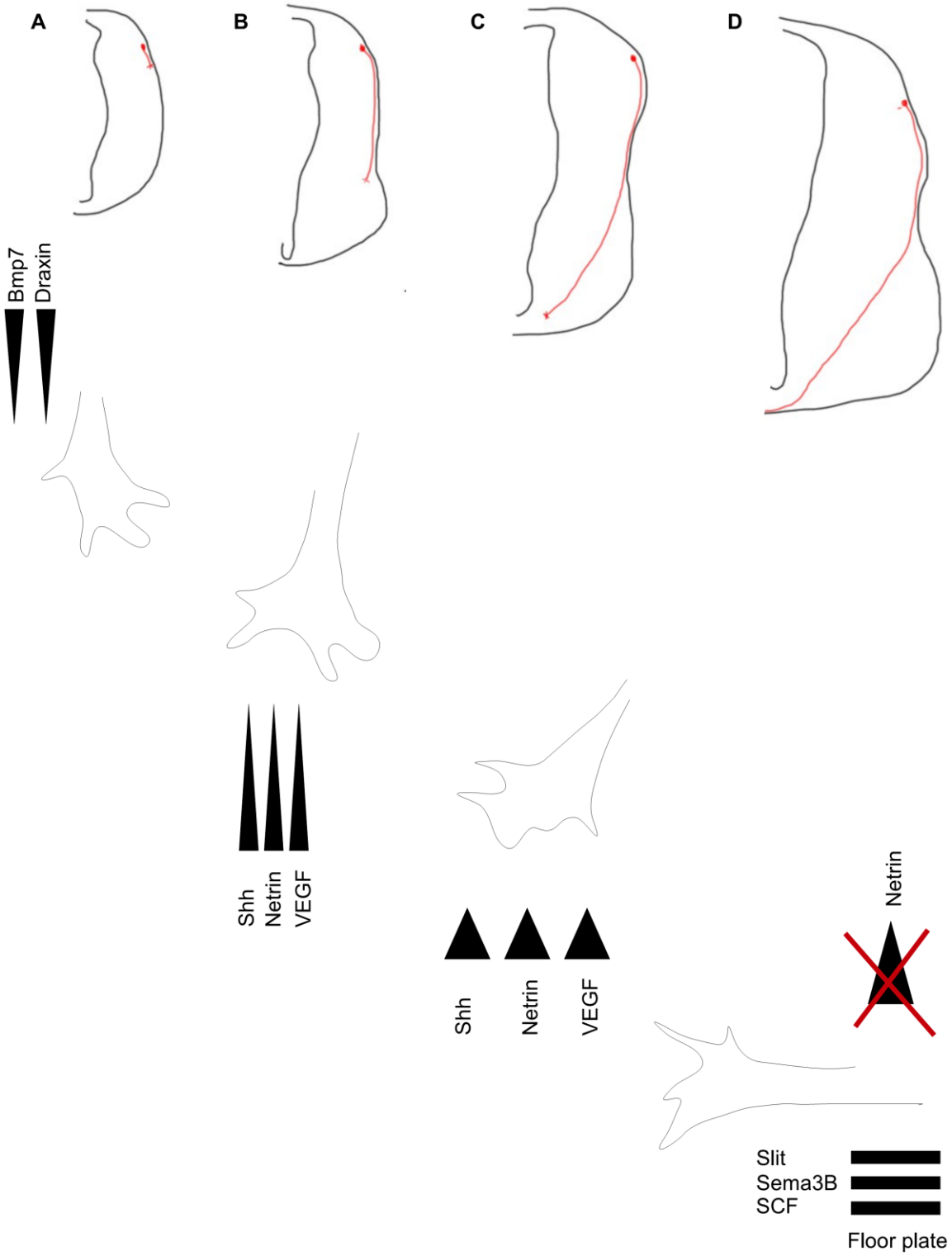
A
B
C
D
Bmp7
Draxin
Shh
Netrin
VEGF
Shh
Netrin
VEGF
Netrin
Slit
Sema3B
SCF
Floor plate

containing DCC, NCK1 and FAK, a protein-tyrosine kinase that provides a direct link between adhesions and intracellular signalling pathways (Li et al., 2002a, Li et al., 2004, Ren et al., 2004). This complex then regulates SFK signaling through the family member Fyn (Li et al., 2004, Meriane et al., 2004), which regulates the activity of the GEFs Trio and Dock180 (Briancon-Marjollet et al., 2008, Li et al., 2008), which then activate the Rho GTPases Rac1 and Cdc42 (Li et al., 2002b, Shekarabi and Kennedy, 2002, Shekarabi et al., 2005).

The mechanism of Shh signaling in commissural axons is much different than Netrin-1-mediated attraction (Figure I.4). Shh ligand binds its receptor Boc (Okada et al., 2006), which removes the repression of Ptch1 on Smoothened. This non-canonical Shh pathyway then diverges from the canonical Shh pathway, as Smo activity leads to activation of Src-family kinase members (Yam et al., 2009), which ultimately leads to regulation of the cytoskeleton through a yet unknown mechanism (Yam and Charron, 2013). Although the downstream mediators of Shh and VEGF signalling in the growth cone are less understood than the molecular mechanisms of Netrin-1 signalling, they are likely to directly or indirectly regulate members of the Rho family of small GTPases, which includes Rho, Rac, and Cdc42, each of which play central roles in the regulation of actin dynamics. The Rho family members cycle between inactive GDP-bound and active GTP-bound states through the action of guanine-nucleotide exchange factors (GEFs) and GTPase-activating proteins (GAPs), respectively.

Although multiple attractant cues guide commissural axons to the same intermediate target, they use distinct signaling pathways, which appear to share a common convergence on the Src-Family Kinases (SFKs). The SFKs are a family of non-receptor tyrosine kinases that are recruited locally to the microtubules within the growth cone (Suter et al., 2004), and when activated can phosphorylate cytoskeletal regulatory proteins. The phosphorylated form of SFK (pSFKs) have been shown to regulate the growth cone traction forces through receptor-cytoskeletal linkages. An increase in tension leads to an increase in tyrosine kinase activation, which in turn

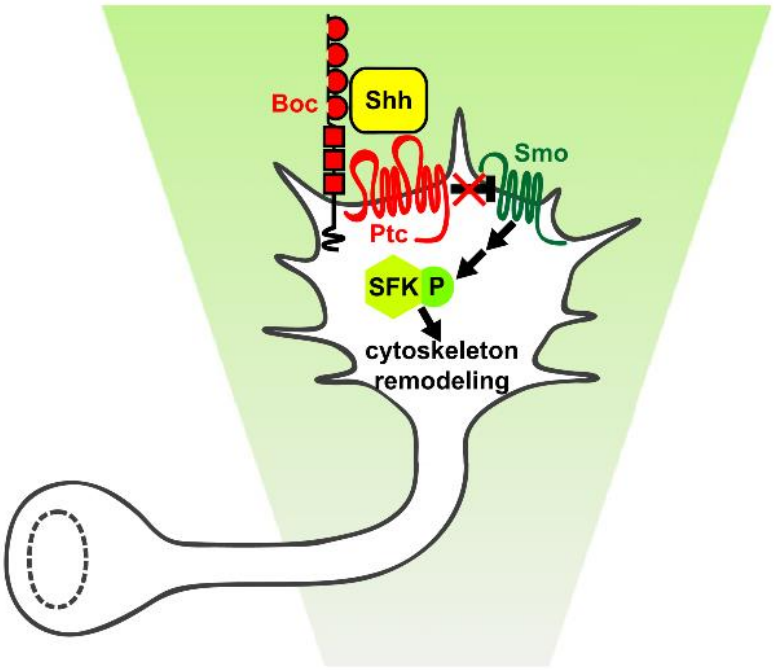

Figure I.4. Shh signaling in axon guidance. Shh mediates axon guidance effects through a non-canonical, transcriptionally independent pathway. In the absence of Shh ligand, the twelve-pass transmembrane protein receptor Ptch1 represses Smo, thereby repressing Shh signaling. When Shh is present, it binds to cell surface receptors Boc and Ptc, relieving the Ptch1 inhibition of Smo. Smo activation leads to phosphorylation of SFKs within the growth cone. The distribution of pSFKs within the growth cone reflects the direction of the extrinsic Shh gradient, wherein the pSFK activity is polarized to the side of the growth cone where there is a higher concentration of Shh. Adapted from Yam et al 2009

strengthens the 'clutch' linkage in a positive feedback loop (Suter and Forscher, 2001). It has been proposed that pSFK activity could link the mechanics of growth cone motility to the intracellular signal transduction events, and that this feedback loop could act as a signal amplifier to enhance cytoskeletal movement towards regions of higher receptor-binding (Jay, 2001). Interestingly, it has been shown that pSFKs are asymmetrically distributed following exposure to a gradient of Shh (Yam et al., 2009), wherein its distribution is polarized to the side of the growth cone exposed to the higher concentration of guidance cue. Moreover, graded pharmacological inhibition of pSFK is sufficient to cause axons to turn (Yam et al., 2009), indicating that a baseline amount SFK is active in growth cones, and asymmetry in its active form is sufficient to drive a polarized response from the growth cone. This suggests that understanding the factors that regulate the phosphorylation of SFKs within the growth cone will aid to understand more generally the mechanism by which a concentration gradient can be internally represented.

I.1.iv. Combinatorial influence of guidance cues

The complexity of combinatorial guidance cue responses is not limited to commissural neurons, as many types of neurons must integrate combinations of guidance cues to reach their targets. Much emphasis has been placed on discovering new guidance cues and elucidating their signalling pathways, while less attention has been paid to how guidance cues cooperate. Several categories of guidance cue integration have been identified. In a recent review (Dudanova and Klein, 2013), the authors described several possible ways that guidance cues could work together at the growth cone, which were broadly categorized as additive or non-additive effects. When growth cone turning is measured quantitatively, it is possible to discern between these alternatives.

When multiple guidance systems act in parallel and operate independently, their effect is purely additive; the sum of the individual responses is equal to the combined effect. This is exemplified by the role of SCF at the floorplate. The presence of this factor itself is not required for the repulsion of Slit and Sema, as demonstrated by the difference between the midline

phenotypes (Zou et al., 2000, Long et al., 2004, Gore et al., 2008). However, the growth impulse that the SCF-Kit mediated signalling produces enables the midline repellants to exert a more notable and timely influence, as the outgrowth of axons is increased (Gore et al., 2008). The push-pull response of LMC_L axons to a counter-gradient of the attractant GDNF and repellant Ephrin-A5 is thought to play an essential role in ensuring appropriate motor innervation of the dorsal hindlimb (Dudanova et al., 2010). When these guidance cues are combined in gradients facing in opposing directions, there is overlapping information provided to the growth cone, which becomes more capable of turning to align with the gradient. In this instance, the attractive 'pull' is encouraged by a repulsive 'push' in the same direction, however each of these pathways act independently in the growth cone.

Alternatively, when there is cross-talk between guidance systems, the influence is non-additive. Within the category of non-additive guidance cue integration, there are three further subdivisions of influence that describe entirely different axonal behaviour: Hierarchical, Permissive and Synergy. Hierarchical interactions have been well described as the growth cones of commissural axons cross the floor plate. Netrin-1-DCC attraction is silenced when growth cones encounter Slit at the midline. Slit binds to Robo, which directly interacts with DCC to impair the attractive response (Stein and Tessier-Lavigne, 2001). Removing the attractive response allows Slit-Robo signalling to dominate, facilitating floorplate exit by repulsion. This is a clear example of crosstalk between signaling pathways, which is the hallmark of non-additive effects. In this case, the coordinated behaviour of multiple signaling ligands presented simultaneously leads to direct interactions between the intracellular domains of the guidance receptors, which allows for a complex maneuver on the part of the axon.

Alternatively, non-additive guidance cue influences can also be permissive. On arrival to the floor plate, commissural growth cones gain responsiveness to Semaphorin-3B following exposure to GDNF (Nawabi et al., 2010, Charoy et al., 2012) and Shh (Parra and Zou, 2010) at the midline. Exposure to the midline cue(s) inhibits the calpain-mediated processing of the Semaphorin-3B co-receptor Plexin-A1, permitting the growth cone to be sensitive to the repellant. This differs from the hierarchical Robo-DCC interaction, as the gained sensitivity to Semaphorin-3B does not appear to cause a loss of sensitivity to Shh.

A combination of guidance cues can also behave synergistically, when the combined response is greater than the sum of the individual responses. Synergy between topographic and chemical cues have been observed for hippocampal neurons grown on topographic gradients (Kundu et al., 2013). Synergy has also been observed between chemoattractants in the developing limb. For example, LMC_L axons can respond synergistically to a combined gradient of GDNF and EphA, when the concentrations for each cue is insufficient to guide with either cue alone (Bonanomi et al., 2012). Outside of the spinal cord, dorsal root ganglion axons are guided synergistically in combined gradients of NGF and NT-3, wherein the gradient threshold required for guidance is lowered in the presence of the second factor (Cao and Shoichet, 2003).

Typically, a synergistic interaction between drugs or guidance cues involves what we will refer to as concentration-limited synergy. When a single guidance cue is provided to the growth cone at a sufficient concentration, it will engage the signalling pathway, and cause the axon to turn. If the concentration is then lowered, there will be a concentration so low that axons will no longer turn (Figure I.5A). This is intuitive, as it represents a situation where there is an insufficient amount of ligand present to properly engage the signalling pathway, and therefore the growth cone has insufficient information to begin a turn. If a second guidance cue is added at a concentration that is also too low to elicit a response on its own, it is possible for the combination of sub-optimal concentrations to induce a synergistic response (Figure I.5B). Since the concentration of guidance cue ligand is limiting in this scenario, we refer to this as concentration-limited synergy. This was observed when Netrin-1 was isolated and a factor contained in the Netrin-depleted high salt extract by-product was capable of lowering the concentration of purified Netrin-1 that was necessary to induce outgrowth (Serafini et al., 1994, Galko and Tessier-Lavigne, 2000). The identity of the factor was undetermined, and named Netrin-Synergizing Activity (NSA) for its functional role.

We propose an alternative model of synergy that is possible when the concentration of both cues is sufficiently high to induce a signaling cascade on their own, but the gradient itself is not strong enough for the growth cone to properly assess the gradient orientation. Since the steepness of the gradient, and not the concentration is limiting, we refer to this as steepness-

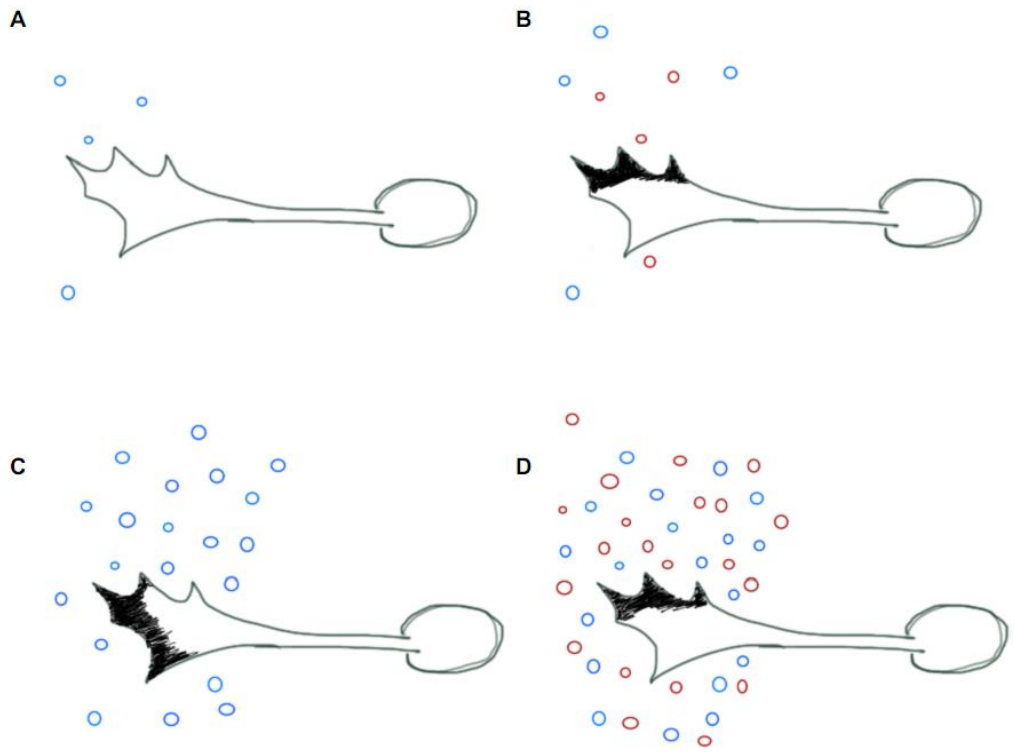

Figure I.5. Distinction between modes of synergy. We propose that it is possible to distinguish between synergistic guidance cue integration. **A)** In the presence of a low concentration of a single guidance cue, there may be insufficient receptor activation present for the intracellular signalling pathways to be engaged. **B)** In the presence of a low concentration of a second guidance cue, a threshold is surpassed, and the downstream signaling pathway is engaged (represented by dark shading). Since the limiting factor for pathway activation is the amount of guidance cue, we refer to this as concentration-limited synergy. **C)** The concentration of a single guidance cue is increased (as compared with A) such that it is sufficient to induce pathway activation. However, since the concentration is higher, there is a less profound difference in the number of molecules on either side of the growth cone. Despite the downstream signaling molecules being active, they are not polarized to reflect the external gradient, and therefore there is no directed turning. **D)** When a second guidance cue is added in a similar gradient to C, the downstream intracellular signaling pathways are activated, and they are spatially polarized to reflect the direction of the external gradient. Since the concentration itself was not limiting in this context, rather the steepness of the gradient was the limiting factor, we refer to this as steepness-limited synergy.

limited synergy. In this model, despite a sufficient amount of ligand being present at the growth cone, the difference between the levels of signaling from one side of the growth cone to the other is too low compared to the overall level of signaling at the growth cone for it to correctly interpret the direction of a single gradient (Figure I.5C). When a second guidance cue gradient is added, the growth cone regains its ability to discern the gradient direction, and turns robustly to align with the gradient (Figure I.5D).

I.2. Concentration gradients

I.2.i. Physics of a concentration gradient

When molecules diffuse away from a point-source, they will naturally create a gradient of molecule density which decreases as a function of the distance from the source (Figure I.6). At the molecular scale, this is a consequence of Einstein's description of Brownian motion (Einstein, 1905). For molecules in solution, this molecular flux results in a concentration gradient, that can be described macroscopically by Fick's laws (Fick, 1855). According to Fick's first law, when the gradient is steady-state a solute will tend to move down a concentration gradient, from a region of high concentration to a region of lower concentration. It follows that the diffusive flux, the number of molecules that will pass through a small area during a given time interval, is proportional to the diffusivity of the molecule and to the concentration gradient. The 'diffusivity' or diffusion coefficient of a molecule is inversely related to the cubic root of the molecular weight. For the purposes of axon guidance and chemotaxis, a concentration gradient can be completely described with three parameters: concentration, the absolute change in concentration, and the steepness. First, the concentration of a molecule is the most straightforward, it is the quantity of molecule per unit volume (Figure I.7A-C). The absolute difference in concentration (ΔC) is the difference in concentration between two points within a gradient. Typically, a relevant length scale is used: in the field of axon guidance, 10 µm is most commonly used to roughly approximate the width of a growth cone. Therefore, the ΔC of the gradient is proportional to the difference in the number of molecules from one side of a

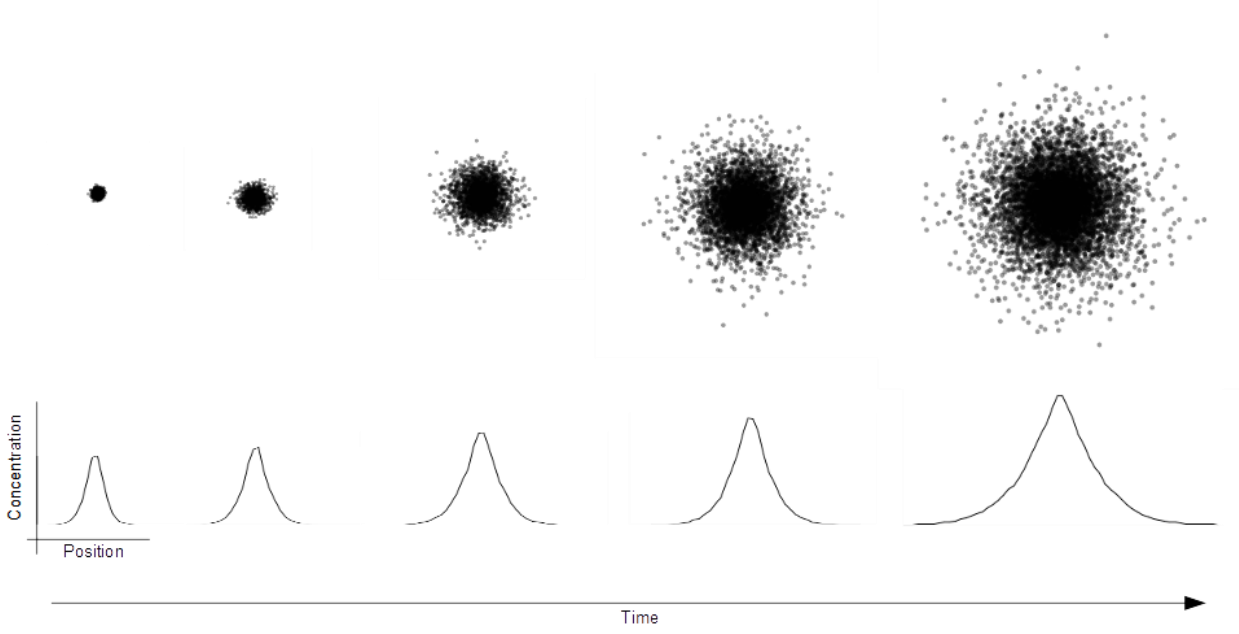

Figure I.6. Concentration gradients result from random molecular diffusion. Molecules released from a hypothetical point source will each move independently according to a random walk, where the direction of any subsequent movement of the particle is independent of any prior direction. Due to the laws of entropy, over time this random movement will result in diffusion away from the source. Given a sufficient number of molecules, a reproducible concentration gradient will be formed, that can be described macroscopically by deterministic differential equations (by Fick's laws). The concentration gradient evolves through time at a rate that is critically influenced by the size of the molecule. The diffusion coefficient, D, is inversely proportional to the cubic root of the molecular weight, $D \cong \frac{1}{\sqrt[3]{MW}}$.

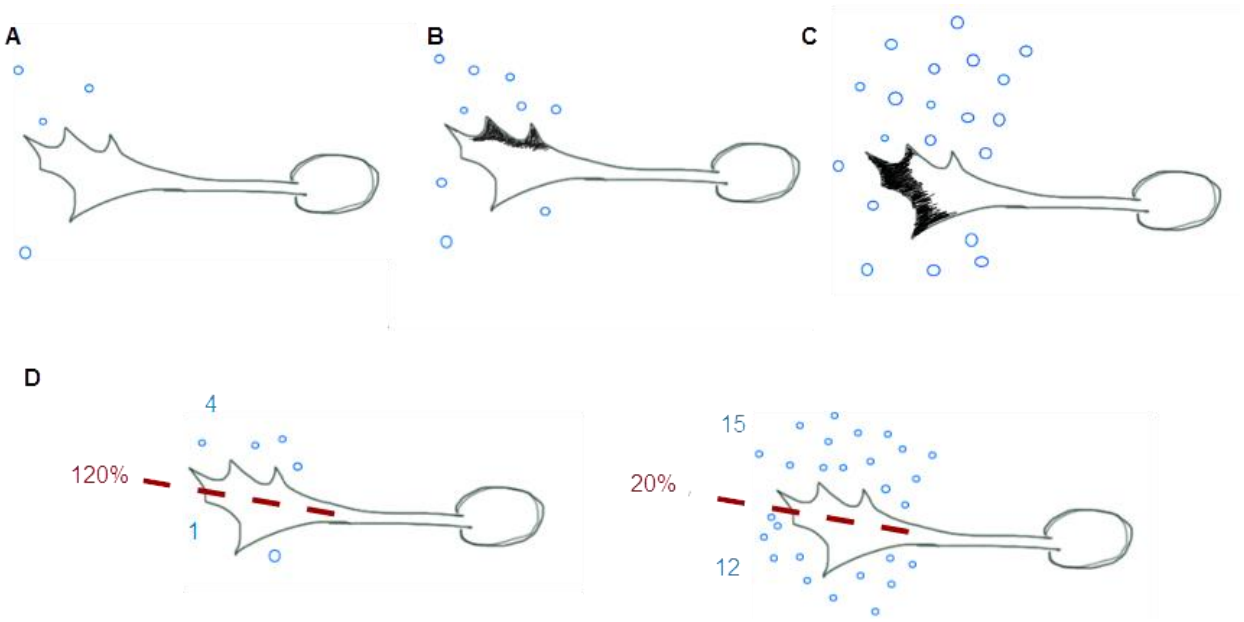

Figure I.7. Parameters describing a concentration gradient. A steady-state concentration gradient can be entirely described by three parameters: the concentration, the absolute change in concentration, and the gradient steepness. The concentration is the standard measure that is proportional to the amount of molecules present in a certain volume. **A)** If the concentration is too low, the signaling mechanisms within the growth cone will not be engaged. **B)** When the concentration is within an appropriate range, signaling pathways are engaged, and the growth cone can sense a difference in the concentration across its width. **C)** When the concentration is too high, all the receptors on the surface are bound, and the growth cone cannot interpret the direction of the gradient. Although the ambient concentration is important, it is critical that the growth cone can sense a concentration difference across its width. The absolute change in concentration across the width of a growth cone (ΔC), is proportional to the difference in the number of molecules from one side to the other. The gradient steepness is the fractional change in concentration across the width of a growth cone, $\delta=\Delta C/C$. **D)** Despite having the same difference in the number of molecules (blue) across the halves of the growth cone, the ambient concentration is different, which results in drastically different gradient steepness (percentage shown in red).

growth cone to the other. The steepness of the gradient is the fractional change in concentration (ΔC/C), which is the difference in concentration across the growth cone, relative to the ambient concentration at the growth cone (Figure I.7D). The steepness is a unit-less value, most often described as a percentage, which provides an intuitive manner to compare gradients between experiments and to theoretical predictions.

I.2.ii. Establishment of concentration gradients *in vivo*

Although the generation of a concentration gradient is in principle quite simple, it is made more complex in a biological setting – as there are many parameters that influence the gradient shape. First, the protein of interest must be produced in abundance and secreted from the cells which produced it, therefore the production rate is critical. It is then released from the producing cell and diffuses through the extracellular matrix. Additionally, the gradient profile depends on the number of receptors that are present in the tissue neighboring where it is produced, and the extent of specific or non-specific binding that occurs within the extracellular matrix (ECM). A well-studied and particularly relevant example to consider is the Drosophila Hh morphogen gradient. There are mechanisms in place to tether Hh to the membrane of producing cells by lipid modification (Peters et al., 2004, Gallet et al., 2006). Once at the membrane, Hh requires coordinated action of Dispatched in order to be secreted by the producing cells (Burke et al., 1999), and to Scube2, a secreted ECM protein that is required for Hh release (Creanga et al., 2012, Tukachinsky et al., 2012). Once released into the extracellular space, Hh requires Heparin Sulfate Proteo-Glycans (HSPGs) of the glypican family to be expressed on the surface of cells in the tissue in order to ensure its proper diffusion (Bellaiche et al., 1998, Bornemann et al., 2004, Takei et al., 2004) and gradient shape (Callejo et al., 2011). The Hh ligand can be titrated or sequestered by specific surface receptors (Yan et al., 2010, Bilioni et al., 2013, Camp et al., 2014), which are also required to maintain the appropriate gradient shape. It is therefore unlikely that a concentration gradient is either entirely soluble or entirely membrane-bound in the developing embryo, and likely transitions continuously between these two states depending on the local physical and chemical interactions. For the

scope of this thesis, I will focus on soluble gradients – with the understanding that this reflects an oversimplification of the *in vivo* environment. Moreover, theoretical modeling has shown the local surface binding would influence the rate of diffusion, but not the shape of a gradient profile (Bergmann et al., 2007, Schwank et al., 2011, Zhou et al., 2012).

I.2.iii. Simulating concentration gradients *in vitro*

The earliest attempts to create gradients for studying axon guidance *in vitro* involved dissecting and co-culturing tissues of interest in a collagen gel, and allowing a gradient of the target-derived factor to form naturally by diffusion. The directed growth of axons could then be easily assessed by light microscopy (Ebendal and Jacobson, 1977a, Tessier-Lavigne et al., 1988). What followed soon after was an experimental manipulation that would allow scientists to study the effect on individual isolated axons. The pipette assay experiments involved holding a high-concentration of soluble guidance cue in a micropipette, and positioning the tip of the pipette a controlled distance and angle with respect to the growth cone. Again, this technique relies on diffusion to establish the gradients, but allowed the gradient to be applied directly to selected growth cones, so that changes in growth direction could be measured quantitatively in real-time. The technique was adapted through the years to be more controlled, and is still frequently used to study mechanisms of axon guidance at the growth cone (Pujic et al., 2008). Other techniques to generate soluble gradients *in vitro* were developed, including the Zigmond chamber (Zigmond, 1988) and the Dunn Chamber (Zicha et al., 1991). Both of these techniques generate a gradient by the same principle: a source of high concentration chemoattractant is separated from a sink containing no chemoattractant by a bridge of defined distance, and a passive gradient is established by diffusion between the source and the sink. The Zigmond chamber was used to study Leukocyte migration and was never applied to study axon guidance. In contrast, the Dunn chamber was also initially developed to study leukocyte migration, later used to study differential axonal outgrowth (Maden et al., 1998), and then adapted for an assay to study growth cone turning in live-imaging experiments (Yam et al., 2009). The Dunn Chamber assay is now becoming more popular for studying signaling mechanisms in axon guidance

(Dudanova et al., 2010, Kent et al., 2010, Ruiz de Almodovar et al., 2011, Bonanomi et al., 2012, Yam et al., 2012).

An alternative to purely diffusion generated gradients was developed to allow arbitrary gradient shapes to be 'printed' into a collagen gel. In this method, drops of solution of known concentration are applied in equally spaced lines (Rosoff et al., 2004). Various gradient shapes can be produced by choosing the concentration of each subsequently printed line appropriately. After printing the lines, guidance molecules diffuse to create a smooth gradient, which remains stable over the course of one day. This method can quickly produce many identical gradients, allowing for a large number of explants to be studied. This technique has been applied to advance the quantitative and theoretical understanding of axon guidance using dorsal root ganglion axons response to NGF gradients as model system (Rosoff et al., 2004, Mortimer et al., 2009, Mortimer et al., 2010, Yuan et al., 2013).

Recently, microfluidic techniques have gained popularity as an alternative to traditional source-sink diffusion gradients. In principal, this involves using microliter volumes of liquid in micron-scale channels to harness the physical laws that govern fluids at this scale, where viscosity dominates over inertia, and mass-transfer happens only by diffusion. In microfluidic networks, known concentrations of reagents can be precisely controlled and dispersed, allowing unprecedented levels of experimental control. The first and most notable of these techniques is the pre-mixer gradient generator (Jeon et al., 2000), which involves sequentially 'mixing' and separating individual known concentrations of guidance cue several times, in order to generate a linear concentration gradient that is stable as long as the fluid velocity is maintained. The pre-mixing paradigm also allows investigators to create a gradient profile that depends minimally on diffusion, but rather depends largely on the geometry of the mixing network and the gradient chamber. This gradient generator has been adapted to study turning of *Xenopus* neurons in live-imaging (Joanne Wang et al., 2008) and has more recently been adapted by us (Sloan et al., 2015) to study turning of rat commissural axons.

Other microfluidic gradient devices based on different gradient generating paradigms have been applied to study axon guidance. Some examples include the 'microjets' device

(Bhattacharjee et al., 2010) or a similar design that implements a porous membrane between fluidic layers (Xiao et al., 2013, Xiao et al., 2014). More recently, a passive-diffusion based microfluidic device (Taylor et al., 2015) has been used to study turning of embryonic cortical axons to gradients of Netrin-1. Each of these designs involve diffusion-based gradients, however they include microfluidic channels for a more precise control of the gradient and minimal use of reagents. While the number of microfluidic gradient generators is always on the rise, there still appears to be a bottleneck separating proof of principle experiments that measure known responses, from studies which use microfluidic devices to make biologically novel observations of axon-guidance phenomena. Moreover, while various gradient generator technology has been used to assess the influence of different gradient parameters on chemotaxis (Zigmond, 1981, Herzmark et al., 2007) and axon guidance (Rosoff et al., 2004, Mortimer et al., 2009, Yuan et al., 2013), no study has attempted to draw a link between the gradients experienced *in vivo* and those generated *in vitro* in the same model axons.

I.2.iv. Cellular interpretation of concentration gradients

There are several cellular processes performed by various cell types that are distinct from- but conceptually related to axon guidance, as they require the cells to interpret a molecular concentration gradient and perform an appropriate response. Whether the end result is to differentiate according to the ligand concentration, or migrate up gradient, several of the physical constraints that limit the ability of any cell or growth cone to make an accurate representation of the gradient are similar. Foremost, the cells are sensitive to the level of protein synthesis at the gradient source, and the rate at which it is secreted by the producing cells. Once the ligand is in a diffusible form, the gradient shape depends on the level of receptor synthesis on the receiving and neighboring cells, which can alter the shape of the gradient, and the sensitivity of the receiving cells. Finally, when the ligand reaches the receiving cells, there is imprecision in receptor occupancy that results from the stochasticity of the ligand-receptor binding, and the uncertainty of the inherently random molecular diffusion (Figure I.8). This final

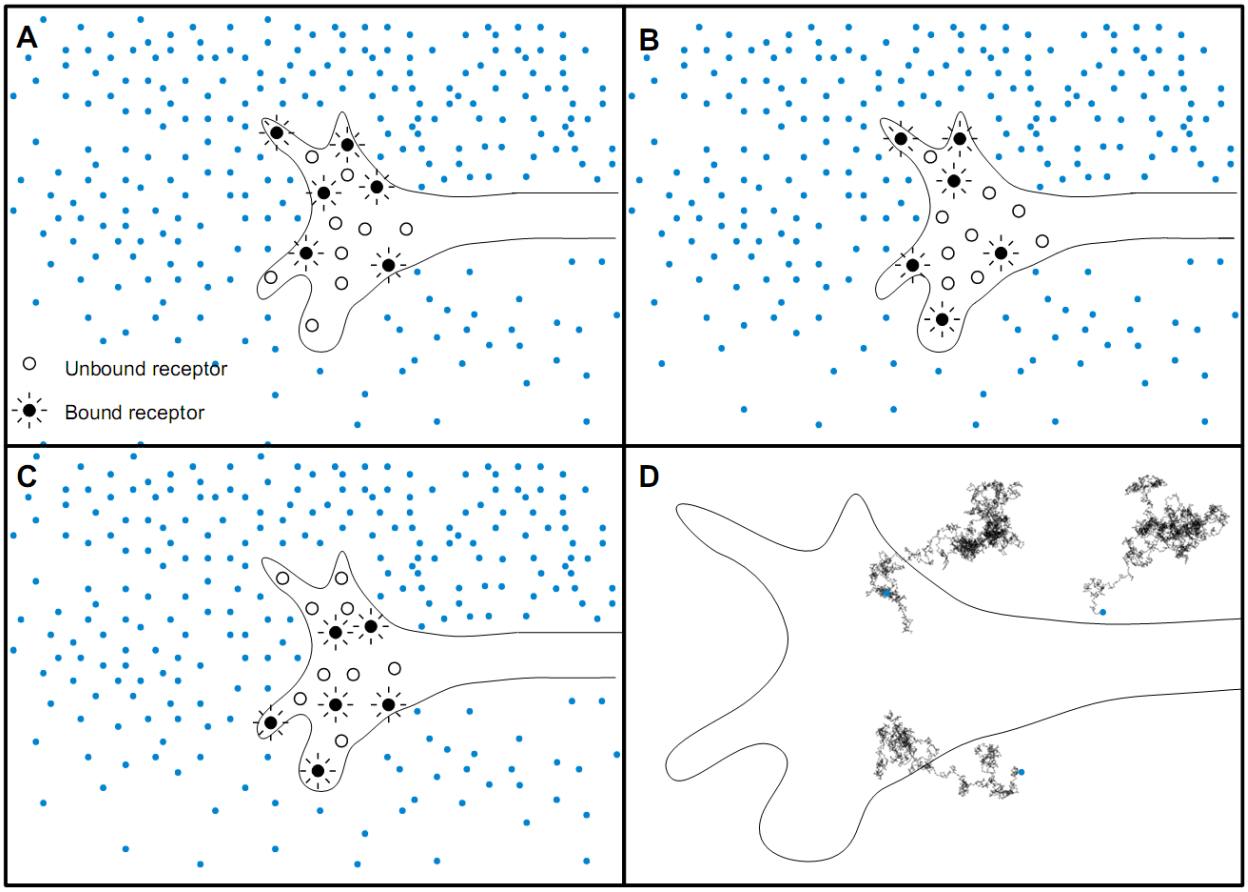

Figure I.8. Stochasticity of binding is a limitation to gradient sensing. Due to the stochasticity of receptor-binding, the pattern of bound receptors on a growth cone depends on the concentration gradient in a non-deterministic manner. **A)** The most likely distribution of bound receptors across the width of a growth cone in a concentration gradient will result in more bound receptors on the side of the growth cone where the concentration is higher. However, since the binding events are random, it is quite possible that at any instance in time, **B)** the number of bound guidance receptors is equally distributed across the growth cone, or that **C)** there are more bound receptors on the side of the growth cone exposed to lower concentration. **D)** Each guidance cue molecule's position is described microscopically as a random walk (traces shown in black). Therefore, the position of any individual guidance molecule is uncertain, and this uncertainty provides a noise constraint on the ability of a growth cone to detect the direction of the gradient. Importantly, this constraint becomes more relevant as the concentration decreases, due to the smaller number of molecules.

source of imprecision increases as the distance from the source increases, as the fewer number of molecules leads to larger fluctuations in receptor occupancy (Lander, 2013).

In this section I will first introduce the interpretation of morphogen gradients. Despite differences in the type of information that is obtained between morphogenesis and axon guidance, the vast literature on the interpretation of morphogen gradients can provide insights to what cellular strategies can enhance the interpretation of a gradient, by reducing the imprecision. I will then introduce the general topic of directed cell migration in various non-neuronal cell types, and discuss how mechanisms that have been identified in both prokaryotes and eukaryotes can provide conceptual insight to how concentration gradients can be interpreted by the growth cone. In both of these subsections, I will highlight instances where multiple concentration gradients are integrated by the cells to provide robustness in the gradient interpretation.

I.2.iv.a. Morphogen gradients

The best studied and most understood function of concentration gradients *in vivo* are morphogen gradients, which define specific cell fates at various positions within the gradient, depending on the local, absolute concentration of morphogen. The influence of the Shh gradient on the patterning of the ventral spinal cord has been well studied. A now classic study determined the molar concentrations of Shh required for different spinal cord identities to be reproduced in culture (Roelink et al., 1995). It is now thought that a mechanism of cell-sorting corrects the initially messy patterning (Xiong et al., 2013). The fact that the initial interpretation of the gradient is imperfect and later corrected by other mechanisms is relevant to how these findings can be extended to axon guidance, as axons which fail to reach their intended intermediate or final targets have made a fundamentally similar error: they've misread the gradient. Notwithstanding, there is a major difference between which gradient parameters are critical in either scenario: for a cell to obtain the appropriate fate from a morphogen gradient, in must receive a specific, absolute amount of protein in order to differentiate using the

appropriate transcription factors. When the determination of the absolute concentration of ligand by these cells is important, the rates of production and secretion from the source are critical, as is the expression level of the receptors in the receiving and neighboring cells.

An interesting clue to how cells may counteract these sources of imprecision comes from the distribution of embryonic morphogen gradients. A major mechanism by which noise can be overcome is through pooled sampling; successive measurements that are uncorrelated (Lander, 2013). One mechanism by which this can be achieved is by integrating the same signal over time. Temporal integration occurs in cells which accumulate intracellular signals which remain active, such as an internalized ligand-receptor complex that continues to signal within the endosome. An alternative mechanism that has been proposed is for cells to pool their sampling by measuring multiple gradients simultaneously (Lander, 2013). This method is employed by morphogen gradients in the vertebrate hindbrain, where a posterior-to-anterior Retinoic Acid gradient is supplemented by FGF and Wnt gradients with the same orientation (Schilling, 2008). Similarly, in the drosophila embryo, the Bicoid gradient works together with independent gradients of Caudal and maternal Hunchback (Gursky et al., 2011). Additionally, during dorsal-ventral patterning of the embryonic spinal cord by BMPs, there are always multiple ligands present (Reversade and De Robertis, 2005, O'Connor et al., 2006). The presence of multiple gradients is consistent with theoretical models which determined the presence of overlapping concentration gradients to give more accurate information, so long as the noise is negatively correlated between gradients (Morishita and Iwasa, 2009). However, the combined effect of multiple morphogen concentration gradients has not been determined experimentally.

I.2.iv.b. Directed cell migration

Growth cones share many features in common with other types of migrating cells, and this ultimately informed Cajal's hypothesis that growth cones can be influenced by chemoattraction. More generally, this important conceptual parallel has benefitted the study of axon guidance by allowing the field to mature more quickly by borrowing concepts learned

from other migrating cells, and assays used to study them. It is no coincidence that many of the gradient generating techniques used in axon guidance were originally developed to study chemotaxis in other cell types. Although growth cones are different in some important respects, as the molecular cues, receptors and signalling pathways are mostly distinct, the conceptual problem of chemotaxis is identical: how can a cell make an informed decision about the orientation of an external gradient, when provided only with a pattern of bound receptors?

Chemotaxis of non-neural cells and growth cones differ from cells which respond to morphogen gradients, as the absolute concentration is not expected to be as critical (Goodhill, 1997, Mortimer et al., 2009), rather it is crucial that a difference between signalling levels from one side of the cell or growth cone to the other can be distinguished. Although the two functional interpretations of the gradient differ in this respect, the cells are still limited in how well they can perceive the gradient by the same physical constraints. For migrating cells and growth cones that are sensitive across a wide range of absolute concentrations, the first two constraints are less important, as the rate of morphogen synthesis and receptor number would mainly influence the interpretation of absolute concentration. However, the imprecision due to binding noise is expected to substantially influence the ability of a cell or growth cone to sense the orientation of a concentration gradient, which has been discussed in depth (Berg and Purcell, 1977, Goodhill and Urbach, 1999, van Haastert and Postma, 2007, Mortimer et al., 2011).

There are several migrating cell types that have been heavily studied and are applicable to the study of growth cone chemotaxis. The simplest is *E.Coli*, which are known to swim up concentration gradients of nutrients such as methyl aspartate and serine. Since the size of the cells are small, they are unable to sense a spatial gradient across their width, and must instead rely on a temporal mechanism of gradient sensing that is conceptually similar to the interpretation of morphogen gradients. In this model, the bacterium swims forward in bursts of a constant distance in a random direction. It then compares the level of accumulated intracellular signaling molecules to the levels it accumulated at a previous time, using the level of signaling as a readout of the absolute concentration extracellularly. If it can detect an increase in concentration, it will be biased to continue to swim in the same orientation. Instead,

if the concentration measured is lower or the same, then the cell will tumble and randomize its orientation (Jin, 2013). A temporal model of gradient sensing has been suggested to play a role in the exquisite sensitivity of axons to concentration gradients (Rosoff et al., 2004, Xu et al., 2005), however this hasn't been demonstrated experimentally.

The slime mould *Dictostelium Discoideum* has been studied in depth, as these cells migrate toward higher concentrations of chemokines and cAMP. Unlike bacteria, *Dictostelium* and other eukaryotes are able to transduce small spatial concentration differences into highly polarized cellular responses. Furthermore, it has been shown that *Dictostelium* chemotaxis depends on both the steepness and concentration of cAMP gradients (Fuller et al., 2010), and that different mechanisms of chemotaxis are used in steep versus shallow gradients. In recent years, the molecular mechanism of their gradient detection has been elucidated through a combination of *in vitro* experiments and mathematical modeling. It is now understood that chemokine ligands bind to G-protein coupled receptors (GCPRs) which modulate Ras proteins through opposing action of GEFs and GAPs to influence the actin cytoskeleton. Furthermore, the dynamics of RasG activation follows a 'Local Excitation Global Inhibition' (LEGI) model (Iglesias, 2012) that had been formulated several years earlier (Levchenko and Iglesias, 2002). This model of chemotaxis explains how a cell can adapt perfectly to an external gradient; binding of the ligand to the G-protein coupled receptor produces rapid activation of an 'excitor' molecule on one side of the cell, in parallel with the slower activation of an inhibitor molecule globally, throughout the entire cell. The global inhibition allows the cell to adapt to the ambient ligand concentration, and the cell becomes more sensitive to the slight differences in receptor occupancy between the leading and trailing edge. This model provides perfect adaptation to the external gradient, but no amplification occurs at the receptor level, therefore it was proposed that the LEGI model is coupled to an excitable network that acts as a switch to turn the graded response into a binary decision. In *Dictostelium*, the role of the excitor is played by PI3K, whereas the role of the inhibitor is played by PTEN (Iglesias, 2012). Although there has been interest in linking this model to the chemotaxis of growth cones, as some similar molecules are involved in both processes (Mortimer et al., 2008), the LEGI model has not been formally demonstrated for neurons. Furthermore, although little is known regarding the

response of *Dictostelium* to multiple gradients, it is expected that multiple attractants can work together, as there are multiple GPCRs expressed that should allow them to detect multiple gradients simultaneously (Jin, 2013).

Another migrating cell type that has been thoroughly studied is the blood neutrophil, as its routine function involves chasing bacteria by following concentration gradients of bacterial derived attractants such as Formyl-met-leu-phe (fMLP) and tissue derived chemoattractants such as interleukin-8 and leukotriene B4 (LTB4). The migration of neutrophils in gradients of the chemotactic peptide fMLP has been shown to depend on both the concentration and steepness of the gradients (Herzmark et al., 2007). Of particular interest, neutrophils routinely use multiple concentration gradients to enhance their pathfinding ability during wound-healing events. In the initial stages following injury, neutrophils migrate to the site of damage by following an intravascular gradient of CXCL2 that is released by necrotic cells. The earliest neutrophils to arrive at the site then form a secondary chemoattractant gradient of LTB4 which has been shown to amplify the response to the primary chemoattractant (Afonso et al., 2012). Therefore, there is precedent in neutrophil chemotaxis indicating that the interpretation of a concentration gradient can be performed more robustly in the presence of a second chemoattractant gradient.

I.2.v. Theoretical models of axon guidance to concentration gradients of guidance cues

The field of axon guidance has reached a stage where there are more implicated molecules than we can comfortably conceptualize, and the techniques have evolved so far as to allow exquisite control of the growth cones' microenvironment. At this stage of maturity, a great amount can be gained by moving proposed mechanistic models beyond a cartoon, and towards formal models of the mechanisms at play. A formal theory allows hypotheses to be tested with more quantitative rigor, and experimental results to be more readily compared between model systems. Fundamentally, the central question of chemotaxis is a computational one: how can a cell or growth cone determine the orientation of an external gradient, when the only

information it possess is the occupancy of its receptors? What follows is a brief, conceptual explanation two models that have been proposed to address this question.

In order for a gradient to be correctly interpreted and a guidance decision to be made, the concentration of guidance cue must be sufficiently high to engage the signalling pathways. Therefore, the concentration must be within several orders of magnitude as the dissociation constant for the ligand-receptor complex. The growth cone must also be able to sense a difference in signalling from one side to the other, as a growth cone with all its receptors saturated would have no difference in receptor occupancy, and would not be able to detect a gradient. Even for growth cones which don't have their receptors saturated, the stochasticity of ligand-receptor binding and the thermal fluctuations in the amount of ligand molecules present at the growth cone fundamentally constrain the gradient detection.

Two formal models have been proposed to describe the ability of a growth cone to detect the gradient direction while taking the molecular noise and receptor saturation constraints into consideration. They provide a theoretical framework to estimate the ability of the growth cone to correctly detect the external gradient as a function of the concentration, gradient steepness, and its orientation within the gradient. In the Bayesian axon turning model (Mortimer et al., 2009, Mortimer et al., 2010) (Figure I.9A), a growth cone makes a measurement of the gradient at every forward step, and turns in a biased-random direction. If the signal of the gradient is high relative to the noise, then the growth cone will be biased to turn towards the gradient, where the bias is proportional to the signal-to-noise ratio. Over many simulations, this model generates trajectories that clearly resemble having turned up the gradient, towards the higher concentration. In the contrasting model of guidance by growth rate modulation (Figure I.9B), the growth cone makes the same calculation of the gradient strength at each step, but the axon grows a longer distance when facing up-gradient than while facing down-gradient. In this model, there is no turning towards the gradient per-se, rather an asymmetric outgrowth in the

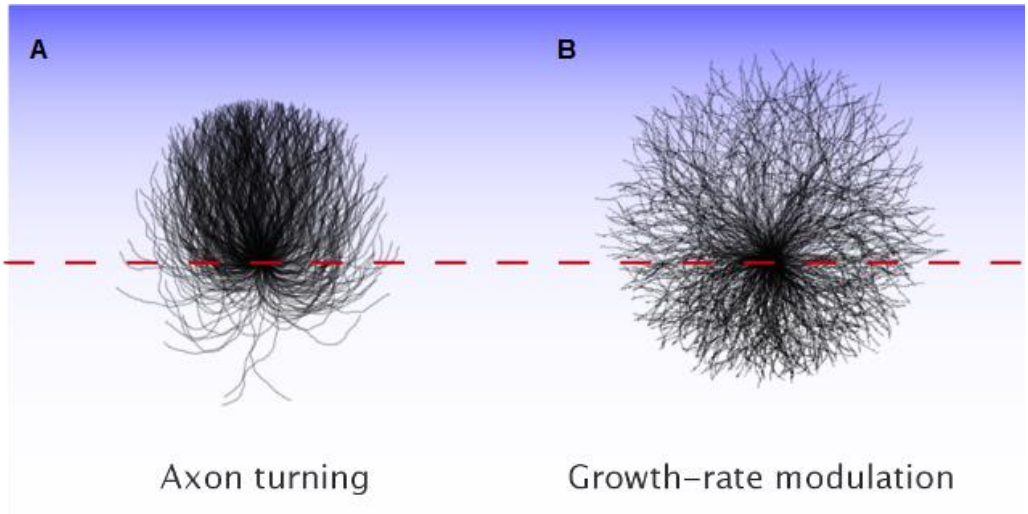

Figure I.9. Formal models of axon guidance. Two models have been proposed to describe the ability of the growth cone to detect the direction of a gradient as a function of the concentration and steepness (Mortimer et al 2010). The models differ in how the growth cone uses its interpretation of the gradient to change its orientation. **A)** Biased and direct turning model (referred to as the axon turning model): before each forward movement, the growth cone computes the direction of the gradient. This measurement is optimal when the gradient is perpendicular to the growth cone. The axon turns a defined angle in a random direction (left or right), where the probability of turning toward the gradient is increased proportionally to the interpretation of the gradient direction. Each movement forward is of a defined distance. In this model, axons may initially grow against the concentration gradient, but will later turn to reorient with the gradient. **B)** Axon guidance by growth rate modulation: For each forward movement, the growth cone calculates the direction of the gradient, while the optimal measurement is made when the growth cone is oriented parallel to the gradient. The growth cone turns randomly a defined angle in either direction with equal likelihood. In this model, the distance a growth cone translates forward is proportional to the strength of the measured gradient, such that growth is further in the up-gradient direction. In this model, axons that are initially oriented down the concentration gradient will grow a shorter distance in this direction. This bias in relative rate of growth in the up-gradient and down-gradient directions is responsible for the directional outgrowth of DRG axons in shallow gradients of NGF (Mortimer et al 2010).

up-gradient direction that leaves the visual impression of turning, without any individual axon having explicitly turned. It was shown that the trajectories of axon outgrowth from DRG explants into collagen gel in response to NGF gradients match more closely the predictions of the growth-rate modulation model than the axon turning model (Mortimer et al., 2010).

Importantly, the equations proposed by Mortimer et al make explicit predictions regarding the integration of multiple attractive guidance cues by the growth cone. They predict that the likelihood of the growth cone to correctly interpret the direction of a concentration gradient is enhanced in the presence of a second guidance cue (Mortimer et al., 2011). Moreover, since the concentration and steepness are independent variables in their model, they implicitly provide a theoretical framework in which concentration-limited and steepness-limited synergy may co-exist as mutually-exclusive phenomena.

I.3. Rationale:

It is known that Shh and Netrin-1 signaling pathways in the growth cone are not redundant, because mice which are deficient for either signaling pathway have a commissural guidance phenotype (Serafini et al., 1996, Fazeli et al., 1997, Charron et al., 2003, Okada et al., 2006). *However, it is not entirely understood why multiple guidance cues are required to guide axons to the same target.* It is known that both Shh and Netrin-1 signaling at the growth cone require the phosphorylation of Src-Family Kinases (Li et al., 2004, Meriane et al., 2004, Yam et al., 2009), as it signals downstream of the guidance receptors in either pathway. It is known that the distribution of pSFK reflects the direction of the gradient of Shh, and that asymmetric pSFK is sufficient to induce an axon to turn (Yam et al., 2009). *However, it is not known whether a combined gradient of both cues can enhance the asymmetric localization of pSFKs.* It is thought that growth cones are sensitive to both the concentration of a guidance cue, and the steepness of the concentration gradient. It has been hypothesized that two attractive gradients can increase the likelihood that an axon will turn the correct direction to align with the gradient (Mortimer et al., 2011). It has been further demonstrated that synergy between guidance cues can occur when the concentration of the guidance cues is limiting (Serafini et al., 1994, Bonanomi et al., 2012). *It has not been determined, however, whether a synergistic interaction between guidance cues can occur when the steepness of the gradient is limiting.*

We hypothesize that the combination of Shh and Netrin-1 can enhance the ability of the growth cone to detect the orientation of a shallow concentration gradient. Additionally, we hypothesize that the two pathways are integrated by the growth cone by converging on pSFKs.

Chapter II: Integration of Shallow Shh and Netrin-1 gradients guides commissural axons

II.1. Abstract

During nervous system development, gradients of Sonic Hedgehog (Shh) and Netrin-1 attract growth cones of commissural axons toward the floor plate of the embryonic spinal cord. Mice defective for either Shh or Netrin-1 signaling have commissural axon guidance defects, suggesting that both Shh and Netrin-1 are required for correct axon guidance. However, how Shh and Netrin-1 collaborate to guide axons is not known. We first quantified the steepness of the Shh gradient in the spinal cord and found that it is mostly very shallow. We then developed an *in vitro* microfluidic guidance assay to simulate these shallow gradients. We found that axons of dissociated commissural neurons respond to steep but not shallow gradients of Shh or Netrin-1. However, when we presented axons with combined Shh and Netrin-1 gradients, they had heightened sensitivity to the guidance cues, turning in response to shallower gradients that were unable to guide axons when only one cue was present. Furthermore, these shallow gradients polarized growth cone Src-family kinase (SFK) activity only when Shh and Netrin-1 were combined, indicating that SFKs can integrate the two guidance cues. Together, our results indicate that Shh and Netrin-1 synergize to enable growth cones to sense shallow gradients in regions of the spinal cord where the steepness of a single guidance cue is insufficient to guide axons, and we identify a novel type of synergy that occurs when the steepness (and not the concentration) of a guidance cue is limiting.

II.2. Introduction

During embryogenesis, axons grow through a complex environment to make specific connections with their targets. The growth cone follows concentration gradients of guidance cues by sensing a difference in receptor occupancy across its width, and turns to align with its interpretation of the gradient direction. Moreover, multiple guidance cues are often needed to correctly guide axons. For example, commissural axons are initially repelled by bone morphogenic proteins (BMPs) in the dorsal half of the spinal cord (Augsburger et al., 1999, Butler and Dodd, 2003). They are then attracted by gradients of Netrin-1 (Kennedy et al., 1994), Sonic hedgehog (Shh) (Charron et al., 2003) and vascular endothelial growth factor (VEGF) (Ruiz de Almodovar et al., 2011) towards the floor plate. While it isn't understood why multiple guidance cues are needed to guide axons to the same targets, it is clear they are non-redundant, as interfering with each of these pathways individually results in guidance errors (Serafini et al., 1996, Fazeli et al., 1997, Charron et al., 2003, Okada et al., 2006, Ruiz de Almodovar et al., 2011).

Both Netrin-1 (Serafini et al., 1994, Kennedy et al., 2006) and Shh (Ericson et al., 1995a, Roelink et al., 1995) diffuse from the floor plate cells which secrete them and establish gradients which guide commissural axons (Charron et al., 2003, Kennedy et al., 2006). Shh signals through its receptor Boc (Okada et al., 2006), while Netrin-1 signals through its receptor DCC (Keino-Masu et al., 1996, Fazeli et al., 1997). Shh- and Netrin-1-mediated axon guidance also both require Src-family kinase (SFK) activity (Liu et al., 2004, Yam et al., 2009), whose asymmetric activation reflects the direction of the external gradient and is sufficient to cause the growth cone to turn (Robles et al., 2005, Yam et al., 2009). While it is known that both Shh and Netrin-1 form gradients, it is not clear how steep the gradients are *in vivo* and how this steepness influences axon pathfinding in gradients formed by single or multiple guidance cues. Although theoretical chemotaxis modeling has suggested that two overlapping attractive concentration gradients could increase the probability of a cell making a correct decision about the gradient direction (Mortimer et al., 2011), this prediction has not been tested experimentally.

There are several potential mechanisms by which multiple guidance cues could collaborate to improve how well the growth cone estimates the direction of the gradient. In one model, the concentration of individual guidance cues is too low to elicit a robust turning response. When the cues are combined, the response is higher than the sum of responses from the same concentration of either cue individually. We will refer to this as concentration-limited synergy, as the concentration of either guidance cue is limiting for the pathway to be engaged. When a second cue is present, there is some crosstalk or convergence between pathways which overcomes the activation threshold. An alternative mechanism, which we will refer to as steepness-limited synergy, is where the concentration of guidance cue present at the growth cone is not limiting; instead, it is the concentration difference of an individual guidance cue across the growth cone that is too small compared to the ambient guidance cue concentration to be accurately detected by the growth cone. When two guidance cues are present, corroborating directional information is supplied and integrated by the growth cone through crosstalk or convergence between the two guidance cue pathways.

We demonstrate that commissural axon guidance errors occur *in vivo* where Shh concentration gradients are relatively shallow. We then use a novel microfluidic guidance assay to show the importance of gradient steepness for commissural axon guidance *in vitro*. We find that a combined gradient of the attractive guidance cues Shh and Netrin-1 can act in steepness-limited synergy to attract axons when the steepness of a single guidance cue is insufficient to guide axons. Mechanistically, we demonstrate that combined Shh and Netrin-1 gradients polarize SFK phosphorylation in the growth cone at the same gradient steepness where the two cues behaved synergistically to attract axons.

II.3. Results

II.3.i. Shallow gradients guide commissural axons en route to the floor plate

To determine the Shh gradient steepness that growth cones of commissural axons are exposed to *in vivo*, we examined spinal cord cross sections of embryonic day 9.5 (e9.5) and e10.5 mouse embryos, stages when axons are actively being guided towards the floor plate. We visualized the distribution of Shh protein in paraformaldehyde-fixed spinal cords using immunofluorescence with an anti-Shh antibody (Tian et al., 2009). The Shh staining present in the floorplate and the spinal cord were not present in *Shh*$^{-/-}$ embryos (Figure II.S1A), demonstrating that the antibody specifically recognized Shh. We then measured the fluorescence intensity profiles of the Shh protein gradient along the dorso-ventral axis at several angles for each image (Figure II.1A) and pooled these measurements from multiple embryos to obtain a prototypical gradient profile (Figure II.1B). Shh fluorescence signal was highest at the floor plate and rapidly decreased for approximately 50 µm from the floorplate, followed by a slower decrease for the remainder of the spinal cord. We observed that the gradient profiles were remarkably consistent between embryos (Figure II.S1B). and that they did not depend on the concentration of the primary antibody (Figure II.S1C). We then demonstrated that there is a linear relationship between the fluorescence intensity and the concentration of Shh protein (Figure II.S1D). Furthermore, the gradient profiles were similar whether the measurements were made medially (as in Figure II.1A), or more laterally, overlapping with Tag-1 positive axons (Figure II.S2).

Both the concentration (C) and steepness of the gradient can influence axon guidance responses. Because growth cones must be able to determine the direction of a gradient, it is essential that they can sense a difference in concentration across their width. This can be expressed as the absolute change in concentration across a growth cone (ΔC). The fractional change in concentration ($\delta = \Delta C/C$) is a measure of the steepness of the gradient across the growth cone, typically estimated at 10 µm (Rosoff et al., 2004). The fractional change is usually

Figure II.1. Axon misguidance phenotypes *in vivo* occur where the Shh gradient is shallow. **(A)** Mouse e 9.5 (*left*) and e10.5 (*middle* and *right*) spinal cord cross-sections immunostained for Shh. We measured fluorescence intensity profiles at multiple angles along the cross-section of the spinal cord; angle range indicated by wedges (*right*). **(B)** Shh concentration was highest at the floor plate and decreased rapidly in the first ~50 µm (relative distance of 0-0.1) from the floor plate. Beyond this steep decline in intensity, there was a residual shallow gradient extending >300 µm, up to a relative distance of 0.8 from the floor plate to the roof plate. 29 sections from two e9.5 embryos and 15 sections from two e10.5 embryos were analyzed. The steepness of the gradient, δ, was defined as the fractional change in concentration ($\delta = \Delta C/C$) over a distance of 10 microns, and was $46 < \delta < 72$ % in the steep region close to the floor plate (black line), and $0.6 < \delta < 0.7$% at e9.5 and $1.9 < \delta < 2.1$% at e10.5 at a relative distance of 0.41-0.56 from the floor plate, where guidance errors have been reported for mice with mutations in Shh signaling (purple line). The guidance errors that have been reported for mice with mutations in Netrin-1 signaling occupy a similar region of the spinal cord. The absolute distance scale from floor plate is for e10.5. **(C)** Schematic spinal cord showing the approximate relative positions of the regions of high and low fractional change, and the range of guidance errors reported previously.

fp, floor plate; nc, notocord. Scale bar (A): 100 µm. See also Figure II.S1, Figure II.S2, and Table II.S1

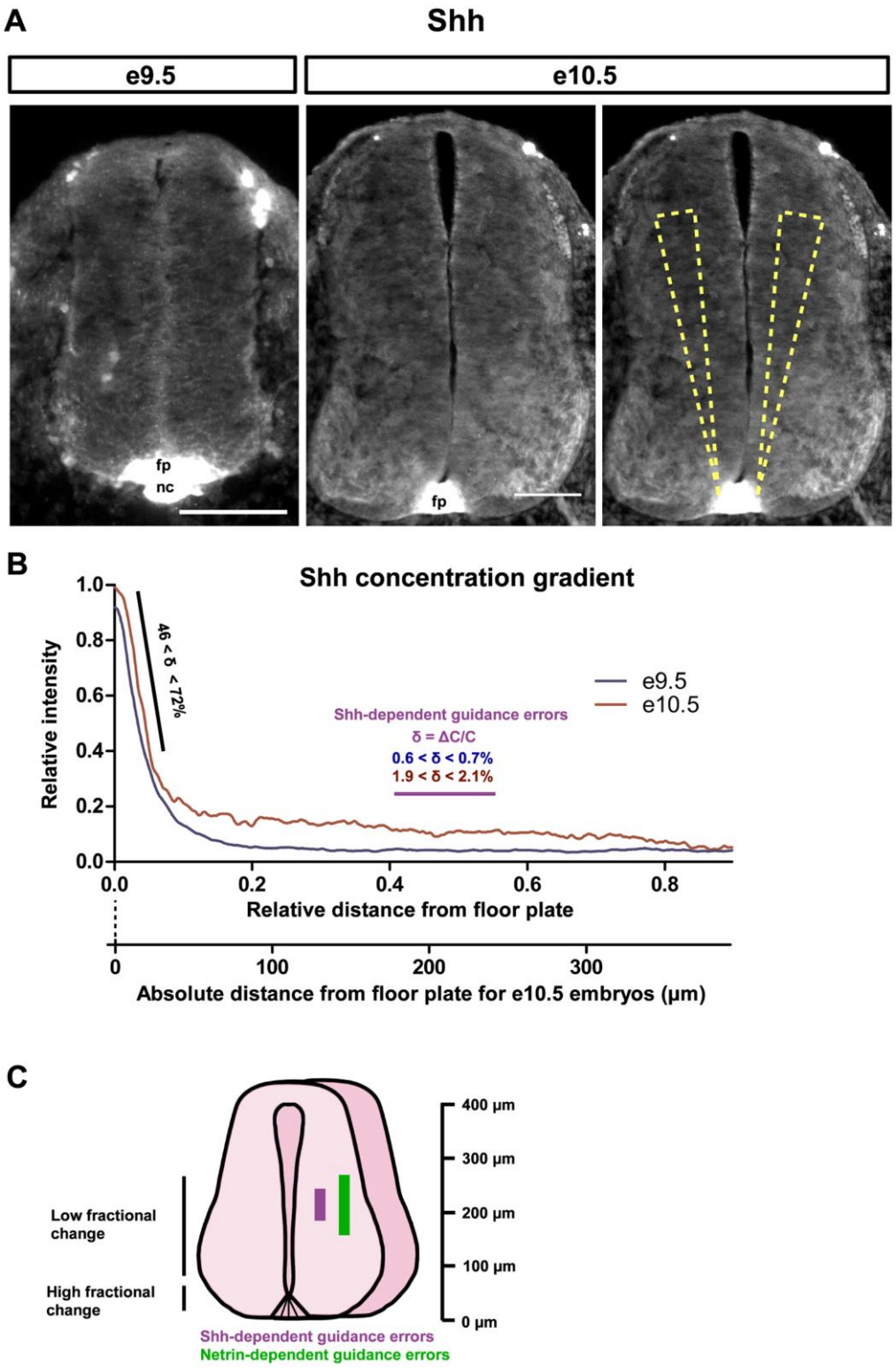
A
Shh
e9.5
e10.5
fp
nc
fp
B
Shh concentration gradient
Relative intensity
1.0
0.8
0.6
0.4
0.2
0.0
46 < δ < 72%
e9.5
e10.5
Shh-dependent guidance errors
δ = ΔC/C
0.6 < δ < 0.7%
1.9 < δ < 2.1%
0.0
0.2
0.4
0.6
0.8
Relative distance from floor plate
0
100
200
300
Absolute distance from floor plate for e10.5 embryos (μm)
C
Low fractional change
High fractional change
400 μm
300 μm
200 μm
100 μm
0 μm
Shh-dependent guidance errors
Netrin-dependent guidance errors

expressed as a percentage and reflects the change in concentration across a growth cone relative to the ambient concentration at the growth cone.

Although it is not possible to accurately quantify absolute protein levels *in vivo* using immunohistological methods, measuring the fractional change in concentration does not require knowledge of the actual concentration of the cues, only the relative concentration of the cue. Thus we estimated the fractional change in concentration using the Shh fluorescence intensity. Within 50 µm of the floor plate (relative distance of 0-0.1 from the floor plate to the roof plate), there is a rapid decrease in Shh, with a fractional change (δ) of 46-72% (Figure II.1B). In the region beyond 50 µm of the floor plate, the Shh gradient was shallower.

We then determined where along the spinal cord guidance defects occur for commissural axons from mice genetically deficient for Shh or Netrin-1 signaling. We analyzed images from previously reported guidance cue or guidance receptor mutants (Serafini et al., 1996, Fazeli et al., 1997, Charron et al., 2003, Okada et al., 2006) and measured the relative distance from the floor plate at which misguided axons begin to deviate from their normal trajectory (S1 Table). For Shh and Netrin-1 signaling dependent defects, guidance errors occurred at a relative distance of 0.35-0.6, which corresponds to 158-270 µm from the floor plate for a spinal cord ~450 µm in height. In the region where Shh dependent errors occur (relative distance of 0.41-0.56), the Shh gradient at e9.5 was very shallow, with a fractional change of $0.6< \delta<0.7\%$. At e10.5, when the majority of the commissural axon growth cones are en route from the roof plate to the floor plate, the fractional change in this region was $1.9< \delta<2.1\%$, slightly higher than that measured at e9.5 (Figure II.1B). The Netrin-1 gradient has been previously visualized at mouse e10.5 using alkaline phosphatase immunohistochemistry (Kennedy et al., 2006). Similarly to what we observed for Shh, Netrin-1 signal is highest at the floor plate and decreases rapidly in the first ~50 µm from the floor plate, with a shallow gradient present in the remainder of the spinal cord, which includes the region from the floor plate where Netrin-1 dependent errors occur (relative distance of 0.35-0.6). This gradient shape is reminiscent of the

gradient shape for Shh, and suggests that the Netrin-1 gradient is also steep close to the floor plate and shallow in the remainder of the spinal cord. However, we were unable to confirm this by more precise quantification using immunofluorescence because the Netrin-1 antibodies that work for immunohistochemistry are no longer available.

Intriguingly, the Shh- and Netrin-1-dependent guidance errors occur in the region of the spinal cord where Shh and most likely Netrin-1 gradients are shallow, not steep (Figure II.1C), indicating that loss of one guidance cue is sufficient to cause guidance defects in shallow gradients. Since guidance defects occur in this shallow gradient region, we hypothesized that having multiple guidance cues may be most important when the fractional change is low; when it is more difficult for a growth cone to obtain an accurate sense of direction from a single gradient.

II.3.ii. *le Massif* microfluidic axon guidance assay

The guidance of commissural neuron axons towards the floor plate in mice occurs between e9.5 and e11.5 (Holley, 1982, Bovolenta and Dodd, 1990). Considering that commissural axons grow at 13-20 µm/h *in vivo* (Bovolenta and Dodd, 1990, Yamauchi et al., 2013) and that the distance from the roof plate to the floor plate is about 500 µm, an individual axon will therefore take ~25-38 h to reach the floor plate. Since neurons vary in when they differentiate and begin their axon outgrowth, we approximate that commissural neurons are exposed to guidance cues en route to the floor plate over 1-2 days.

We thus developed a guidance assay capable of simulating, over 1-2 days, the shallow Shh gradients which we observed in the spinal cord *in vivo*. Microfluidic mixing networks allow gradients to be controlled in space and time allowing for long-term gradients to be established, in contrast to passive source-sink diffusion gradients (e.g. pipette assay and Dunn chamber). We used a linear gradient generator because it allowed us to test a range of fractional change

(δ) values. We modified a pre-mixer microfluidic gradient generator (Jeon et al., 2000) by increasing both the length and width of the gradient region, thus maximizing the surface area on which neurons could be exposed to the gradient and thus the sample size. By increasing the width of the gradient, we also decreased the range of gradient steepness to physiologically relevant levels, as determined *in vivo* (Figure II.1B). Our wider gradient chamber required an increase in the number of sequential mixing channels (Figure II.2A), which offered the added benefit of increasing the overall resistance, thus decreasing the flow velocity and resulting shear stress, which can be harmful to axons (Joanne Wang et al., 2008). With these device improvements, we were thus able to generate stable, long-term gradients.

In our microfluidic device (Figure II.2A), gravity driven flow (Figure II.2B**)** directs fluid into the mixing network (Figure II.2C), resulting in a linear gradient throughout the chamber (Figure II.2C-E). We used fluorescent dextran to measure the concentration and fractional change of the gradient, and found that as predicted, the gradient is linear and maintained throughout the chamber (Figure II.2F,H), and stable over a 24 h period (Figure II.2J-K). Furthermore, the measured fractional change (δ) values match the predicted values, ranging between 0.3 and 2.2 % (Figure II.2G,I). Since the gradient is linear (Figure II.2F,H), the fractional change increases as the concentration decreases across the device (Figure II.2G,I). The device was biocompatible, as dissociated commissural neurons could be cultured in the device and were observed to extend axons (Figure II.2L-M). To test whether the slow flow rate present in the chamber would bias the direction of axon growth, we measured the angle at which the axon emerged from the cell body and the angle at which the tip of the axon was oriented. We found that the presence of fluid flow did not change the random distribution of these angles (Figure II.S3), and therefore the shear stress in our device is negligible and does not bias the direction of axon initiation from the cell body nor the direction of axon growth. Therefore, we have developed an assay, which we named *le Massif*, to challenge commissural neurons with physiologically relevant gradients.

Figure II.2. *le Massif* microfluidic gradient generator can produce shallow linear concentration gradients which are stable through space and time. **(A)** Drawing of the *le Massif* microfluidic device. The blue line represents the upstream limit of the gradient chamber; the red line represents the downstream limit. The device generates linear concentration gradients using a pre-mixing microfluidic paradigm, where a known concentration of cue is added to a reservoir at inlet 1, and culture media without guidance cue is added to inlet 2. **(B)** Schematic cross-section of *le Massif* microfluidic gradient generator. The fluid filled inlet reservoirs drive a flow from left to right, with the fluid accumulating in the hole at the outlet. **(C-E)** The gradient visualized using trimethylrhodamine-conjugated 40 kDa dextran. When the streams from inlets 1 and 2 converge, the concentrations are mixed and divided at 18 discrete steps throughout the premixers **(C)**, generating 20 discrete concentrations which then enter into the gradient chamber **(D)**. The overall gradient shape smoothens rapidly by diffusion to become continuous, while maintaining its overall profile until the downstream region (red line in **E**), where the media flows to the outlet. **(F, G)** Theoretical calculation of the concentration **(F)** and fractional change in concentration, δ, **(G)** of guidance cue in the gradient chamber. The fractional change range ($0.3 \leq \delta < 2.2\%$) encompasses the shallow gradients observed *in vivo*. **(H, I)** Measured fluorescence intensity **(H)** of the upstream (blue line in **D**) and downstream (red line in **E**) limits of the gradient chamber, as well as the fractional change in concentration **(I)** calculated from the upstream concentration profile. Mean ± SEM of 14 independent gradient devices are shown. The measured values match the theoretical predictions (green line in I), with a mean-square-error of 0.091 compared with the theoretical fractional change. **(J, K)** Gradient profile over time for the upstream **(J)** and downstream **(K)** limits. The red boxes in **(K)** represent 450 µm which are excluded due to the gradient flattening which occurs at the boundaries of the device resulting from the no-slip condition. **(L)** Stitched inverted fluorescence image of the downstream area shown in **(E)**, seeded with commissural neurons which were fluorescently stained with rhodamine-conjugated phalloidin. **(M)** Representative higher-magnification inverted fluorescence image of rhodamine-phalloidin-stained commissural neurons in the gradient chamber. After 45 h in culture, most neurons have extended an axon. Scale bar (**C-E,L**): 1 mm. **(M)**: 25 µm.

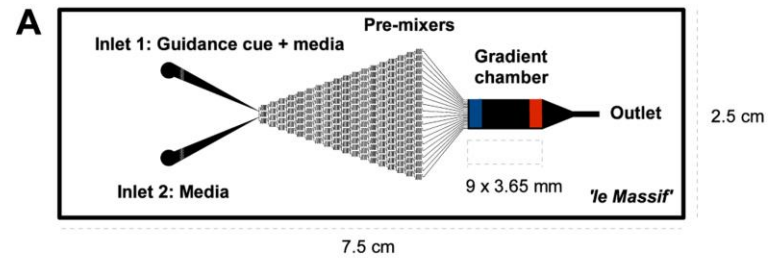
A
Pre-mixers
Inlet 1: Guidance cue + media
Gradient chamber
Outlet
2.5 cm
Inlet 2: Media
9 x 3.65 mm
'le Massif'
7.5 cm

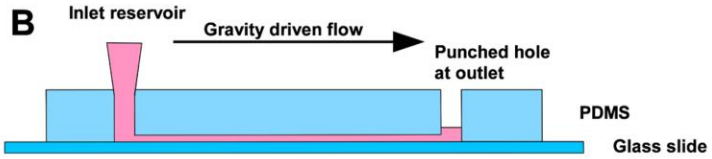
B
Inlet reservoir
Gravity driven flow
Punched hole at outlet
PDMS
Glass slide

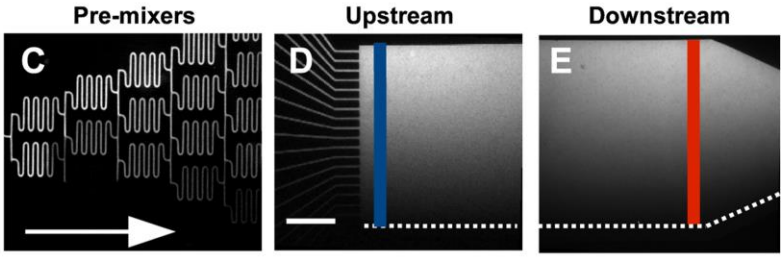
Pre-mixers
Upstream
Downstream
C
D
E

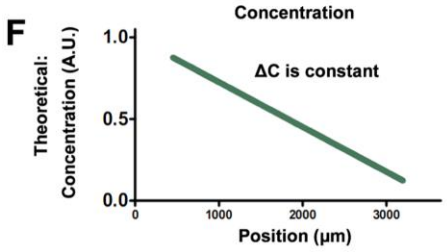
F
Concentration
Theoretical:
Concentration (A.U.)
ΔC is constant
Position (μm)

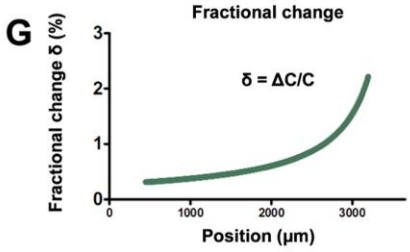
G
Fractional change
Fractional change δ (%)
δ = ΔC/C
Position (μm)

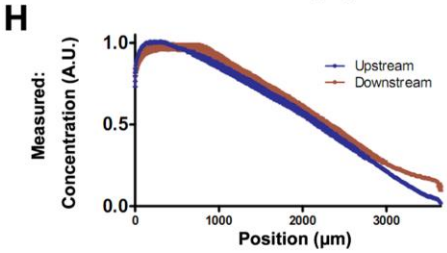
H
Measured:
Concentration (A.U.)
Upstream
Downstream
Position (μm)

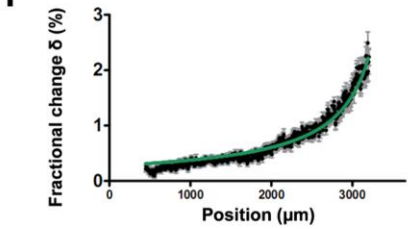
I
Fractional change δ (%)
Position (μm)

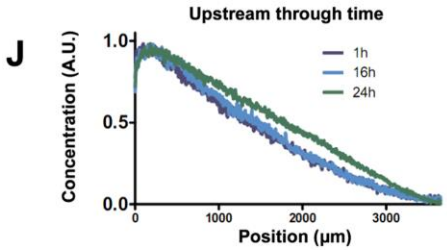
J
Upstream through time
Concentration (A.U.)
1h
16h
24h
Position (μm)

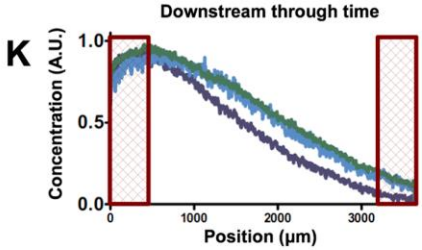
K
Downstream through time
Concentration (A.U.)
Position (μm)

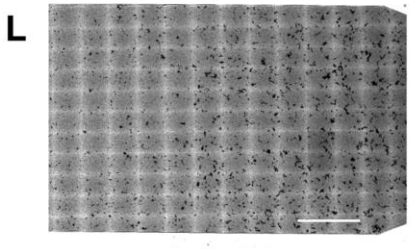
L

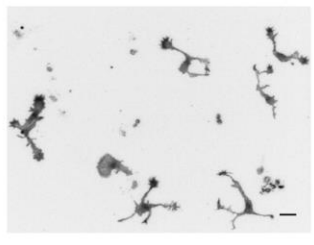
M

II.3.iii. Axons turn up a gradient of Shh or Netrin-1 in *le Massif*

We established gradients of Shh or Netrin-1 after commissural neurons had been cultured for 24 h, when the majority of neurons had already initiated an axon. We calculated the turned angle of an axon as the difference between the base and tip angles (Figure II.3A), and scored the angle as positive if the axon turned towards the gradient, and negative if it turned away. By varying the maximal concentration of ligand in a particular chamber, we could test a wide range of concentrations. In a control gradient (PBS/BSA), we observed a wide range of turned angles towards and away from the gradient, resulting in a net turned angle of 0° (Figure II.3B,E). Neurons exposed to a gradient of Shh (Figure II.3C,E) or Netrin-1 (Figure II.3D,F), however, turned towards the higher concentration of chemoattractant. For either cue, we observed axon turning in response to a wide range of concentrations at the growth cone (Figure II.3E,F). The distribution of turned angles of individual axons confirmed that wide concentrations of Shh and Netrin-1 induced biases towards attraction (Figure II.3G,H). To eliminate the possibility that Shh or Netrin-1 influences the orientation at which the axon exits the cell body (axon base angle), thus confounding our measurement of the angle turned, we performed experiments where gradients were established 4-6 h after the neurons were plated, before the majority of neurons had initiated an axon. We found that Shh and Netrin-1 gradients induced no significant bias in the distribution of axon base angles facing up-gradient (higher concentration) compared to those facing down-gradient (lower concentration) (Figure II.3I-J). Therefore, *le Massif* generates gradients that can induce axon turning without any effect on axonal initiation.

II.3.iv. Axons turn more when the fractional change in concentration is high

Since we observed similar turning over a wide range of concentrations (Figure II.3E-F), we then analyzed axon turning as a function of the fractional change in concentration, δ, across a

Figure II.3 Axons turn up gradients of Shh and Netrin-1 in *le Massif*. **(A)** The turned angle is defined as the angle between the line representing the proximal 20 μm of the axon at the cell body (axon base, turquoise) and the line representing the distal 20 μm of the axon at the growth cone (axon tip, red). The sign of the turned angle is positive if the turn is in the direction of the higher concentration of chemoattractant, and the sign of the turned angle is negative if the turn is in the direction of the lower concentration. **(B-D)** Images of commissural neurons grown for 1 day in culture followed by the application of **(B)** control vehicle gradient (BSA), **(C)** Shh gradient or **(D)** Netrin-1 gradient for 24 h. Wedge represents the gradient orientation. The average turned angles of axons as a function of the absolute concentration of **(E)** Shh and **(F)** Netrin-1 at the growth cone. Axons turn to a similar extent over a wide range of concentrations. The number of axons in each group is indicated in parentheses. **(G, H)** Circular distribution of individual turned angles. The angular deviation from vertical represents the magnitude of the turned angle, such that points to the right of the center are attracted (green) and those to the left are repelled (red). Neurons which turned between -5º and 5º are considered to be neutral (yellow). The distance of each point from the center represents the axon length. A random sample of 60 axons for Shh and Netrin-1 are plotted. A small shift in distribution towards attraction is seen across a wide range of concentrations for either cue. **(I, J)** To exclude the possibility that the gradients influence the angle at which the axon protrudes from the cell body, a gradient was applied 6 h following plating the neurons, before most neurons had initiated an axon. Axon base angle frequency distributions for axons grown in **(I)** Shh and **(J)** Netrin-1 were measured. Green bars represent the number of axons with a base angle facing up-gradient, and red bars indicate axons with angles facing down gradient. There is no significant bias in angle distribution for either cue (Rayleigh test for uniformity, Shh: n = 2028; Netrin: n = 2805). Scale bars (**B-D**): 10 μm. (**G-H**): 25 μm. Error bars represent SEM. cb, cell body; gc, growth cone. See also Figure II.S3.

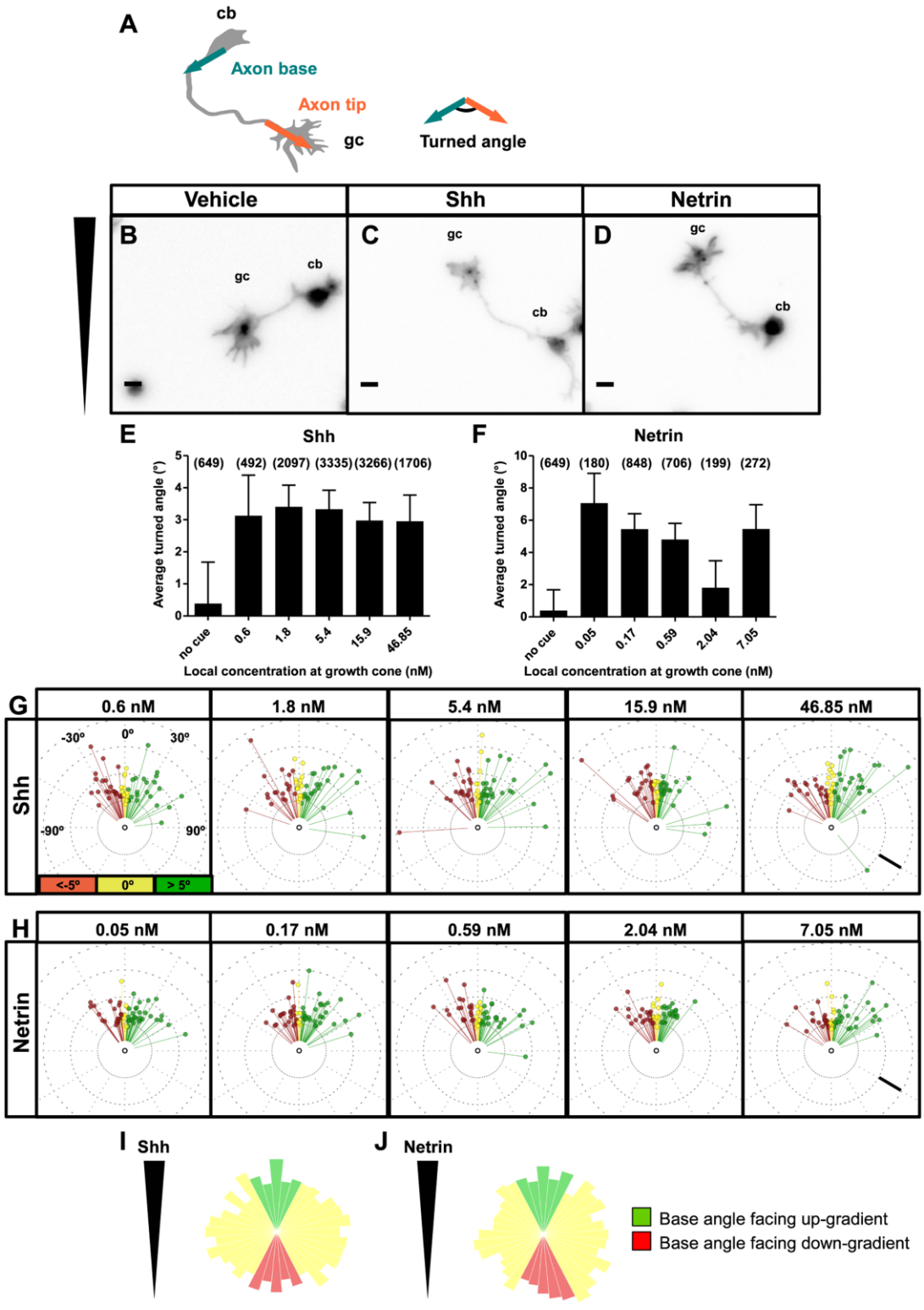
A
cb
Axon base
Axon tip
gc
Turned angle
Vehicle
Shh
Netrin
B
C
D
gc
cb
E
Shh
F
Netrin
(649) (492) (2097) (3335) (3266) (1706)
(649) (180) (848) (706) (199) (272)
Average turned angle (°)
no cue
0.6
1.8
5.4
15.9
46.85
0.05
0.17
0.59
2.04
7.05
Local concentration at growth cone (nM)
G
H
0.6 nM
1.8 nM
5.4 nM
15.9 nM
46.85 nM
0.05 nM
0.17 nM
0.59 nM
2.04 nM
7.05 nM
-30°
0°
30°
-90°
90°
<-5°
0°
> 5°
I
Shh
J
Netrin
Base angle facing up-gradient
Base angle facing down-gradient

growth cone. The fractional change is a function of the chamber geometry, and not of the maximum concentration used (Figure II.4A). Therefore, the fractional change is independent of the maximum concentration in the gradient chamber, so long as the minimum concentration is 0. We found that axon turning increased as a function of fractional change for both gradients of Shh and Netrin-1 (Figure II.4B-C). This corresponded with an increase in the ratio of axons which turned towards the gradient compared with those turning away (Figure II.4D-E). Thus, there seems to be fewer guidance errors as the fractional change across the growth cone increases. This was also illustrated with the distribution of turned angles of individual axons (Figure II.4F). At low fractional change, the population of axons have variable turned angles, with a slight bias toward attraction. As the fractional change increased, a bias towards attraction became more pronounced, as there were fewer axons which were erroneously repelled. We then compared the turned angles of axons experiencing the same fractional change ($\delta>1\%$) with different concentrations at the growth cone. When $\delta>1\%$, we observed no trend toward increased turning as the concentration at the growth cone increased (Figure II.4G-H). Therefore for commissural neurons in gradients of Shh or Netrin-1, the turning response is more sensitive to changes in the fractional change than the local concentration at the growth cone.

II.3.v. Axons turn more robustly in combined gradients of Shh and Netrin-1

Since guidance errors occur in the region of the spinal cord where Shh and Netrin-1 gradients are shallow, and not steep (Figure II.1), we hypothesized that multiple guidance cues might be most important for guiding axons in shallow gradients. Therefore, we next tested whether combining gradients of two guidance cues might modulate the axon turning response in relation to fractional change. We performed guidance assays with 20 nM Shh and 0.69 nM Netrin-1 in the inlet, generating local concentrations ranging from 2.5 to 18.55 nM for Shh and 0.08 to 0.65 nM for Netrin-1, encompassing the range for which we see axon turning (Figure II.3E-H, Figure II.4G-H). Gradients of Shh or Netrin-1 alone and in combination were established 6 h after neurons were plated and maintained for 45 h. In either Shh or Netrin-1 gradients, the

Figure II.4. Commissural axon turning depends more on the gradient fractional change than the concentration. **(A)** Schematic of the concentration gradient within the microfluidic chamber. Because the concentration gradient is linear, the fractional change, δ, is highest when the concentration is low. Regardless of the maximum concentration used, the fractional change at a given position in the chamber is the same. **(B-E)** Both **(B)** Shh and **(C)** Netrin-1 gradients induce more turning as the fractional change increases. The average turned angle is plotted as a function of a moving window of 0.5% fractional change. Error bands represent mean and error of all neurons within the window at each position. The slope of the linear regression was 4.5 ± 2.0 degrees/% for Shh and 6.5 ± 2.4 degrees/% for Netrin-1. This increased turning response corresponds to an increase in the ratio of axons which turned in the correct direction in **(D)** Shh and **(E)** Netrin-1 gradients. (Shh: $43 < n \leq 1302$; Netrin: $17 < n \leq 569$ from ≥ 4 independent microfluidic devices). **(F)** Circular distribution of individual turned angles. A random sample of 60 axons for Shh and 20 axons for Netrin-1 are plotted. For either cue, as the fractional change increases, turning is more robust, with a clear bias in the distribution of turned angles towards attraction and a decrease in the proportion of guidance errors. **(G, H)** For fractional change $\delta > 1\%$, there is no improvement in turning with increasing absolute local concentration of **(G)** Shh or **(H)** Netrin-1 at the growth cone. The number of axons in each group is indicated in parentheses. One-way ANOVA with Newman Keuls' multiple comparison test indicated no significant differences between the groups. Scale bar **(F)**: 25 μm. Error bars represent SEM.

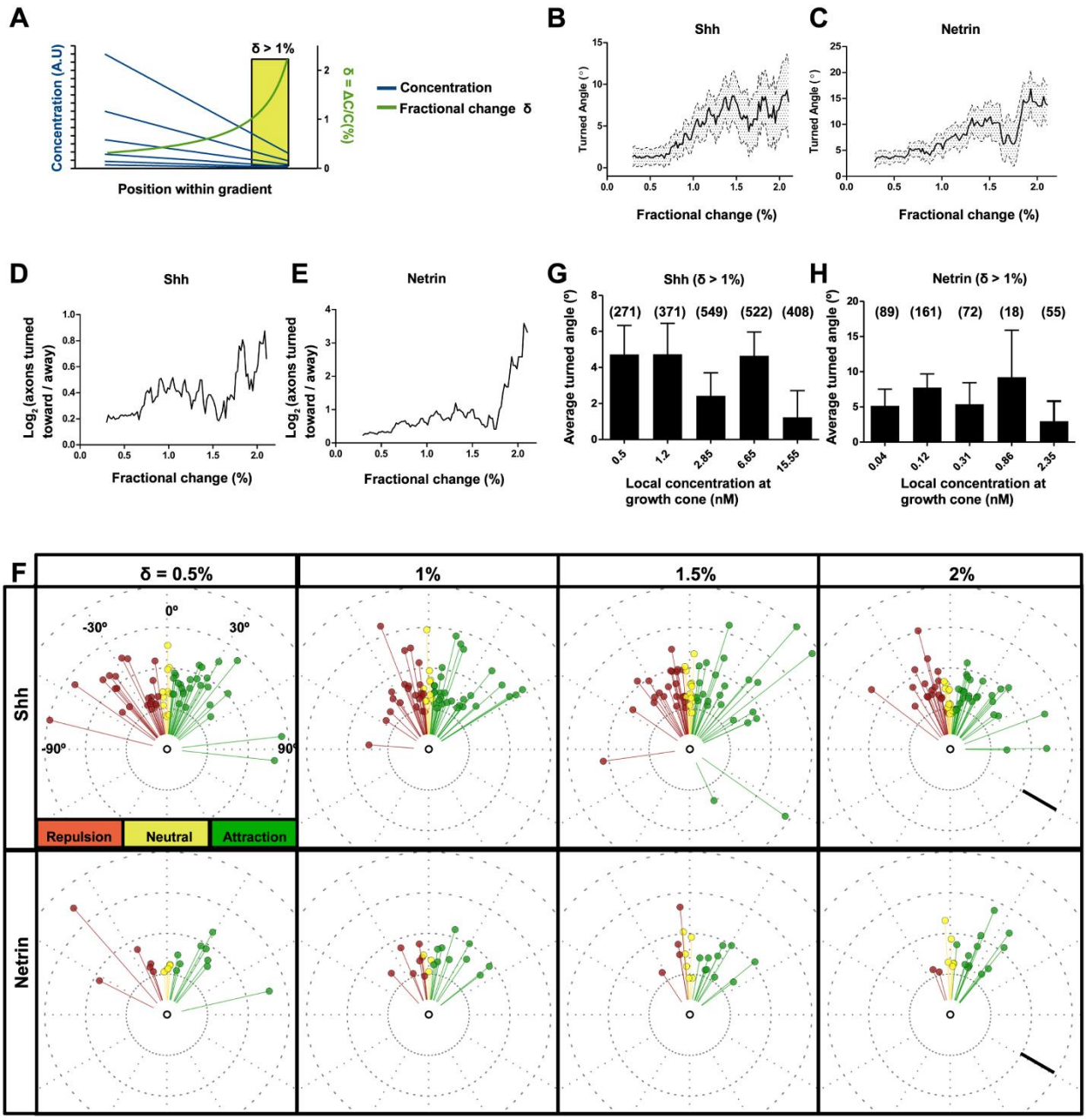
A
δ > 1%
Concentration (A.U)
δ = ΔC/C(%)
Concentration
Fractional change δ
Position within gradient
B
Shh
Turned Angle (°)
Fractional change (%)
C
Netrin
Turned Angle (°)
Fractional change (%)
D
Shh
Log2 (axons turned toward / away)
Fractional change (%)
E
Netrin
Log2 (axons turned toward / away)
Fractional change (%)
G
Shh (δ > 1%)
(271) (371) (549) (522) (408)
Average turned angle (°)
0.5 1.2 2.85 6.65 15.55
Local concentration at growth cone (nM)
H
Netrin (δ > 1%)
(89) (161) (72) (18) (55)
Average turned angle (°)
0.04 0.12 0.31 0.86 2.35
Local concentration at growth cone (nM)
F
δ = 0.5%
1%
1.5%
2%
Shh
Netrin
0°
-30°
30°
-90°
90°
Repulsion
Neutral
Attraction

turned angle peaked at the highest fractional change, $\delta = 2.2\%$ (Figure II.5A). Upon applying both Shh and Netrin-1 simultaneously, the average turned angle increased more quickly as a function of fractional change, such that axons were turning robustly in a region of the double gradient where a single cue was not eliciting much turning , ($1.4 < \delta < 1.8\%$). Interestingly, at the maximal zone of fractional change ($1.8 < \delta < 2\%$), there was no observable difference in the angle turned induced by the individual or combined cues (Figure II.5A).

To assess the relationship between the combined cues compared to the individual cues, we calculated the synergy quotient as the turned angle in the combined gradient divided by the sum of the turned angles to both cues individually (described in the Materials and Methods section). With this measurement, a value below 1 indicates sub-additive effects, 1 is defined as additive, while a value above 1 is synergistic. We observed additive and sub-additive effects for the majority of the fractional change range, apart from fractional change range of $1.44 < \delta < 1.82\%$ where the effect of the combined cues is much greater than the sum of the individual cues, demonstrating synergy (Figure II.5B). Hence the synergistic effect of the combined gradient is greatest when the fractional change is below the maximum.

At this fractional change ($1.44 < \delta < 1.82\%$) where the combined gradients lead to synergy, axons responded much more robustly to the combined cues than for either cue individually, resulting in a higher average turned angle (Figure II.5C). This effect was remarkably consistent, with every independent gradient chamber with combined cues having strong positive turning in this range of fractional change, whereas the gradient chambers with the single cues had variable turned angles with no consistent bias (Figure II.5D). The synergy occurring when the two cues are present was also demonstrated by the larger proportion of axons which turn up the combined gradient than for either cue individually (Figure II.5E). The influence of combining cues on the proportion of correct versus incorrect guidance decisions was also apparent when we observed the distribution of the turned angles in the different conditions (Figure II.5F). For the control gradient (vehicle) and gradients of Shh and Netrin-1 there was no bias towards either attraction or repulsion. Remarkably, when both cues were presented as a combined

Figure II.5. A combined gradient of Shh and Netrin-1 enhances axon guidance when the fractional change is sub-optimal for guidance towards a single cue. **(A)** Average turned angle as a function of fractional change when axons are exposed to gradients for 45 h. Axons exposed to gradients of Shh (green) or Netrin-1 (blue) have a maximum response when the fractional change is at its highest, $\delta = 2.2\%$. A combined gradient of Shh and Netrin-1 (red) induce turning to a similar magnitude as either cue individually at $\delta = 2.2\%$, but induce turning that is higher than for either cue individually when the fractional change is below its maximum ($1.4 < \delta < 1.8\%$). Mean and error of the average turned angle within a window of 0.5% are shown (Shh: $31 < n \leq 1004$; Netrin: $38 < n \leq 1107$; Shh+Netrin: $40 < n \leq 1164$). **(B)** We defined the synergy quotient as the ratio of the turning towards the combined gradient to the sum of the turning to either cue individually (calculated using the means from A). For the majority of the combined gradient, the combined influence is sub-additive. However, the combined cues act synergistically when the fractional change is ($1.44 < \delta < 1.82\%$), just below its maximum value. **(C)** At this fractional change ($1.44 < \delta < 1.82\%$), axons responded much more robustly than for either cue individually, resulting in a higher average turned angle. **(D)** The synergy observed when $1.44 < \delta < 1.82\%$ is consistent between independent experiments (Shh: n=5; Netrin: n=9; Shh+Netrin: n=5; p=0.043 1-way ANOVA with Newman-Keuls Multiple Comparison Test) **(E)** The increase in turned angle results from a larger ratio of axons turning toward than away from the gradient in the combined gradient (Shh: n=55; Netrin: n=92; Shh+Netrin: n=73). **(F)** Angular distribution of the turned angles of a random sample of 60 neurons for $1.44 < \delta < 1.82\%$. No bias in distribution is observed in the control gradient, nor in gradients of Shh or Netrin-1 alone. However, when axons are exposed to the combined gradient, there is a clear bias in the distribution of turned angles towards attraction. Therefore, in the presence of shallow combined gradients, there are fewer guidance errors occurring than for either cue individually.

Scale bar **(F)**: 25 μm.

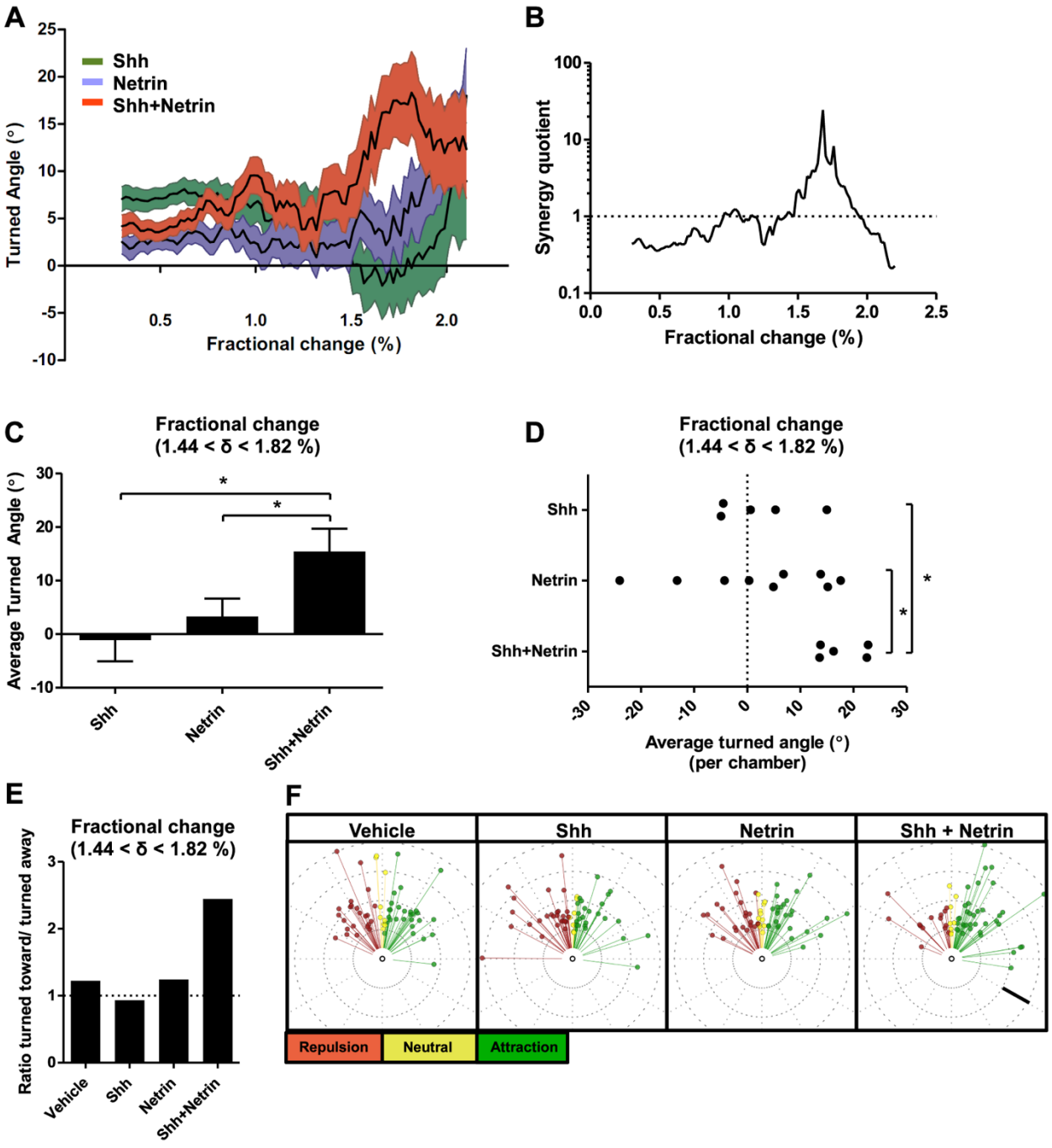
A
Shh
Netrin
Shh+Netrin
Turned Angle (°)
Fractional change (%)
B
Synergy quotient
Fractional change (%)
C
Fractional change
(1.44 < δ < 1.82 %)
Average Turned Angle (°)
Shh
Netrin
Shh+Netrin
D
Fractional change
(1.44 < δ < 1.82 %)
Shh
Netrin
Shh+Netrin
Average turned angle (°)
(per chamber)
E
Fractional change
(1.44 < δ < 1.82 %)
Ratio turned toward/ turned away
Vehicle
Shh
Netrin
Shh+Netrin
F
Vehicle
Shh
Netrin
Shh + Netrin
Repulsion
Neutral
Attraction

gradient, there was a clear bias towards attraction, wherein very few axons failed to reorient their direction. Together, these results indicate that a combination of guidance cues can act in synergy to guide axons where the gradient steepness is sub-optimal for the growth cone to sense the direction of a single cue gradient.

II.3.vi. Combined gradients of Shh and Netrin-1 induce polarized Src-family kinase activation in the growth cone

Since SFKs act downstream of Shh (Yam et al., 2009) and Netrin-1 (Liu et al., 2004) to guide commissural axons, it has been proposed in a recent review by Dudanova and Klein (Dudanova and Klein, 2013) that Shh and Netrin-1 signaling may converge on SFKs. Furthermore, the active form of SFKs, phosphorylated at Y418 (pSFK), accumulates on the side of the growth cone proximal to the higher concentration of Shh and is sufficient to relay the direction of the gradient (Yam et al., 2009). Using *le Massif*, we challenged commissural growth cones with gradients of either Shh, Netrin-1, or a combination of both for 2 h, and then assessed the distribution of growth cone pSFK along the direction of the gradient (Figure II.6A). Growth cone pSFK distribution was measured by the fractional change in signal intensity across the width of a growth cone (δ_{GC}), which represents the difference in the amount of pSFK at the proximal versus the distal side of the growth cone, relative to the overall levels. Growth cones with more pSFK on the proximal side closer to the higher guidance cue concentration had positive δ_{GC} values and growth cones with more pSFK on the distal side closer to the lower guidance cue concentration had negative δ_{GC} values. For axons exposed to a fractional change of $1.44 < \delta < 1.82\%$ in single cue gradients of Shh (Figure II.6B) or Netrin-1 (Figure II.6C), there was no consistent bias in the direction of pSFK distribution (mean and median δ_{GC} ~0%, Figure II.6E-F). In the combined gradient however, more growth cones had a proximally biased pSFK distribution (Figure II.6D-F).

Figure II.6. Combined shallow gradients of Shh and Netrin-1 synergize to polarize activated Src family kinase within the growth cone. **(A)** pSFK asymmetry across each growth cone was measured as the fractional change in pSFK fluorescence (δ_{GC}). This was defined as the difference between mean intensities in the proximal third (green rectangle) and the distal third (red rectangle) of the mean intensity profile spanning the width of the growth cone, divided by the mean intensity of the entire growth cone area. Growth cones exposed to shallow $1.44 < \delta < 1.82\%$ gradients of **(B)** Shh alone or **(C)** Netrin-1 alone do not show a directional bias in pSFK distribution after 2 h. However **(D)** in the combined gradient, pSFK is asymmetrically localized to the proximal side of the growth cone (in this example, there is an 18% pSFK fractional change, similar to the mean fractional change that we observe in (**E**)). This results in a higher **(E)** mean and **(F)** median fractional change in pSFK across the growth cones. Polarized pSFK growth cone asymmetry was assessed by using a Wilcoxon signed-rank test against a hypothetical median of 0 (Shh: n=99; Netrin: n=107; Shh+Netrin: n=126; $p = 0.018$ for Shh+Netrin). **(G)** The ratio of the number of growth cones with proximal versus distal pSFK asymmetry for each independent gradient device for ($1.44 < \delta < 1.82\%$) demonstrates that while the devices with single cue gradients of Shh and Netrin-1 alone have no bias for a proximal versus a distal distribution, those with combined gradients have consistently equal or more growth cones that are proximally than distally polarized ($p = 0.025$, Chi-square analysis).

Wedge represents direction of gradient (**A-D,G**). Scale bar (**B-D)**: 10 µm. Error bars represent SEM.

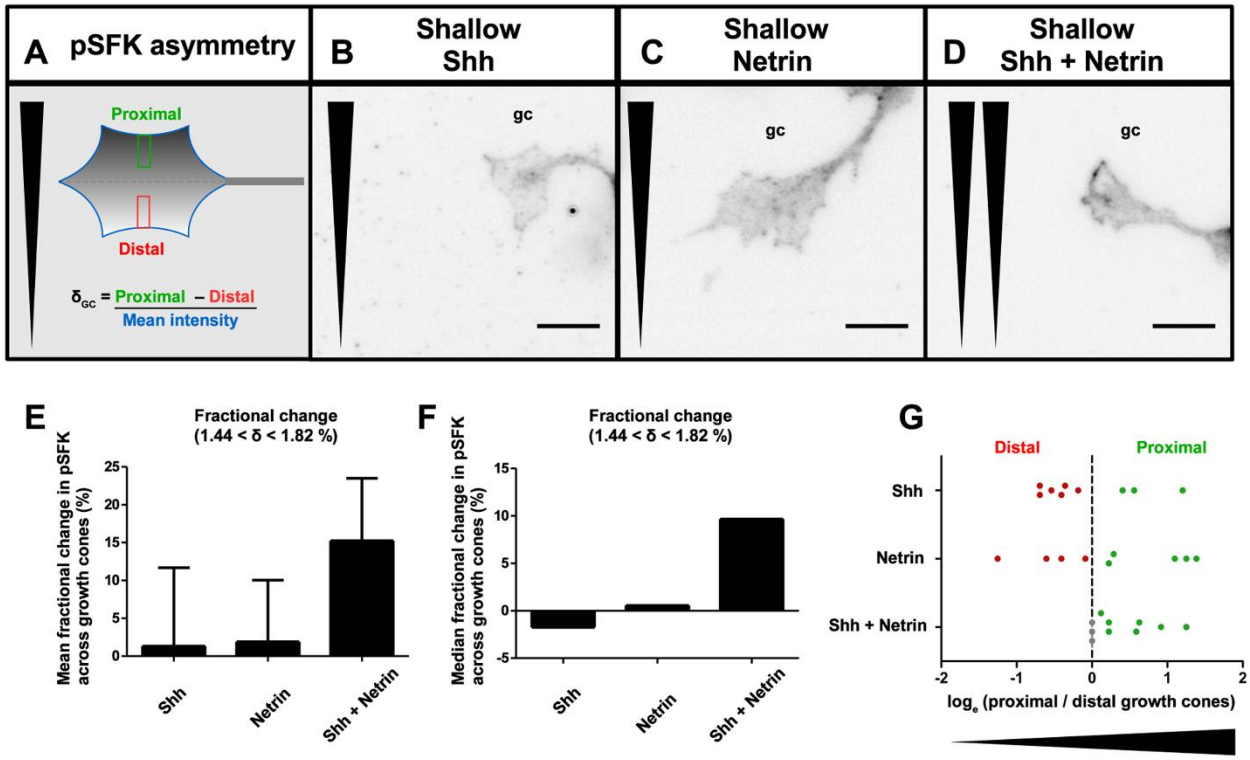
A pSFK asymmetry
Proximal
Distal
δGC = Proximal – Distal / Mean intensity
B Shallow Shh
C Shallow Netrin
D Shallow Shh + Netrin
gc
E
Fractional change (1.44 < δ < 1.82 %)
Mean fractional change in pSFK across growth cones (%)
25
20
15
10
5
0
Shh
Netrin
Shh + Netrin
F
Fractional change (1.44 < δ < 1.82 %)
Median fractional change in pSFK across growth cones (%)
15
10
5
0
-5
Shh
Netrin
Shh + Netrin
G
Distal
Proximal
Shh
Netrin
Shh + Netrin
-2
-1
0
1
2
log e (proximal / distal growth cones)

This shift towards proximally distributed pSFK was also apparent when we calculated the ratio of the number of proximal to distally polarized growth cones in each independent gradient chamber, for $1.44 < \delta < 1.82\%$. Independent chambers with single cue gradients of Shh or Netrin-1 vary between having a net proximal or distal pSFK growth cone distribution. In contrast, for the combined Shh and Netrin-1 gradient, there are consistently more chambers with a net proximal pSFK growth cone distribution and not a single chamber where there is a net distal pSFK growth cone distribution (Figure II.6G). Therefore, single cue gradients of Shh and Netrin-1 that do not elicit axon turning (Figure II.5), also do not elicit a polarized pSFK distribution (Figure II.6). Remarkably, when the Shh and Netrin-1 gradients synergize to elicit turning, this also corresponds to a higher pSFK distribution on the side of the growth cone facing the high concentration of guidance cues. Taken together with our quantification of gradients and guidance defects *in vivo*, these results indicate that a combination of guidance cues can act in synergy to polarize growth cones in regions where the gradient steepness is sub-optimal for the growth cone to be polarized by a single cue gradient.

II.4. Discussion

II.4.i. Summary

In this study, we developed a microfluidic gradient generator that enabled us to directly measure long-term axon turning responses with a physiological gradient steepness. We demonstrate that commissural axons turn more when the fractional change is high for both Shh and Netrin-1. Additionally, we show that when the steepness of the gradient is limiting, a combined gradient of Shh and Netrin-1 induces axon turning at a gradient steepness where either cue alone cannot (Figure II.7A). Furthermore, at this same gradient steepness, we observe polarized growth cone activation of SFK only when Shh and Netrin-1 are presented in combined gradients (Figure II.7A). Therefore we propose that collaboration between Shh and Netrin-1 results in synergy specifically in circumstances where both gradients are shallow. In this steepness-limited synergy, multiple overlapping signals are necessary for the growth cone to properly interpret the orientation of the gradient when the gradient is shallow. In the

Figure II.7. Shh and Netrin-1 synergize to guide commissural axons when their gradients are shallow. **(A)** In shallow individual cue gradients, commissural axon turning is random (*left* and *middle*). In the presence of combined Shh and Netrin-1 shallow gradients (*right*), axons turn toward the higher concentration of guidance cue. When either gradient alone is insufficient to promote axon turning, pSFK activation is also not polarized up the gradient. However, the combined Shh and Netrin-1 gradient biases pSFK distribution to the side of the growth cone facing up the gradient. **(B)** In the developing spinal cord, the gradients of Shh and Netrin-1 proximal to the floor plate are steep (high fractional change), whereas further from the floor plate, the gradients of Shh and Netrin-1 are shallow (low fractional change). **(C)** When either the Shh or Netrin-1 signaling pathway is disabled, guidance errors occur at approximately the midpoint of the spinal cord, where the gradients are shallow. Our results suggest that in this shallow gradient region, integrating multiple guidance cues is necessary for correct growth cone guidance.

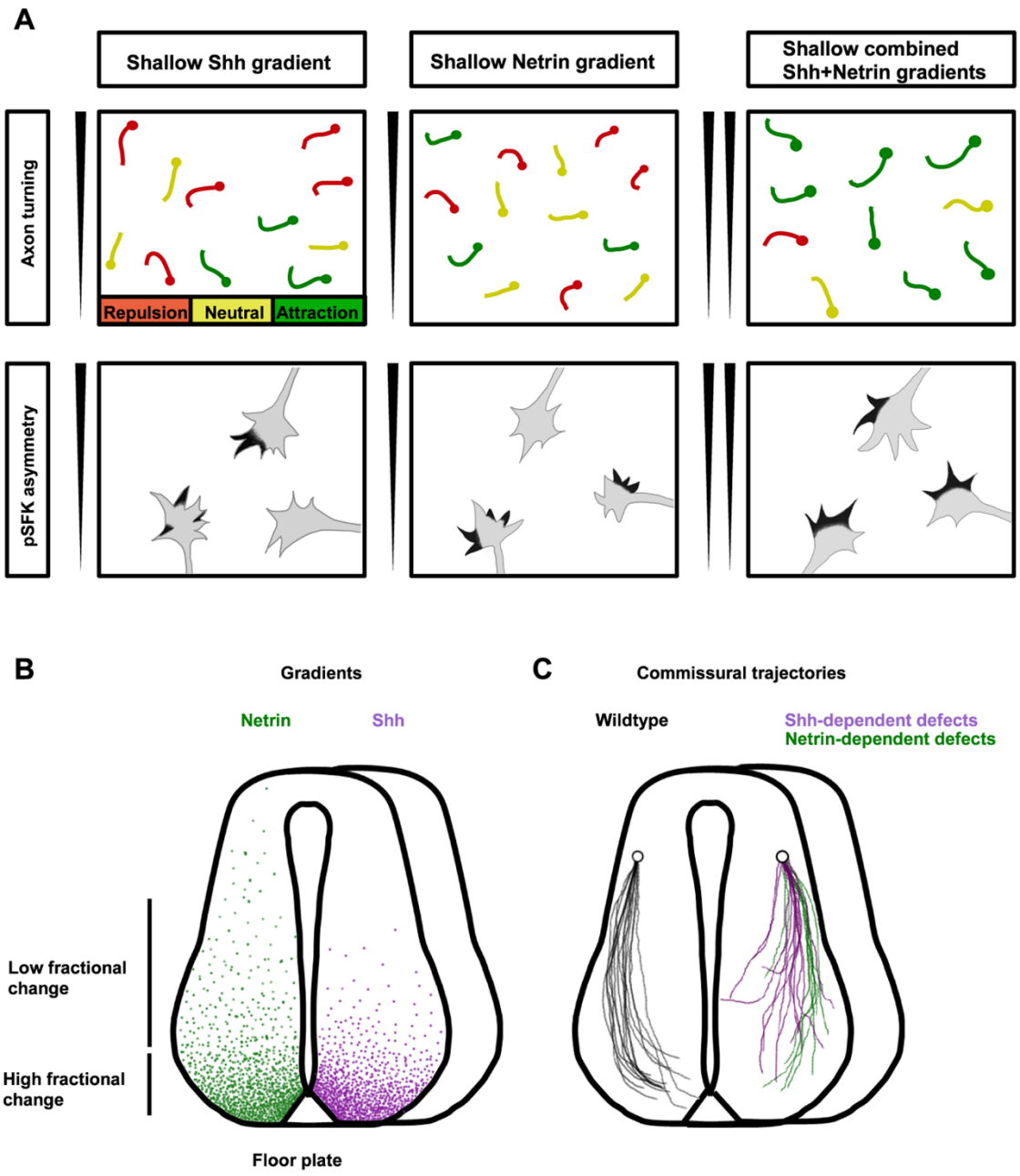
A
Shallow Shh gradient
Shallow Netrin gradient
Shallow combined Shh+Netrin gradients
Axon turning
Repulsion
Neutral
Attraction
pSFK asymmetry
B
Gradients
Netrin
Shh
Low fractional change
High fractional change
Floor plate
C
Commissural trajectories
Wildtype
Shh-dependent defects
Netrin-dependent defects

developing spinal cord, we propose that this corresponds to a region midway along the commissural axon trajectory (Figure II.7B). Notably, the analysis of the phenotype of 4 different mouse models (*Netrin-1, DCC, Boc,* and *Smo* conditional mutants) shows that when one of these pathways is impaired, guidance errors occur in this shallow gradient region (Figure II.7C). Therefore, our data support a model where guidance cue collaboration is essential to guide axons when the gradient steepness is sub-optimal for them to be guided by a single cue.

II.4.ii *le Massif* microfluidic gradient device generates temporally and spatially stable physiologically relevant gradients

An essential component of the current study is the use of microfluidic mixing networks to generate spatially and temporally stable concentration gradients. *Le Massif* guidance assay allows us to assess axon turning over the course of days. Since an image only has to be taken at the final time point, it is compatible with high-content screening microscopes, allowing assays to be performed in a high-throughput manner, such that a large number of axons can be imaged and analyzed (over 200 per chamber).

An additional advantage of *le Massif* over other axon guidance assays is that it generates gradients with low-to-moderate fractional change ($0.3 < \delta < 2.2\%$) which sits near the lowest fractional change eliciting detectable guidance responses (Figure II.4B-C). This is critical for studying the influence of fractional change on axon turning. This contrasts with techniques such as the pipette assay, which generates gradients with a steep fractional change ($5 < \delta < 35\%$) (Pujic et al., 2008). While printed gradient assays allow precise control over the gradient parameters (Baier and Bonhoeffer, 1992, Rosoff et al., 2004, von Philipsborn et al., 2006, Mai et al., 2009), the gradient is printed prior to the addition of the neurons, making it difficult to distinguish the effect of the gradient on direct axon turning, rather than differential axon outgrowth or growth rate modulation (A notable exception to this is Mortimer et al. 2009, which tested the effect of printing the guidance cue before and after addition of explants). Furthermore in these assays, axons are either growing along pre-defined corridors or are

growing from an explant, making individual axon trajectories often difficult to identify. In contrast, individual axon trajectories can be easily visualized in *le Massif* because the dissociated neurons are grown at low density, so we can clearly measure directed turning of individual axons. Also, by imposing the gradient after axon outgrowth has commenced, we avoid the gradient influencing the orientation of axon protrusion from the cell body (Mai et al., 2009). Thus, owing to the versatile process of microfluidic design, we were able to create a customized gradient generator and generate gradients with physiologically relevant steepness that are stable over days.

II.4.iii. Gradient steepness is a critical determinant of axon turning responses to guidance cues.

In addition to axon turning, axon growth (Baier and Bonhoeffer, 1992) and growth rate modulation (Rosoff et al., 2004, Mortimer et al., 2010) are also processes important in guiding axons to their correct targets. Compared to direct axon turning, growth rate modulation occurs when axons growing up-gradient grow faster than those growing down-gradient (Mortimer et al., 2010). Previous studies have found that gradient steepness affects axon growth (Baier and Bonhoeffer, 1992) and growth rate modulation (Rosoff et al., 2004, Mortimer et al., 2010). We found that gradient steepness also influences axon turning, with robust turning observed for steepness δ~1-2%. This contrasts with what has been reported for growth rate modulation by NGF gradients, where steepness as low as 0.1% is sufficient to bias DRG axon trajectories (Rosoff et al., 2004, Mortimer et al., 2010). Consistent with our results, these 0.1% NGF gradients had no effect on direct axon turning (Mortimer et al., 2010). Similarly, growth of axons is also modulated by gradients with steepness of ≥0.4% (1% over 25 μm), possibly also by influencing the growth rate (Baier and Bonhoeffer, 1992). Therefore, our results suggest that steeper gradients of 1-2% are required to induce direct axon turning than growth rate modulation, as hypothesized by Mortimer and colleagues (Mortimer et al., 2010).

The gradient steepness at which robust turning occurs is ~1-2%, within a similar range to our estimate of Shh gradient steepness in the spinal cord (Figure II.1B). For Netrin-1, the lack of effective antibodies for Netrin-1 for use in immunofluorescent staining hampers our ability to directly measure the Netrin-1 gradient steepness in the spinal cord. Previously published images of Netrin-1 in the spinal cord are not amenable to precise quantification because they use alkaline phosphatase immunohistochemistry combined with darkfield imaging (Kennedy et al., 2006). However, examination of the pattern of Netrin-1 staining in the spinal cord (Kennedy et al., 2006) does show that the Netrin-1 gradient is steeper closer to the floor plate and shallower further away from the floor plate, consistent with what we observe with Shh and consistent with our hypothesis that Netrin-1-dependent guidance errors occur in shallow, not steep, regions of the gradient.

II.4.iv. Additive and synergistic cooperation between guidance cues

While significant evidence indicates that multiple guidance cues act on the same axons, precisely how these cues converge to regulate the behavior of the growth cone is poorly understood. The response to two combined cues may be additive or synergistic, depending on whether the output is equal to or above the combined response of either cue individually. Dudanova and Klein (Dudanova and Klein, 2013) define additivity as resulting from cues that act in parallel pathways, and synergy as resulting from cues that have crosstalk between pathways.

Additive effects of guidance cues have been observed with ephrin-A and GDNF on lateral motor column (LMC_L) axons (Dudanova et al., 2010), whereas a synergistic attractive response was seen between EphA and GDNF for the same axons (Bonanomi et al., 2012). The former demonstrates that ephrin-A and GDNF act in parallel pathways, while the latter demonstrates crosstalk between EphA and GDNF. EphA and GDNF signal through their respective GPI-anchored receptors ephrin-A and GFRα1 respectively, and they crosstalk by sharing a common co-receptor, Ret. The co-activation of ephrin-A and GFRα1 through sharing Ret acts as a coincidence detector and generates synergy (Bonanomi et al., 2012). The interaction between

EphA and GDNF is an example of concentration-limited synergy, as the combination of low concentrations of guidance cues induced turning when neither cue alone was sufficient.

One of our major findings is that synergy occurs between Netrin-1 and Shh to guide commissural axons. In contrast to Bonanomi and colleagues (Bonanomi et al., 2012), we find that this synergy is steepness-limited rather than concentration-limited. Steepness-limited synergy occurs when the gradient of individual cues is too shallow to guide axons, but a combined gradient of two cues elicits axon turning. We know that in our case the concentration of the individual cues are not limiting because we observe axon turning when the fractional change is high, despite this corresponding to a lower absolute concentration (Figure II.4A). Furthermore, the range of concentrations used in our experiments all elicit axon turning, when the steepness is not limiting (Figure II.4G-H). Thus, we demonstrate for the first time that synergy can also be steepness-limited, when the amount of ligand is not limiting, but instead the steepness of the gradient is insufficient for the growth cone to estimate the direction of a single cue gradient.

We also identify SFKs as a downstream signaling molecule that integrates Shh and Netrin-1 signaling when the two cues synergize. Both Shh and Netrin-1 can activate SFKs, and SFKs are required for Shh and Netrin-1-mediated axon guidance (Liu et al., 2004, Yam et al., 2009). Furthermore, pSFK polarization at the growth cone reflects the direction of the external gradient (Yam et al., 2009). Gradients of Shh and Netrin-1 too shallow to guide axons were also insufficient to correctly polarize pSFKs at the growth cone. Only in the presence of Shh and Netrin-1 together was the direction of the gradient correctly reflected by the growth cone pSFK polarization. Hence activated SFKs appear to be a node where information from the Shh and Netrin-1 gradients are integrated. In addition to synergy resulting from sharing a common co-receptor as for EphA and GDNF, we find that for Shh and Netrin-1 synergy can arise from shared intracellular signaling molecules. Therefore, diverse mechanisms exist at which synergy between two guidance cues can occur and more mechanisms likely remain to be discovered.

In the developing nervous system, it is likely that many types of synergistic interactions play a role in the correct guidance of axons to their targets. In the developing limb, where guidance cues act at a choice point for motor axons, concentration-limited synergy may be more important than steepness, because the gradient is very abrupt. For commissural axons, which climb a shallow gradient of guidance cues over a long distance, steepness-limited synergy may initially be more critical. Later in their journey, when they reach the steep part of the gradient, it appears that one cue alone may be sufficient to guide axons – for example, the axons in *Boc* mutant mice that cannot respond to Shh but by chance make it close to the floorplate do eventually reach the floorplate (Okada et al., 2006), possibly due to the effect of the steep Netrin-1 gradient in the ventral spinal cord. Thus it appears that single steep gradients can guide axons over short distances, and allow for more precise guidance near the floorplate whereas midway along the commissural axon trajectory, synergy between shallow gradients of Shh and Netrin-1 allows these gradients to guide axons that are far from the floor plate, thus extending the distance that guidance cues can act in the spinal cord.

II.5. Materials and Methods

II.5.i. Immunostaining

All animal work was performed in accordance with the Canadian Council on Animal Care Guidelines. Wildtype C57Bl6 or *Shh*$^{-/-}$ mouse embryos were sacrificed at e9.5 or e10.5 and fixed in 4% paraformaldehyde (PFA) in phosphate buffered saline for 1-1.5 h at 4ºC and cryoprotected in 30% sucrose. 12-20 µm thick serial sections were cut with a cryostat. Sections were rinsed several times in buffered saline, and then treated for 1 h with a blocking solution containing 0.1% Triton X-100 and 10% heat-inactivated goat serum (HiGS). Spinal cord sections were stained with anti-Shh antibody (kindly provided by S. Scales, Genentech) to detect Shh protein (Tian et al., 2009). This antibody is specific as no signal is detected in *Shh* mutant embryos (Figure II.S1A). The primary antibody was then replaced with a buffered solution containing 1% HiGS and Alexa Fluor 546-coupled secondary antibody (Molecular Probes; 1:1000) or Cy3 conjugated secondary antibody (Jackson Immunoresearch, 1:1000) for 1 h. After staining, slides were mounted with Mowiol (Sigma) and allowed to dry for at least 24 h before imaging. Dot blot immunochemistry was performed by pipetting serial dilutions of recombinant human NShh C24II (R&D) onto a glass microscopy slide, followed by the same procedure and reagent concentrations as above.

For pSFK asymmetry assays, guidance cues were added, then the microfluidic devices were returned to the incubator for 2 h, after which they were fixed with 4% PFA at room temperature for 15 min. Phosphorylated Src-family kinase was detected using a phosphospecific (pY418) primary antibody (Invitrogen, 1:1000), followed by Alexa Fluor 488-coupled secondary antibody (Molecular Probes; 1:1000). Chambers were imaged with an IXM high-content screening microscope (Molecular Devices) using a 40X Nikon objective.

II.5.ii. Imaging and analysis of gradients

Spinal cord cross-sections were imaged on a Leica upright microscope with 10X and 20X objectives at multiple exposure times to ensure that the images contained the entire dynamic range of the gradients which had been revealed by immuno-histochemistry. Images were then analyzed with a custom ImageJ macro, which measured the intensity profile along the dorso-ventral axis at 5 discrete angles ranging from 95° to 105° emanating from a region just outside the floor plate. This was performed for both sides of the spinal cord for each image (Figure II.1A). The data was then pooled and visualized using a custom MATLAB script to calculate the mean intensity of the Shh gradient. The background fluorescent signal contribution from both the primary and secondary antibodies was determined by measuring the staining intensity in the neural tube of *Shh*$^{-/-}$ littermates, which were processed simultaneously and imaged identically. The background signal was then subtracted from each quantified Shh gradient profile, before the fractional change was calculated. To calculate the fractional change of the measured gradient, the mean intensity profile of the regions of interest were fit to a straight line using Open Office Calc (Maryland), and the fractional change calculated from the fit line. See Appendix.2.iii for a detailed description of the quantification of the Shh gradient profile from spinal cord sections.

II.5.iii. Microfluidic device fabrication

A microfluidic gradient generator (Jeon et al., 2000) was modified to increase the surface area over which the gradient can be applied. Positive relief master molds were fabricated from a 17.78 cm (7”) chrome photomask (FineLine Imaging, Colorado) by the McGill Nanotools Microfabrication Facility by spin coating SU-8 2050 (Microchem) to a height of 50 µm onto a 15.24 cm (6") silicon wafer. The silicon master wafer with positive relief features was exposed to CHF_3 plasma for 1 minute, then treated with 3,3,3 trifluoroperfluoro-octylsilane in a vacuum desiccator for 30 min to ensure that the polydimethylsiloxane (Silgard 184 - PDMS) would not stick to the SU-8 features. PDMS was then mixed thoroughly as per manufacturer's

recommendations (10:1 base polymer : curing agent) before being degassed for >15 minutes in a vacuum, and poured onto the silicon master wafer. The PDMS was cured for >3 days at 60ºC. The PDMS was then peeled off from the master and cut to individual chips. Through-holes at the two inlets and outlet were made using a biopsy punch. Glass slides (Schott Glass D) were soaked in concentrated nitric acid for 24-36 h, before being rinsed in milliQ water 12 times over 2 h, and sterilized by baking at 225°C for 4-6 h. On the day prior to beginning the experiment, both glass slides and PDMS chips were exposed to an oxygen plasma (Plasmaline 415 Plasma Asher, Tegal Corporation, 0.2 mbar for 30 s at 75 W) before bringing the surfaces into contact to form an irreversible bond. Within 20 min following bonding, devices were filled with 0.1 µg/ml poly-D-lysine (PDL; Sigma) to generate an adhesive substrate onto which neurons could attach. After coating for 1h, the PDL was removed and the microfluidic chamber rinsed twice by adding sterile milliQ water to the outlet. Fluid reservoirs were crafted by cutting the bottoms from 200 µl PCR tubes, and positioning the tubes into the punched holes such that both tubes were an equal height. The tubes were both filled with 200 µl of Neurobasal media containing serum, generating a forward gravity driven flow, which was left to further rinse the PDL coated channels overnight. See Appendix.1.i for a detailed description of the le Massif gradient generator fabrication.

II.5.iv. Premixer microfluidic gradient generator

The range of ligand concentration imposed on the axons in the gradient chamber depended on the guidance cue concentration added to the reservoir at inlet 1 (Figure II.2A). The reservoir at inlet 2 was filled with culture media without guidance cue. To visualize and quantify the gradient, we used 40 kDa tetramethylrhodamine-dextran. Hydrostatic pressure was created by filling the inlet reservoirs higher than the outlets (Figure II.2B), which drove fluid flow uni-directionally from left to right throughout the device. When fluid from the two inlets converge, the concentrations at inlet 1 and inlet 2 are mixed and subsequently divided to three discrete concentrations (Figure II.2C). This mixing and splitting occurs a total of 18 times, generating 20 discrete concentrations which are spaced at linear gradations between the concentration at

inlet 1 and inlet 2 (no cue). The 20 discrete concentrations then flow from the premixer channels into the gradient chamber, where they meet and diffuse to establish a linear concentration gradient (Figure II.2C). Because the fluid volume is on the microliter scale and the Reynold's number is low (Re<1), the flow is laminar and there is no convective mixing (Capretto et al., 2011). Because diffusion is slow over long distances, the diffusion of the guidance cue is slow relative to the flow velocity and the gradient remains linear for the entire 9 mm length of the gradient chamber (Figure II.2E) as long as there is a continuous flow driving the mixing. Consequently, long-term gradients can be maintained without actively controlling the flow rate, so long as the reservoir at the outlet is emptied periodically (~every 24 h). The upstream and downstream regions of the gradient chamber were imaged using a 2.5X objective on an upright fluorescence microscope (Leica).

II.5.v. Primary commissural neuron culture

Commissural neurons were prepared from the dorsal fifth of E13 rat neural tubes as described previously (Yam et al., 2009, Langlois et al., 2010). Cells were re-suspended in plating media composed of Neurobasal (Gibco) supplemented with 10% heat-inactivated FBS and 2mM GlutaMAX (Life Tech). 50 µl of plating media was added to both inlet reservoirs and 50 µl of cell suspension (3,160,000 - 5,630,000 cells/ml) was added to the outlet. One of the inlet reservoirs was removed and a reverse flow induced by connecting a syringe to the inlet hole via a short rubber hose and pulling on the plunger. While observing with an inverted microscope, neurons were drawn into the gradient chamber, after which the flow was stopped by releasing the plunger, disconnecting the syringe, and then returning the reservoir to the hole. After 4-6 h, inlet reservoirs were filled with 200 µl of plating media, again inducing a forward flow. ~15 h later, the plating media was replaced with serum-free growth media composed of Neurobasal (Gibco) supplemented with 2% B27 (Gibco), 2mM GlutaMAX (Gibco) and penicillin/streptomycin (Gibco).

II.5.vi. Guidance assay

Shh guidance experiments were performed using the recombinant human NShh C24II (R&D). Netrin-1 guidance experiments were performed using the VI,V peptide (Bin et al., 2013), which was a kind gift from Dr. Tim Kennedy. The guidance assay was started within 24 h of plating, when most of the neurons had initiated a neurite. Culture media (200 µl) was added to one of the inlet reservoirs and guidance cue or vehicle control (0.1% BSA; Sigma) diluted in culture media (200 µl) to the other. Gradient devices were then returned to the incubator until the following morning (~20 h following gradient application), at which point a Pasteur pipette was used to remove any fluid which had accumulated in the outlet. The devices were then returned to the incubator for a further 4 h, for the remainder of the 24 h assay. Guidance assays over 45 h were performed as described above, except the gradient was established 4-6 h after the neurons were loaded into the device.

The assay was ended by quickly removing all culture media from the inlets and outlets by aspiration and adding 4% PFA (100 µl) to the outlet reservoir. After 15 min, the PFA was removed and replaced with a staining buffer consisting of DAPI (Sigma, 1:10,000) to stain cell nuclei, TRITC-phalloidin (Molecular Probes, 1:250) to stain F-actin, and Triton (Sigma, 1:400) to permeabilize the cells. Neurons were left to stain overnight (~12 h) and the staining buffer was replaced with buffered saline for 1-2 h before imaging. See Appendix.1.i for a detailed description of the le Massif guidance assay protocol.

II.5.vii. Image acquisition and analysis of axon turning

Fixed specimens were imaged using an IXM high content screening automated microscope (Molecular Devices) with a laser-based auto-focus and a 20X objective (Nikon). 275-300 images were obtained to include the entire area of the gradient chamber using MetaExpress imaging software (Molecular Devices). All analyses were performed by an observer naive to the gradient conditions for each device. For each image, we traced all isolated axons in each field of view

using a custom ImageJ macro. So that the observer would be blind to the direction of the gradient, every image had a 50% chance of being flipped vertically when opened. Image files were analyzed by Flatworld Solutions (Bangalore).

All calculations of neuron position, concentration, fractional change, axon length and turned angle were performed using a custom MATLAB script. We defined the axon base angle as the angle between the proximal 20 µm of the axon and the direction of flow, and the axon tip angle as the angle between the distal 20 µm of the axon and the direction of flow (parallel to the arrow in Figure II.2C). We defined the turned angle as the difference between the base and tip angles of the axon, where the sign of the difference was positive if the axon turned toward the gradient, and negative if the axon turned away from the gradient (Figure II.3A). We considered only axons which faced against the direction of the flow, and excluded those facing directly towards or against the gradient (within 20º of the gradient direction). We excluded from further analysis axons which were shorter than 20 µm. Because of the local flattening of the gradient near the boundaries caused by the no-slip condition, we excluded any neurons positioned within 450 µm of either boundary (red boxes Figure II.2K).

To estimate the concentration of guidance cue at each growth cone position, we calculated each neuron's position relative to the gradient chamber, and thus relative to the gradient itself. We assumed a growth cone width of 10 µm for fractional change calculations, which we calculated using the difference in concentration between a point 5 µm above and 5 µm below the neuron, divided by the concentration at the neuron's position. All included growth cones experience fractional change within the range $0.3 \leq \delta < 2.2\%$. See Appendix.2.i for a detailed description of the quantitative analysis of axon turning and estimation of the guidance cue concentration and fractional change.

To calculate the synergy quotient, we first calculated a central moving average (CMA) of the turned angle of all axons within a window of 0.5% fractional change for each Shh, Netrin, and the combined gradient Shh+Netrin (Figure II.5A). We then calculated the synergy quotient (SQ) as:

$SQ = CMA_{Shh+Netrin} / (CMA_{Shh} + CMA_{Netrin})$.

II.5.viii. Measurement of growth cone pSFK asymmetry

After being exposed to the gradient(s) for 2h, neurons were fixed and stained for pSFK. Chambers were imaged with an IXM high-content screening microscope (Molecular Devices) using a 40X Nikon objective. Each growth cone was outlined. Then a line was placed spanning the width of the growth cone outline, parallel to the direction of the concentration gradient. The intensity profile was measured across 5 parallel lines spaced 1 pixel apart. The average intensity profile of the 5 lines was then processed using a custom MATLAB script. The fractional change in staining intensity across each growth cone (δ_{GC}) was then calculated as the difference in mean intensity between the proximal and distal thirds, divided by the mean intensity of the entire area of the growth cone (Figure II.6A). This value was scored as positive if the higher staining intensity was on the side of the growth cone proximal to the gradient, and negative if the higher staining intensity was on the side of the growth cone distal to the gradient. See Appendix.2.ii for a detailed description of the quantification of the asymmetric localization of pSFK in the growth cone (δ_{GC}).

II.5.ix. Statistical analysis

All analysis of variance, Chi-square and Wilcoxon signed-rank tests were performed using Graphpad Prism 5 (La Jolla, CA). All Rayleigh tests for unimodal deviation from uniformity were performed using the circStat toolbox for MATLAB.

II.5.x. Data visualization

The majority of graphs were generated using GraphPad Prism or Open Office Calc (The Apache Software Foundation), unless otherwise mentioned. Tricolour radial scatter plots (Figure II.3G-H, 4F, Figure II.5F) and radial frequency histograms (Figure II.3I-J, Figure II.S3) were scripted manually with Processing, an open-source sketchpad software (www.processing.org). Random samples of axons were generated with a Processing script using a uniform probability distribution, wherein each axon was equally likely to be selected as the next data point was plotted, and the same data point could not be plotted twice.

II.6. Supporting information

II.6.i. SI Figures

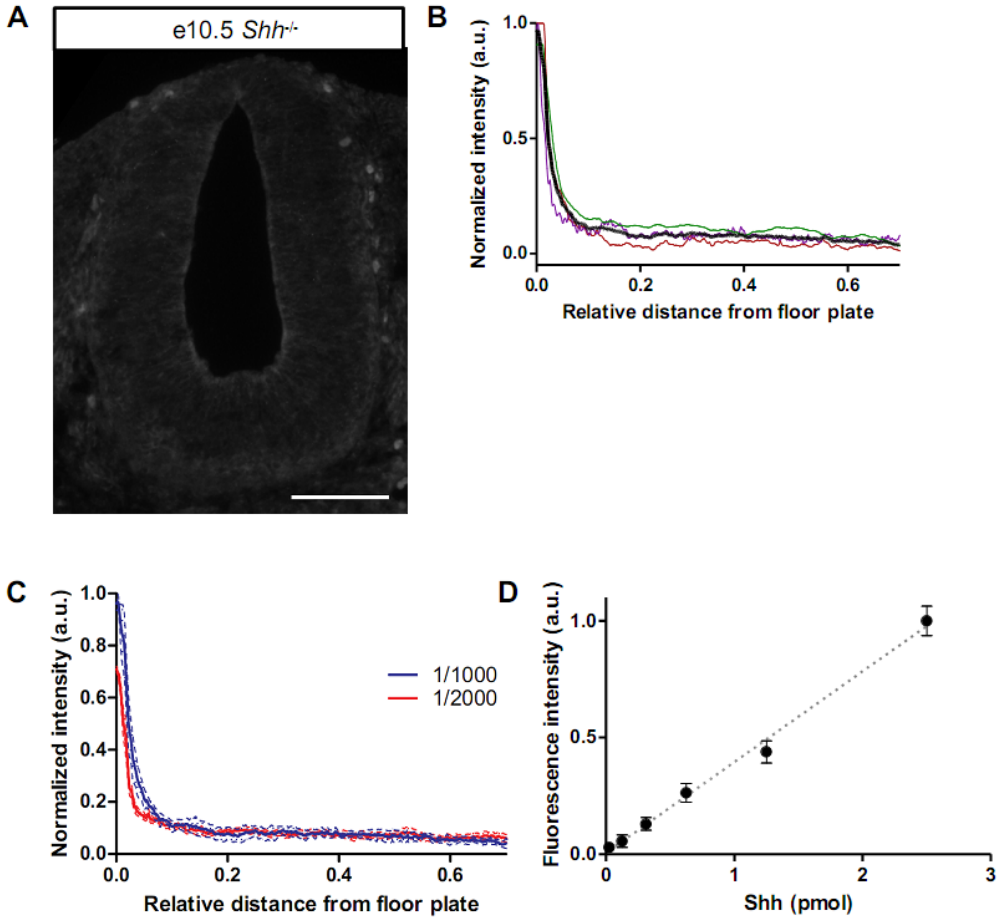

Figure II.S1. Related to Figure II.1. The Shh gradient profile is similar between embryos and does not depend on the concentration of the primary antibody. **A)** The anti-Shh antibody specifically recognizes Shh. The Shh staining present in WT floor plate and spinal cord was not present in Shh-/- e10.5 embryos. **B)** Quantification of the Shh gradient on a relative distance scale, where the mean gradient profiles from three different e10.5 embryos are shown. The mean value is indicated by the thick black line. **C)** Quantification of the Shh gradient profile at antibody concentrations of 1:1,000 (n = 3) or 1:2,000 (n = 8). The intensity profiles are almost entirely overlapping, despite a 2-fold change in primary antibody concentration. Error bands represent SEM. **D)** Quantification of the relationship between Shh concentration and fluorescence intensity by dot blot. Error bars represent SD (n = 5). Scale bar (A): 100 µm.

Figure II.S2. Related to Figure II.1. The measured gradient profile does not depend on the exact position of measurement. **A)** We compared intensity profiles measured using wedges in the spinal cord of e10.5 mouse embryos (as in Fig. 1A) with measurements made more laterally (overlapping with Tag-1 positive axons) on the same images from the same sections. **B)** Quantification of Shh protein intensity as a function of the relative distance from the floor plate to the roof plate. Although the measurements made laterally appear noisier, the two gradient profiles look similar.

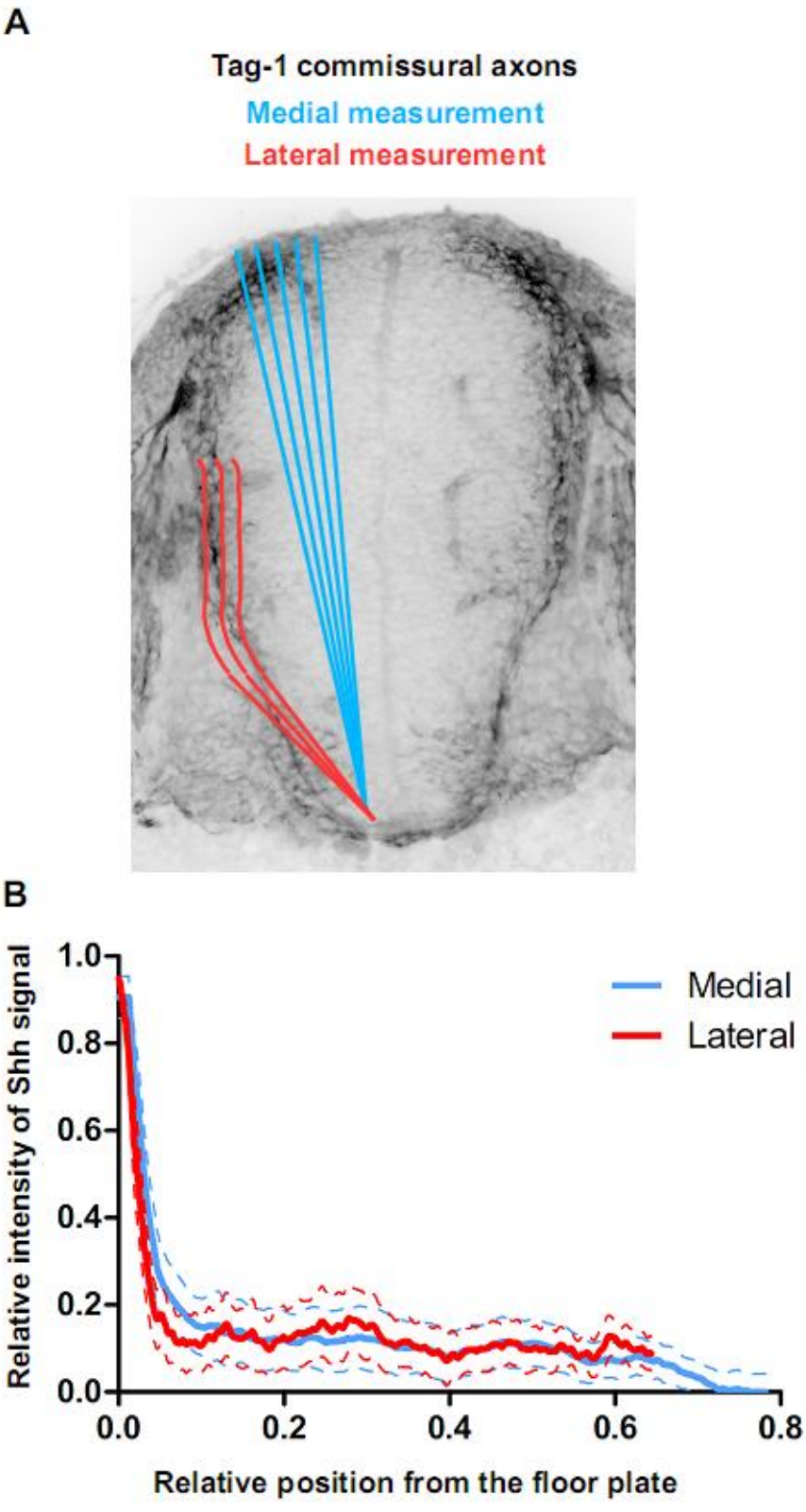
A
Tag-1 commissural axons
Medial measurement
Lateral measurement
B
Relative intensity of Shh signal
1.0
0.8
0.6
0.4
0.2
0.0
0.0
0.2
0.4
0.6
0.8
Relative position from the floor plate
Medial
Lateral

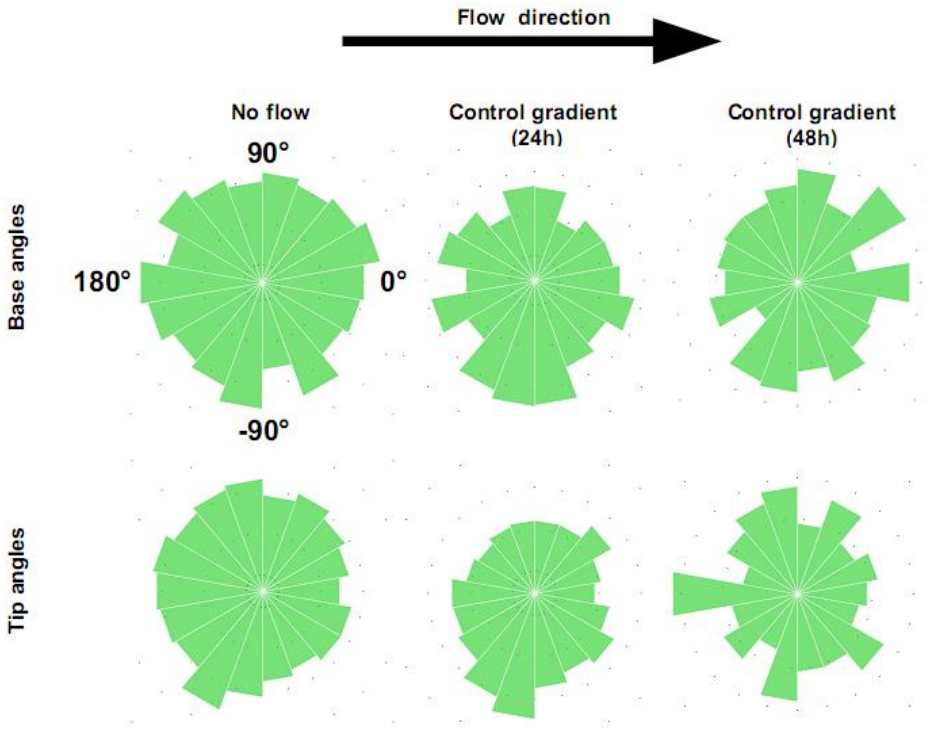

Figure II.S3. Related to Figure II.3. The flow does not bias the direction at which the axon originates from the soma, nor the axon tip orientation. The base angle and tip angle were measured as described in Figure II.3A. Circular frequency distribution for the axon base and tip angles in gradient devices with no flow or a control (BSA) gradient for 24 h or 48 h are shown. There is no significant directional bias for any of the distributions (Rayleigh test for uniformity, $n \geq 403$).

II.6.ii. SI Table

Genotype	Range of guidance error; proportion of the spinal cord (%)	Reference
Netrin-1$^{-/-}$	37 – 60	Serafini et al 1996
DCC$^{-/-}$	35 – 49	Fazeli et al 1997
Wnt1-Cre; Smo$^{null/conditional}$	43 – 47	Charron et al 2003
Boc$^{-/-}$	41 – 56	Okada et al 2006

Table II.S1. Relative position of Shh and Netrin-1 signaling dependent guidance errors. Using previously published images from mice genetically deficient for Netrin-1 (Netrin-1$^{-/-}$ and DCC$^{-/-}$) or Shh (Wnt1-Cre;Smo$^{null/conditional}$ and Boc$^{-/-}$) signaling, we determined at what position along the spinal cord guidance defects occur for commissural axons by measuring the relative distance from the floor plate to the roof plate at which misguided axons begin to deviate from their normal trajectory (expressed as %). We used these relative distances to define the range of guidance errors.

Chapter III: General Discussion

III.1. Summary

It is known that disrupting either Shh or Netrin-1 signaling pathway is sufficient to induce guidance errors of the commissural tract (Serafini et al., 1996, Fazeli et al., 1997, Charron et al., 2003, Okada et al., 2006), indicating that these two cues are not entirely redundant. However, it is not understood how these guidance cues act collaboratively to ensure robustly targeted growth of axons toward the floorplate.

It has been observed that guidance cues can collaborate in concentration-limited synergy, such that the lack of function of a single cue at limiting concentration can be enhanced in the presence of a similarly low concentration of a second guidance cue (Bonanomi et al., 2012). I hypothesized that Shh and Netrin-1 could collaborate to enhance the chemotactic sensitivity of growth cones when instead the gradient steepness is limiting.

I tested this hypothesis by quantifying the steepness of the Shh concentration gradient *in vivo*, specifically where guidance errors occur in the absence of Shh signaling, and found that the gradient steepness is low (< 2%). I then assessed whether the gradient steepness is a critical parameter for the ability of axons to turn in individual gradients of Shh or Netrin-1 *in vitro*. Critically, I demonstrated that a combined gradient of Shh and Netrin-1 is capable of guiding commissural axons synergistically in a region of the gradient where the steepness is insufficient to guide axons with a single cue. I further demonstrated that in the same gradient steepness, only gradients of both cues induced the asymmetric activity of phosphorylated Src-Family Kinase within the growth cone.

Thus, I demonstrated that Shh and Netrin-1 collaborate to guide commissural axons in steepness-limited synergy.

III.2. Quantification of the Shh concentration gradient *in vivo*.

An essential component of this work was to quantify the Shh concentration gradient *in vivo*, as it allowed us to make a direct comparison with our systematic evaluation of the gradient parameters required for axon turning *in vitro*. We observed that there is a steep decrease in Shh concentration approximately 25 µm adjacent to the floorplate, followed by a shallow decrease that spans the remainder of the spinal cord (Figure II.1B). Although the steepness of Netrin-1 concentration gradient has been measured previously (Kennedy et al., 2006), there have been no attempts to measure the steepness of the Shh concentration gradient.

The graded Shh distribution in the spinal cord has been quantified using a Shh:GFP fusion protein (Chamberlain et al., 2008), but the gradient steepness was not available for comparison. One striking difference between our quantification of the gradient profile and theirs is that they could not detect any Shh:GFP fusion protein beyond 25 µm from the floorplate. This could only partially be explained by the decrease in diffusivity imposed by the larger molecule (estimated 1.3-fold decrease), thus the difference more likely results from the fact that the fusion protein was produced in much less abundance than unmodified Shh (Chamberlain et al., 2008). Given the probabilistic nature of concentration gradients, the lower production rate would result in a limited range of diffusion. Therefore, it is possible that the modification could have interfered with the formation of the gradient. Several other studies have imaged the Shh concentration gradient *in vivo* using immunochemistry (Roelink et al., 1995, Chen et al., 2004, Cohen et al., 2015). The major difference between our study and all previous measurements of the gradient by immunochemistry is the Shh-antibody used. The 5E1 monoclonal antibody was used for all previously reported measurements of the Shh concentration gradient in the spinal cord. However, in our study we used a more recently purified polyclonal Shh-antibody, which does not have to compete with Ptch1 for binding (Tian et al., 2009), unlike 5E1. Prior to obtaining this new antibody, we had attempted immunostaining with 5E1, but we were only able to reveal the high-intensity staining immediately within and adjacent to the floorplate, consistent with the aforementioned studies. This was unsatisfactory, as it is known that Shh patterns the entire ventral half of the spinal cord (Jessell, 2000). When we used the polyclonal Shh-antibody, we were able to image the

gradient with much more sensitivity, and were able to detect low-levels of Shh protein that is present more dorsally than has been previously reported. In order to determine a true background value, we subtracted tissue-background intensity values from the neuro-epithelium of $Shh^{-/-}$ littermate embryos imaged from the same slides. This ensured that our quantification was limited to signal resulting from Shh protein. To further justify our quantitative interpretations, we demonstrated that the gradient profile was not dependent on the concentration of primary antibody being used (Figure II.S1). Therefore, our measurement of the Shh gradient is consistent with the substantial body of evidence that Shh acts at a distance to specify the fate of the entire ventral half of the spinal cord (Ericson et al., 1995b, Ericson et al., 1996, Ericson et al., 1997a, Ericson et al., 1997b, Briscoe et al., 1999, Briscoe et al., 2000), and in the absence of Ptch1, this influence can even extend into the dorsal half (Briscoe et al., 2001). Thus, the difference between the Shh gradient profile we report and the profile seen in previous studies most likely results from technical limitations, rather than by the absence of biological activity in this region *in vivo*.

We found that the concentration gradient of Shh is relatively shallow ($1 \leq \delta \leq 2\%$) in the region of the gradient where commissural guidance errors occur in the absence of Shh signaling (Figure II.1B). This suggests that it may be most crucial for growth cones to integrate multiple guidance signals when the gradients are shallow. Our results are consistent with a noteworthy study by Isbister and colleagues (Isbister et al., 2003), where the authors observed immunostained sections of the grasshopper limb, and identified guidance errors of Ti1 pioneer growth cones *in vivo*. They then quantified both the absolute change (ΔC) and the steepness ($\delta = \Delta C/C$) of the Sema2A gradient along the path of migrating axons, in order to determine which of these parameters was critical to guide the growth cone. Since they identified more guidance errors *in vivo* where the ΔC was high and the steepness low, they concluded that it was the steepness of the gradient that was responsible for the chemoattractive property. We built on this *in vivo* approach and took it a step further by relating the gradient steepness in the region where guidance errors occur in mutant mice *in vivo* to the turning of the same axons *in vitro*. We have performed the first quantitative comparison of the gradient parameters required for axon turning both *in vivo* and *in vitro*. Interestingly, the range of gradient steepness

observed in this zone of the neural tube *in vivo* corresponds to the same range of steepness where the synergy occurs between Shh and Netrin-1 signaling *in vitro*.

There is a notable difference between our measurements of the Shh concentration gradient, and the steepness reported of the Netrin-1 concentration gradient (Kennedy et al., 2006). While there is no reason to expect the gradients to be identical, as their molecular weight would predict the rate of diffusion to be 1.5-fold slower for Netrin-1, there are nonetheless slight differences between the measurements that are worth discussing. They report that the gradient steepness of Netrin-1 ranges from 27% at the apex to 11% at the low end, across a growth cone width of 25 µm. Adjusted for the differences in the growth cone size, this ranges from 4.4 - 10.8% across 10 µm, which is still higher than we observed for the Shh gradient. Since the Netrin-1 gradient was quantified in chick, these differences may be accounted for by differences between rodent and chicken stages of development. Furthermore, the Netrin-1 gradient measurements were made along the circumferential trajectory along the neuro-epithelial basement membrane, where the intensity is visibly higher. While many of the commissural axons are still migrating circumferentially by this age (e10.5), the intensity measurements may be confounded by signal originating from the axons themselves, rather than the external gradient. While we found that the measured Shh gradient profile was quite similar whether measured laterally or medially within the spinal cord (Figure II.S2), we noticed the lateral measurement was noisier, quite possibly due to the presence of commissural axons. It remains a possibility that the different measurement position could lead to different quantitative results for the Netrin-1 gradient.

III.3. Novel microfluidic guidance assay: *le Massif*

A major technical advance that allowed us to perform the present work was our development of a microfluidic guidance assay that was optimized to study axon turning in response to physiologically relevant, shallow gradients. Specifically, we assessed turning over the course of 1-2 days, which is consistent with the time taken for the population of commissural neurons to make their trajectory towards the floorplate. This contrasts with common guidance assays such

as the pipette and Dunn chamber assays, which assess axon turning on the timescale of 1-2 hours.

A major factor which we consider necessary for creating a high-throughput guidance assay is the massive surface area upon which the neurons can be plated. This is critical, because in order to look in detail at specific ranges of concentration or gradient steepness, the gradient area must be subdivided, which further reduces the number of axons exposed to either gradient parameter. To obtain a substantial experimental throughput, we optimized several critical steps of the procedure. Initially, rapid prototyping of microfluidic devices allowed larger experiments to be performed than if the devices were commercially purchased or re-used. While we chose to perform experiments ranging in size from 10 to 30 microfluidic devices in parallel, there is no fundamental limit on how many experiments could be performed simultaneously, if needed. Moreover, the use of an automated high-content screening microscope allowed for many experiments to be imaged in a short period of time, so the rate-limiting step was then shifted to the analysis of the axonal trajectories. As a result, the *le massif* turning assay can be used to assess axon turning with a sample size that is nearly unheard-of in the field of axon guidance. The largely automated imaging and analysis make the method scalable, which could make it of particular interest to neurobiology laboratories, and also to investigators studying non-neuronal chemotaxis. In addition to the experimental throughput, the range of gradient steepness generated in the *le Massif* assay is at the lower boundary of what can be perceived by the growth cone (Figure II.4 B-C), so this allowed us to evaluate guidance cue combination in a context where the steepness of the gradient was the limiting factor. For these reasons, the established axon turning assays were incompatible with the present study.

For example, the pipette assay has been considered to be the gold standard for assessing axon turning for well over the last decade. Controlled bursts of guidance cue from the tip of a micropipette generates a steep gradient that can vary greatly if several key parameters are not precisely controlled (Pujic et al., 2008). In the pipette turning assay, each axon must be imaged for 1h, and the experiment must remain on microscope stage for the duration of the experiment. Therefore, the number of simultaneous experiments that can be performed is

limited by the number of microscopes with dedicated cameras and pico-spritzers. To fully illustrate the influence this has on throughput, the graph shown in Figure II.3E would have taken over 2 years performing pipette assays, for 12h hours each day. Additionally, the range of gradient steepness generated by the pipette assay is in the range of $5 < \delta < 35\%$, which is quite high relative to *le Massif*. Since the pipette assay has been optimized to study turning to a single guidance cue, it is not clear that it would be possible to observe steepness-limited synergy with this approach.

The Dunn Chamber is an increasingly popular tool to assess axon turning, as it allows experimenters to image 30-40 axons simultaneously over the course of 2h (Yam et al., 2009), with a moderate gradient steepness ranging from $1 < \delta < 10\%$. The throughput is substantially higher than the pipette assay, and it is relatively simple to set up. However, the Dunn chamber is incompatible with the present study because the gradient it generates is a passive source-sink gradient which flattens approximately 10h after being established (Yam et al., 2009), making a 24-45h assay impossible.

The collagen co-culture assay (Ebendal and Jacobson, 1977b) is another robust guidance assay that remains widely used, as guidance effects are often visible without strictly requiring quantification. A further benefit is that it does not rely on live imaging, so many assays can be performed simultaneously. While some authors correctly argue that the growth of axons into a 3D collagen gel is more similar to the *in vivo* environment than a 2D glass substrate (Rosoff et al., 2004, Kothapalli et al., 2011), collagen is not present in the brain or spinal cord, and alone it is not a permissive substrate for axonal outgrowth. As a result, using collagen gels as a culture platform may be, in principle, unsuitable for studying guidance cues with no inherent influence on axonal outgrowth, as is the case with Shh, which requires Netrin-1 to be present in the media for axons to grow into collagen (Charron et al., 2003). Additionally, the gradients produced by this method cannot be easily controlled or quantified, making the level of quantitative investigation in our study impossible.

Of the several microfluidic gradient generator designs that have been used to study axon guidance, none have yet become standard. Each device has been tailored to find a solution to

the major challenge facing all microfluidic gradient generators; they each offer a unique strategy to render the microfluidic device compatible with axons and growth cones. While some groups have prioritized designs that allow rapid switching of gradients, this relies on high flow-rates, which increases the shear stress imposed on the neurons. For delicate processes such as axons and growth cones, it is known that these forces can be quite harmful. Since our device uses gravity to generate the hydrostatic pressure-driven flow, we were able to experimentally determine the minimum volume of fluid required to maintain a stable gradient. We then demonstrated that the resulting shear stress was sufficiently low to not bias or impair axon outgrowth (Figure II.S3), circumventing the need for a more complex solution.

Others have solved the problem of shear stress by isolating the neurons from the flow. In a pioneering study, the shear stress was reduced by etching wells into the glass coverslips so that the neurons could be protected from the high flow velocity (Joanne Wang et al., 2008). Other designs have eliminated the shear stress by isolating the neurons from the flow with a series of 'microjets' (Bhattacharjee et al., 2010) or a porous membrane (Taylor et al., 2015). While each of these gradient generators have excellent spatio-temporal control over the onset of the gradient, the complicated fabrication and experimental procedures make performing multiple assays simultaneously difficult or impossible. Our approach to reducing the shear stress was simpler, which is a benefit in itself; Ultimately, the extent to which any technique will become widely adopted as a standard will rely on how easily it can be learned, and how readily results can be obtained and repeated.

We provide a case study for the adaptability and customizability of microfluidics-based tools. Rather than developing an entirely novel gradient generator, we used a published design and improved it to suit our needs. Whereas other groups have adapted the original pre-mixer gradient generator to prioritize rapid gradient application or switching (Herzmark et al., 2007, Joanne Wang et al., 2008), we produced a variation of the design that was suited to address our specific experimental requirements of a large sample size and long-term gradient stability. At the time of this writing, this customization step is nontrivial, and not particularly cheap. Before a single microfluidic device can be used in an experiment, an upfront cost of several hundred dollars and a substantial time investment is required, with no guarantee that a working device

will result. The ability of ourselves and others to make improvements to the original pre-mixer design in order to make novel biological discoveries makes a strong argument in favour of open-source microfluidic designs that are accessible to non-engineers. So far however, issues with biocompatibility and the high barrier-of-entry have likely delayed microfluidic technology from reaching its full potential for widespread use in quantitative biology. I believe that that customizable, commercially-available, open-source microfluidic devices together with low-cost, rapid-prototyping stereo-lithography instruments will act together as a catalyst to allow microfluidic tools to become more accessible and mainstream.

III.4. Gradient steepness is critical for axon turning

We have demonstrated that gradient steepness is indeed critical for axon turning (Figure II.4B-C), as predicted by the Bayesian model (Mortimer et al., 2009). Our finding is consistent with previous reports that the steepness is an important parameter for the migration of non-neuronal cell types in chemoattractant gradients (Zigmond, 1981, Herzmark et al., 2007, Fuller et al., 2010), and for the guidance by growth rate modulation of DRG explants in gradients of NGF (Rosoff et al., 2004, Mortimer et al., 2009, Mortimer et al., 2010).

In the Bayesian model of gradient sensing, the growth cones ability to detect the gradient depends linearly on the gradient steepness, while the dependence on concentration spans several orders of magnitude (Mortimer et al., 2009). We have demonstrated an approximately linear relationship between the turned angle and steepness (Figure II.4B-C), consistent with the Bayesian model and previous experimental results (Rosoff et al., 2004, Mortimer et al., 2009). Unexpectedly, we did not see a similar dependence on the absolute guidance cue concentration in our assay as predicted by the model (Figure II.4G-H), which lead us to conclude that the gradient steepness is the most critical parameter. However, it is certainly also critical that the concentration is itself sufficiently high to be sensed by the growth cone, and not too high so as to saturate all its receptors (Figure I.7 A-C); this provides an upper and lower bound on the useful concentration range. However, the range of concentration shown theoretically

and experimentally to be relevant for outgrowth spans two orders of magnitude above and below the dissociation constant of the receptor-ligand complex (Mortimer et al., 2010); their model predicts that all guidance activity occurs in a 10,000-fold range of concentrations. To put this into context with our *in vitro* results, we consider the sample of axons in the region of the gradient with steepness ranging from $1 \leq \delta \leq 2.2\%$. This subset of neurons experiences a 31-fold range of concentrations of Shh, and a 59-fold range for Netrin-1 (Figure II.4 G-H). If we consider that the dissociation constant reported for Shh binding to Boc is 42.2 ± 15.9 nM (Okada et al., 2006) and for Netrin VI-V-FC binding to DCC is 5.4 nM (Keino-Masu et al., 1996), then we would expect a subtle increase in the turned angle as the concentration of either cue increases (Figure III.1). Therefore, while the Bayesian model would lead us to expect that concentration-related changes in the turned angle would be relevant within this range of concentrations, we were unable to detect a significant trend (Figure II.4 G-H). One potential explanation is that the ligand-receptor affinity measured in cell binding assays may not accurately reflect the affinity of the receptor and ligand at the growth cone. An alternative explanation is that this model has only been demonstrated to be valid for axon guidance by growth-rate modulation in response to shallow gradients, and has not been experimentally verified to describe immediate and biased turning of any model axon. However, a response that is maximal at the dissociation constant of the ligand-receptor complex has been reported for migrating *Dictostelium discoideum* (Fisher et al., 1989) and polymorphonuclear leukocytes (Zigmond, 1981), both of which migrate in a manner that resembles axon turning. Therefore it seems unlikely that the dependence on concentration would be drastically different for axon turning.

Additionally, the Bayesian model was formulated to describe the high-affinity binding of NGF to a single binding site of the TrkA receptor. However, in both Shh and Netrin-1 guidance systems, there are multiple receptors present. While Boc is the guidance receptor for Shh in commissural growth cones, Ptch1 is present and forms a complex with Shh and Boc with a dissociation constant of 0.92nM ± 0.15 (Okada et al., 2006), much higher affinity than for Shh with Boc alone. For Netrin-1, recent reports have implicated a role (albeit a minimal one) for Neogenin in commissural axon guidance, which has a dissociation constant ~0.73x the binding of Netrin-1 to

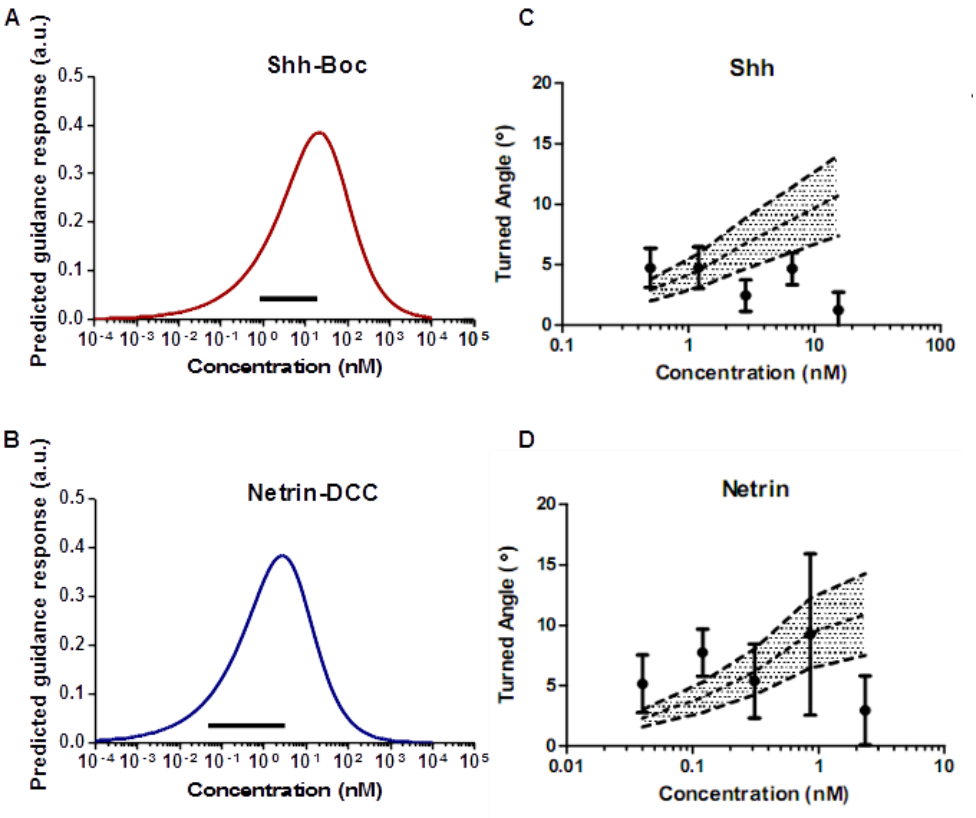

Figure III.1. Bayesian model predictions for growth cone guidance response as a function of the concentration of guidance cue. **A-B)** Based on the reported dissociation constant for Shh with Boc of 42.2 nM ± 15.9 (Okada et al 2006) and Netrin VI,V-FC with DCC of 5.4nM (Keino-Masu et al 1996), the curve represents the expected turning response as a function of the ligand concentration for a steepness of δ=1.45%. The thick black line above the x-axis represents the range of concentrations that we evaluated experimentally (in Figure II.4 G-H). For both Shh and Netrin-1, the ranges of concentration tested were below the reported K_d for the guidance receptor, and therefore the model predicts an increasing turning response as a function of the concentration. **C-D)** Data from Figure II.4 G-H replotted with the predictions from the Bayesian model. To map the Bayesian predicted values onto turned angles, I simply considered the peak response of the curves in A and B to match the highest turned angle obtained for either guidance cue in Figure II.4. As a rough approximation, this allows us to compare our results quantitatively with the Bayesian model predictions. Although the model predicts a subtle increase in turned angle that is notable within the range of concentrations tested, we do not observe an increase in turned angle experimentally.

DCC (Xu et al., 2014). Additionally, Netrin-1 can bind directly to α3 and α6 integrins with unknown affinity (Lemons et al., 2013), which could potentially influence the response. Therefore, there remains a distinct possibility that the Bayesian model is not sufficiently elaborate to describe the behaviour of growth cones with multiple receptors which bind to the same ligand with different affinities (Figure III.2). Future mathematical models should consider the special case of multiple receptors whose respective dissociation constants for the same ligand are separated by as much as an order of magnitude. It should be determined whether this mechanism could theoretically increase the range of ligand concentration that can be detected by the growth cone in a meaningful way.

III.5. Intracellular amplification of an extracellular gradient

An interesting question arises as to if and how a growth cone can amplify the external gradient, as is expected to be necessary in order to turn a graded signal into a polarized, binary response (Mortimer et al., 2008). Because the steepness, δ, of the concentration gradient in our study is known, and the steepness of the intracellular gradient, δ_{GC}, of pSFK is measured (Figure II.6A), we can directly compare between these values to get an approximation of the extent to which the growth cone can amplify the shallow, external gradient (Figure III.3). In our study, the mean and median values of δ_{GC} are both ~10% (Figure II.6E-F), so a back-of-the-envelope calculation would imply an average amplification of > 6-fold in steepness, within the combined gradient that ranges in from $1.4 < \delta < 1.6\%$. While the mean and median well reflect the overall shift in the central tendency for the δ_{GC} measurements, the variability is quite large. As a result, either measure masks extreme values, as some outlier growth cones have $\delta_{GC} > 100\%$, and growth cones with $\delta_{GC} > 50\%$ or $\delta_{GC} < -50\%$ are not uncommon. Due to the volatility of these measurements, it is difficult to make a general conclusion regarding amplification, however our results provide evidence that, on average, the steepness of the pSFK gradient in the growth cone is several fold steeper than the steepness of the combined gradient. Although these results are not conclusive, we provide a novel framework to evaluate a mechanism by which such an amplification could occur. Future studies could localize the step(s) in the intracellular

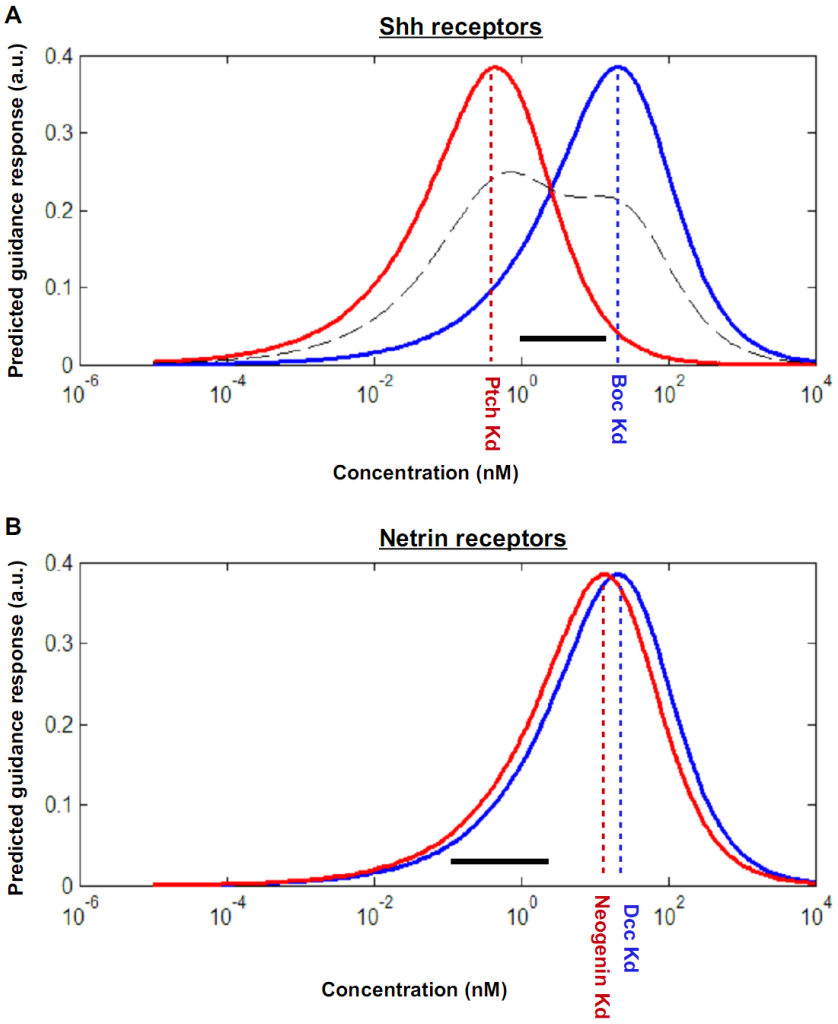

Figure III.2. Bayesian model predictions for guidance receptors with distinct affinities. Plotted curves reflect the Bayesian model predictions (Mortimer et al 2009) as a function of the ligand concentration, for a steepness of $\delta = 1.45\%$. The dotted line reflects the concentration of the reported dissociation constant (K_d) for the ligand-receptor complex. The thick black bar above the x-axis reflects the range of concentrations that we evaluated experimentally (Figure II.4 F-G). **A)** Commissural neurons also express Ptch1, which forms a complex with Boc and Shh with high-affinity. Interestingly, the range of concentrations we've tested is between the K_d of Ptch1 and Boc. The dashed line reflects the mean value of the Ptch and Boc functions, which leads to a slight decrease in turning response in the range of concentrations tested. **B)** Commissural axons have been recently shown to be partially guided by the Neogenin receptor, which has a very similar dissociation constant to DCC (Xu et al 2015).

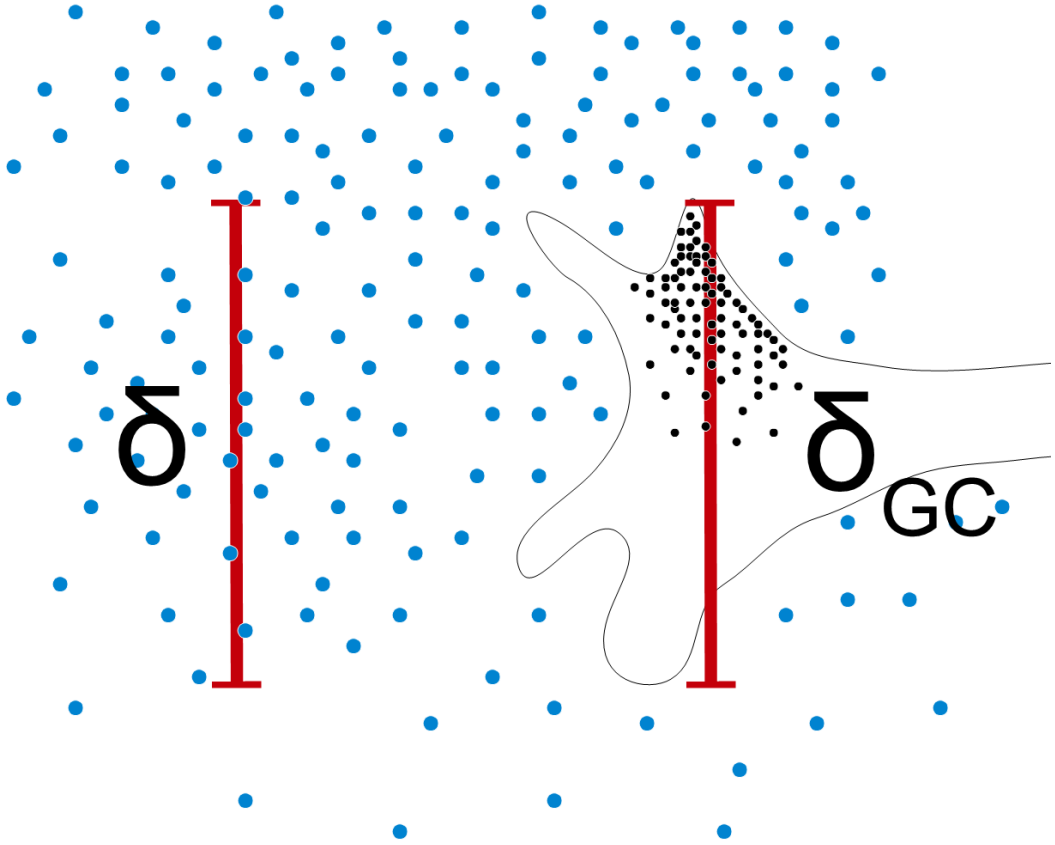

Figure III.3. Growth cone amplification of the guidance cue gradient. A schematic to represent the principle of amplification by the growth cone. In the presence of a concentration gradient of guidance cue (blue) of steepness δ, a growth cone reflects the direction of the gradient internally by asymmetrical activation of a downstream signalling molecule (in this case, pSFK). The steepness of the intracellular gradient, δ_{GC} uses the same unit-less measurement as the concentration gradient steepness δ. Therefore, if $\delta_{GC} > \delta$, this implies that the growth cone has amplified the concentration gradient, and the amplitude of the amplification is proportional to δ_{GC}/ δ.

signalling cascade that are responsible for the pronounced increase by measuring the δ_{GC} for various pathway members, including surface receptors, kinases and adaptor proteins. The δ_{GC} values could be directly compared to the experimentally controlled gradient steepness, δ, and it could be determined which step in the cascade is responsible for the amplification of δ_{GC} relative to δ (Figure III.3).

One possibility is that an amplification of the gradient occurs with the guidance receptors themselves. In this sense, it is conceivable that the growth cone may share a common mechanism with migrating neutrophils, which have been observed to have more folding of the plasma membrane at their leading edge. This leads to an increase in the total amount of chemoreceptors at the side of the cell proximal to the gradient, supposedly thereby amplifying the interpreted gradient (Servant et al., 1999). A similar phenomena has been reported with the redistribution of GABA receptors on the plasma membrane of growth cones exposed to a gradient of GABA (Bouzigues et al., 2007, Morel et al., 2012), and such a mechanism could potentially explain how pSFK is so strongly polarized in such shallow gradients.

III.6. Mechanisms of synergistic guidance cue integration

Genetic analysis of Shh and Netrin-1-pathway mutants indicate that Shh and Netrin-1 act together in the spinal cord, as interfering with either signaling pathway is sufficient to cause commissural misguidance phenotypes (Keino-Masu et al., 1996, Serafini et al., 1996, Charron et al., 2003, Okada et al., 2006). However, it is not clear how these signaling pathways are integrated by the growth cone. We demonstrate that Shh and Netrin-1 collaborate synergistically to guide commissural axons (Figure II.5), and that these pathways appear to converge on pSFKs in the growth cone (Figure II.6).

This finding adds an interesting nuance to an already complex system. The question naturally arises as to whether Shh may have played the role of 'Netrin Synergizing Activity' which was observed to enhance the potency of Netrin-1 (Serafini et al., 1994), as the identity of the

compound remains unknown. Individually, several candidate proteins were ruled out, and it was determined that the synergizing activity resulted from a basic protein in the 25-35 kDa range (Galko and Tessier-Lavigne, 2000). Although the cholesterol modified N-terminal of Shh has a molecular weight of ~23 kDa, it has been determined that the majority of the soluble Shh exists in multimeric form ranging from 25 kDa to 150 kDa in size (Ciepla et al., 2014). While this does not exclude the possibility that Shh acted to synergize with Netrin-1 in the original outgrowth assays, the fact that the fact that the synergistic response was an increase of outgrowth into collagen (Serafini et al., 1994), and that Shh itself has no outgrowth-promoting effect (Charron et al., 2003), makes it unlikely that Shh is responsible for their observed synergy.

Interestingly, we demonstrated that Shh and Netrin-1 collaborate in steepness-limited synergy. Shallow gradients of either guidance cue alone provide insufficient directional information for the growth cones to properly orient and align with the gradient. However, when a second guidance cue was added with the same low steepness, axons were able to respond robustly by turning up the combined gradient (Figure II.5A). Importantly, we know that the concentration of the individual cues is not limiting because we observe axon turning when the steepness is high, despite this corresponding to a lower absolute concentration (Figure II.4A, Figure II.5A). Furthermore, we have identified pSFK as an integration point of synergy between Shh and Netrin-1 signaling pathways in the growth cone (Figure II.6). It is interesting to speculate that the location of the integration node within the signaling cascade may result in different modes of synergy; a co-receptor which binds to two ligands allows crosstalk at the receptor level, which may provide higher sensitivity to low concentrations of guidance cues. This notion is supported by the observation that concentration-limited synergy occurs in LMC_L growth cones between GDNF and EphA through the co-receptor Ret (Bonanomi et al., 2012), and in LMC axons in response to Netrin and ephrin-B2, mediated by a complex of Unc5c and EphB2 (Poliak et al., 2015). Alternatively, integration at a shared intracellular signaling molecule could allow growth cones to integrate shallower gradients – when the concentration is sufficient, but noise reduction is necessary. It is not clear whether the synergy observed between NGF and NT-3 is concentration- or steepness-limited, or a combination of both (Cao and Shoichet, 2003).

Although the mechanism was not further elucidated, it was hypothesized to be related to the expression of both TrkA and TrkC receptors by the DRG growth gone, each of which responds maximally to different cues. Furthermore, both NGF and NT-3 are known to also bind to P75NTR, which is thought to form a complex with TrkA. These ligands are notably promiscuous, as NGF also binds NT-3 (Segal, 2003), so it seems most likely that pathway crosstalk occurs at the receptor level and within the growth cone.

Our results open up several avenues of inquiry related to how growth cones integrate guidance cues from a signal processing point of view. Specifically, it would be interesting to determine if steepness-limited and concentration-limited synergy are determined by the point at which the signaling pathways converge in the growth cone. It would be relevant to know from a theoretical standpoint, if information is optimally integrated according to different strategies when crosstalk occurs at the receptors or at a shared signaling molecule within the growth cone. Future experiments could be devised to test for both concentration-limited and steepness-limited synergy for the same combination of guidance cues. Pairs of guidance cues whose signaling pathways are known to or expected to converge could be assessed for both modes of synergy. Using what is known of the localization of the receptors and downstream signaling molecules, it should be possible to determine whether one mode of synergy predominates for a specific spatial configuration of receptors or subcellular localization of signalling molecules within the growth cone.

There also remains a possibility that the spatial configuration of the receptors and downstream mediators of the various signaling pathways are not as critical to the signal integration as the behavioural influence that each signaling pathway elicits on the growth cone. For example, Shh has no outgrowth-promoting effect, and influences specifically the guidance of commissural axons (Charron et al., 2003). In contrast, Netrin-1 influences both the outgrowth and turning of these axons, which leads to the appearance of a stronger phenotype in DCC and Netrin-1 mutant mice (Keino-Masu et al., 1996, Serafini et al., 1996). Consistent with the growth-rate modulation hypothesis, the average length of the axons facing up a concentration gradient of Netrin-1 were slightly longer than axons facing down the gradient, which we did not observe for Shh. This raises the interesting possibility that synergy can result from mixed modes of directed

growth. In this hypothetical model, an increase in the rate of growth in the up-gradient direction would lead to more pronounced turning of axons that have already begun to turn. Conversely, a higher incidence of axons that turn towards the gradient would necessarily lead to more axons facing in the up-gradient direction, which would then be more strongly guided by the mechanism of growth-rate modulation. It would also be very interesting to determine experimentally whether a combined gradient of a guidance cue that has no outgrowth promoting influence (such as Shh) can synergize with a cue that enhances outgrowth, but does not guide axons, such as Stem Cell Factor (Gore et al., 2008). Therefore, there is substantial room for the formal models of axon guidance to be further elaborated in order to account for differences in the signaling cascades and the resulting axonal behavior.

III.7. Beyond the embryo: applications for combined shallow gradients

I anticipate an increased interest in shallow concentration gradients in a nerve regeneration context, where the distances that need to be traversed are on the order of centimeters. In principle, the shallower a gradient is, the longer the distance over which an axon can be guided, provided the sensitivity to absolute ligand concentration remains the same (Tessier-Lavigne and Placzek, 1991). Given a constant upper- and lower-bound to the useful concentration, decreasing the ΔC of the gradient will allow the same concentration values to be stretched across a wider portion of space, keeping the concentration within a biologically useful range across a larger distance (Figure III.4). However, our results confirm the steepness as a key constraint to the growth cone's perception of the gradient, which creates a limit on how far the gradient can be stretched. Since the steepness of a linear gradient depends on its length, then stretching a gradient out across the space of many millimeters will lead to larger and larger regions where the steepness is too low to reliably guide axons (Figure III.5). Therefore, in a regeneration context, it is extremely useful to know the lower bound of perceptible gradient steepness. Although our results confirm the gradient steepness as a key constraint, we also demonstrate that it can be partially overcome by providing a second, overlapping guidance cue. The second guidance cue appears to lower the perceptible gradient steepness, thus increasing

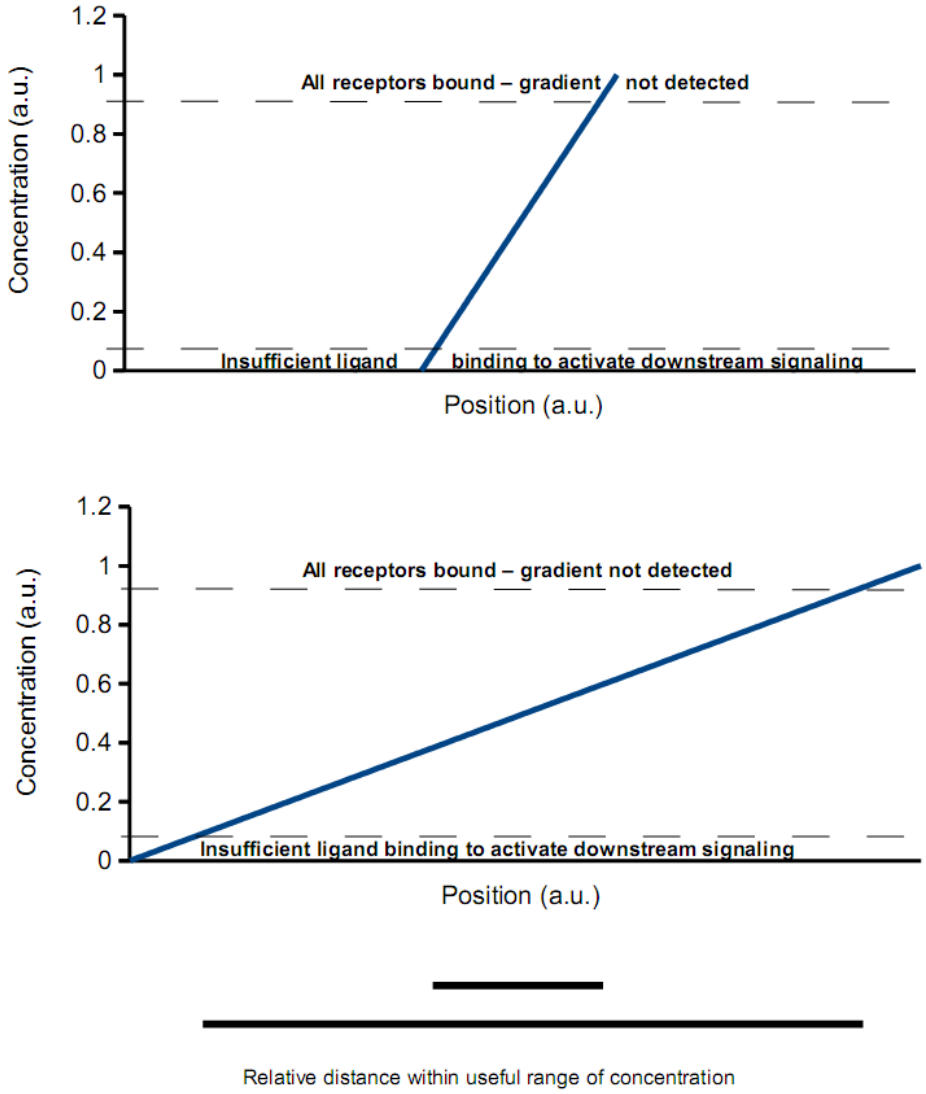

Figure III.4. Stretching the useful range of a concentration gradient. We consider an arbitrary concentration gradient where the high-end of the gradient is a concentration so high that it saturates the guidance receptors, and the low end of the gradient is of insufficient concentration to engage the downstream signaling pathways. When the minimum and maximum concentrations of the gradient are kept constant, and the gradient is stretched across 4x the distance, then the distance where a guidance cue is within a useful range of concentration is scaled proportionately.

Figure III.5. Influence of stretching a linear gradient on the gradient steepness. **A)** 3 sample linear concentration gradients are shown, each of which covers the same range of concentration, but span different distances of 1, 2 or 4 mm. **B)** Calculation of the gradient steepness at each position demonstrates that the range of steepness in each gradient is overlapping on the low end of the concentration gradient. This means that stretching the gradient across more space will lead to any additional distance having lower steepness values. Since the gradient steepness is a critical parameter for axon turning, then this will lead to larger portions of the gradient where the concentration is sufficient, but the steepness is too low to robustly guide axons. **C)** A replica of B where the overlapping plots have been nudged by 1% for clarity. Differences in the steepness in this plot are artificial, as the true values are overlapping as in B. Therefore, the steepness of the gradient places a constraint on how far a gradient can be stretched.

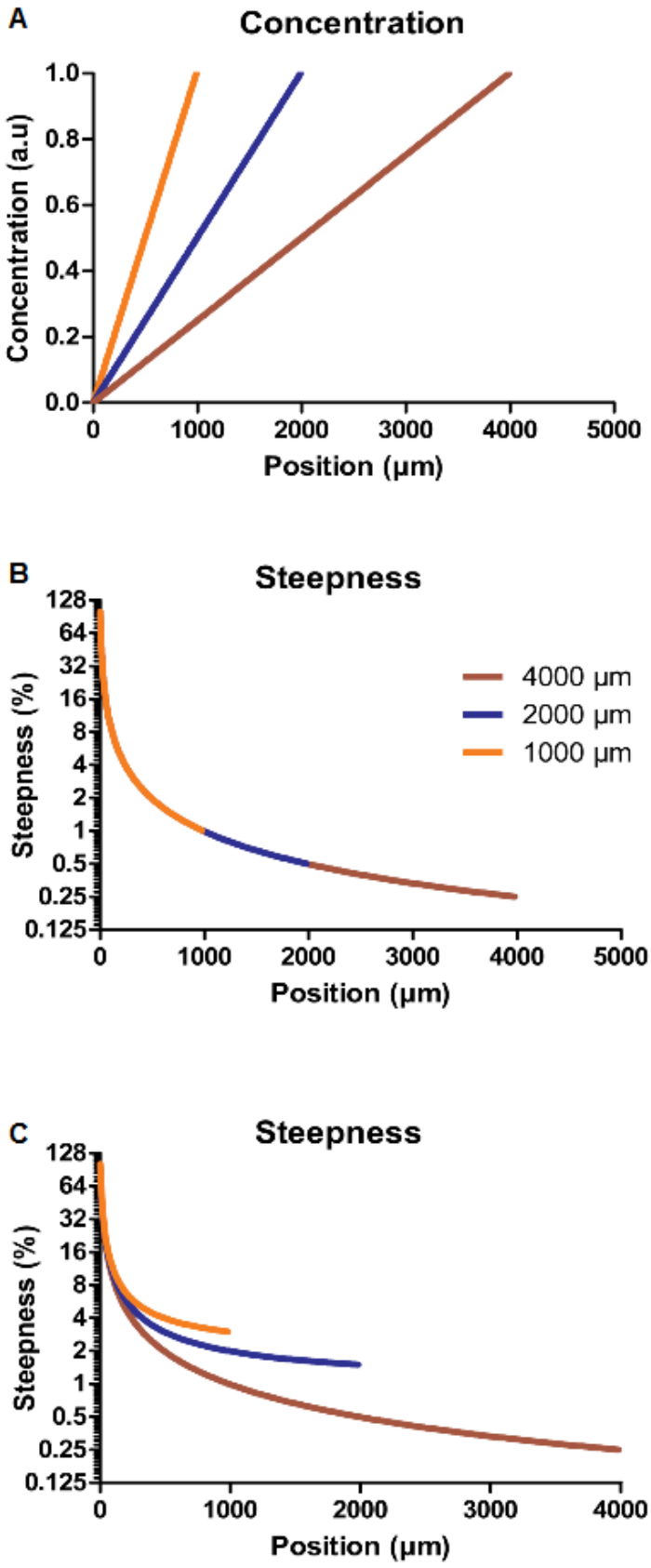
A
Concentration
Concentration (a.u)
1.0
0.8
0.6
0.4
0.2
0.0
0
1000
2000
3000
4000
5000
Position (µm)
B
Steepness
Steepness (%)
128
64
32
16
8
4
2
1
0.5
0.25
0.125
4000 µm
2000 µm
1000 µm
Position (µm)
C
Steepness
Steepness (%)
Position (µm)

the effective distance across which an axon can be guided. Using the steepness values from Figure II.5A, I estimate that over the course of the 45h assay, the single cue gradients begin to attract axons at $\delta \cong 1.8\%$, while the combined gradient begins to attract axons at $\delta \cong 1.4\%$. If we consider a linear gradient of an arbitrary length, I calculate that the second cue allows the axons to be guided for an additional distance of ~150 µm (Figure III.6A). Our finding that a combined gradient can attract axons over a longer distance is consistent with results obtained by Cao and Stoichet (Cao and Shoichet, 2003), where they estimate that DRG axons could be guided over longer distances by a combined NGF and NT-3 gradient than by a gradient of either cue alone. It is true that 150 µm is small on the scale of guidance conduits spanning centimeters, but it is large on the scale of the sub-millimeter pre-crossing commissural trajectory (Figure III.6B). I expect that this finding will be significant in the study of nerve regeneration following injury, where the distances that need be traversed are large, and even an incremental increase in the distance across which axons can be guided would be beneficial. It would be interesting to translate our finding to an animal model of spinal cord injury, where implantable patterned guidance conduits could be designed to optimally present overlapping guidance cue gradients in an attempt to maximize the distance that axons can be guided during recovery.

Although our finding is presently limited to one type of axon in the developing rodent spinal cord, it will be interesting to determine if steepness-limited synergy is a guidance strategy that will generalize to other systems where axons are guided across long distances, or to the chemotaxis behaviour of other cell types. I optimistically share in the century-old tradition in axon guidance research of expecting this phenomena to generalize, not only to other models of developing axons, but also to regenerating axons from the adult central nervous system.

It was precisely one hundred years ago that Cajal and Golgi shared the Nobel Prize in Physiology and Medicine for the discovery of discrete nerve elements. The past century has seen progress in neurobiology that would have left either man in need of a new pair of shorts. Neurosurgeons can sew together peripheral nerves and 3D-print axon scaffolds. Researchers can witness the ensemble of the axonal prominences of an organism in three-dimensional technicolor, seemingly blurring the boundaries between science and art. Cajal's annoyance with the

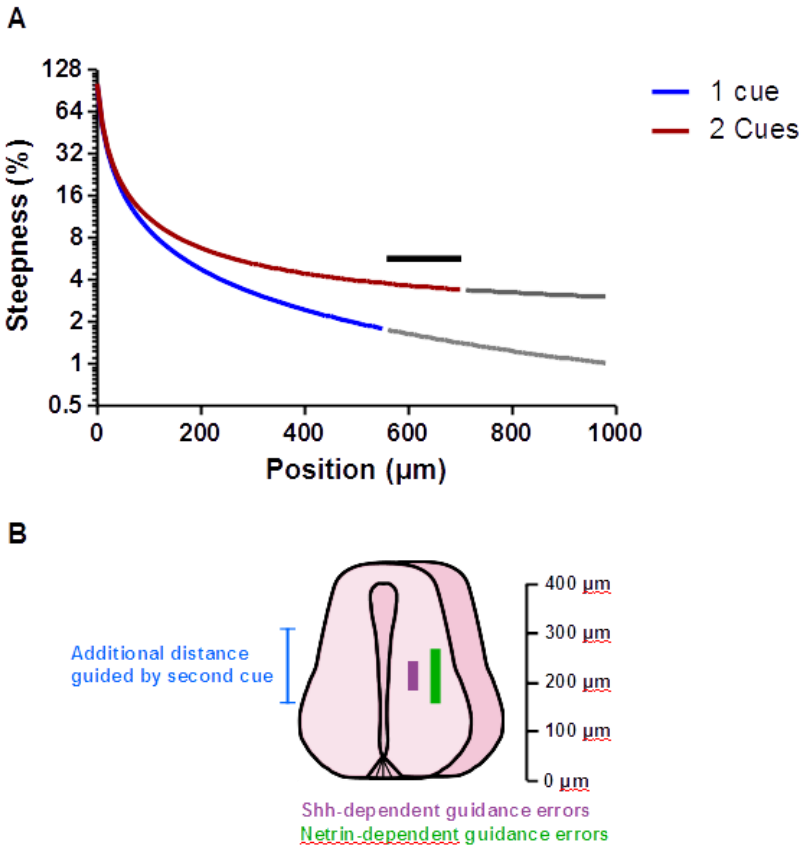

Figure III.6. Guidance distance is extended in the presence of a second guidance cue. **A)** Using the plots in Figure II.5A, I estimated the steepness value where the turned angle begins to increase, for each condition. Therefore, I estimate that the minimum perceptible steepness of a single guidance cue gradient to be approximately $\delta \cong 1.8\%$, and for a combined gradient to be approximately $\delta \cong 1.4\%$ (for a 45h guidance assay). The proportion of the single cue gradient that is above this value is plotted in blue, while the remaining length with δ below this value is plotted in grey. The proportion of the gradient that is above the threshold for two cues is plotted in red. Note, the red plot in A has been offset by 1% to avoid overlap, for clarity. The black line reflects the difference in the distance across which axons can be guided for the one cue and two cue scenarios. Therefore, our results suggest that the presence of a second, overlapping guidance cue could allow axons to be guided for an additional ~150 µm. **B)** To put this distance into the context of the developing spinal cord, the blue bar represents the additional distance of 150 µm that is gained by the presence of a second, overlapping guidance cue.

inadequacy of the tools of his time to test his chemotactic hypothesis has been countered with a multitude of techniques, generating terabytes of quantitative information of which we are presently only able to scratch the surface. A hundred years ago, not a single guidance cue was known, whereas a few decades of biochemistry is approaching a near-complete causal description from stimulus to response. We are in an age where a single-page schematic cannot contain all that is known about the convoluted promiscuity of the cell- signaling cascades. For this reason, the next hundred years will face a new challenge that is the inverse to that of Cajal's day; whereas the techniques at his disposal were insufficient to test his theory, soon the theoretical framework will need to be unified to clarify the marvelous, complex assembly of his discrete nerve elements.

Chapter IV: Bibliography

Afonso PV, Janka-Junttila M, Lee YJ, McCann CP, Oliver CM, Aamer KA, Losert W, Cicerone MT, Parent CA (2012) LTB4 is a signal-relay molecule during neutrophil chemotaxis. Dev Cell 22:1079-1091.

Ahmed G, Shinmyo Y, Ohta K, Islam SM, Hossain M, Naser IB, Riyadh MA, Su Y, Zhang S, Tessier-Lavigne M, Tanaka H (2011) Draxin inhibits axonal outgrowth through the netrin receptor DCC. J Neurosci 31:14018-14023.

Aratyn-Schaus Y, Gardel ML (2010) Transient frictional slip between integrin and the ECM in focal adhesions under myosin II tension. Curr Biol 20:1145-1153.

Augsburger A, Schuchardt A, Hoskins S, Dodd J, Butler S (1999) BMPs as mediators of roof plate repulsion of commissural neurons. Neuron 24:127-141.

Baier H, Bonhoeffer F (1992) Axon guidance by gradients of a target-derived component. Science 255:472-475.

Bard L, Boscher, C. Lambert, M. Mege, R.M., Choquet, D., and Thoumine,). (2008) A Molecular Clutch between the Actin Flow and N-Cadherin Adhesions Drives Growth Cone Migration. Journal of Neuroscience 28:5879-5890.

Bellaiche Y, The I, Perrimon N (1998) Tout-velu is a Drosophila homologue of the putative tumour suppressor EXT-1 and is needed for Hh diffusion. Nature 394:85-88.

Berg HC, Purcell EM (1977) Physics of chemoreception. Biophysical journal 20:193-219.

Bergmann S, Sandler O, Sberro H, Shnider S, Schejter E, Shilo BZ, Barkai N (2007) Pre-steady-state decoding of the Bicoid morphogen gradient. PLoS Biol 5:e46.

Bhattacharjee N, Li N, Keenan TM, Folch A (2010) A neuron-benign microfluidic gradient generator for studying the response of mammalian neurons towards axon guidance factors. Integr Biol (Camb) 2:669-679.

Bilioni A, Sanchez-Hernandez D, Callejo A, Gradilla AC, Ibanez C, Mollica E, Carmen Rodriguez-Navas M, Simon E, Guerrero I (2013) Balancing Hedgehog, a retention and release equilibrium given by Dally, Ihog, Boi and shifted/DmWif. Dev Biol 376:198-212.

Bin JM, Rajasekharan S, Kuhlmann T, Hanes I, Marcal N, Han D, Rodrigues SP, Leong SY, Newcombe J, Antel JP, Kennedy TE (2013) Full-length and fragmented netrin-1 in multiple sclerosis plaques are inhibitors of oligodendrocyte precursor cell migration. Am J Pathol 183:673-680.

Bonanomi D, Chivatakarn O, Bai G, Abdesselem H, Lettieri K, Marquardt T, Pierchala BA, Pfaff SL (2012) Ret is a multifunctional coreceptor that integrates diffusible- and contact-axon guidance signals. Cell 148:568-582.

Bornemann DJ, Duncan JE, Staatz W, Selleck S, Warrior R (2004) Abrogation of heparan sulfate synthesis in Drosophila disrupts the Wingless, Hedgehog and Decapentaplegic signaling pathways. Development 131:1927-1938.

Bourikas D, Pekarik V, Baeriswyl T, Grunditz A, Sadhu R, Nardo M, Stoeckli ET (2005) Sonic hedgehog guides commissural axons along the longitudinal axis of the spinal cord. Nat Neurosci 8:297-304.

Bouzigues C, Morel M, Triller A, Dahan M (2007) Asymmetric redistribution of GABA receptors during GABA gradient sensing by nerve growth cones analyzed by single quantum dot imaging. Proceedings of the National Academy of Sciences of the United States of America 104:11251-11256.

Bovolenta P, Dodd J (1990) Guidance of commissural growth cones at the floor plate in embryonic rat spinal cord. Development 109:435-447.

Briancon-Marjollet A, Ghogha A, Nawabi H, Triki I, Auziol C, Fromont S, Piche C, Enslen H, Chebli K, Cloutier JF, Castellani V, Debant A, Lamarche-Vane N (2008) Trio mediates netrin-1-induced Rac1 activation in axon outgrowth and guidance. Mol Cell Biol 28:2314-2323.

Briscoe J, Chen Y, Jessell TM, Struhl G (2001) A hedgehog-insensitive form of patched provides evidence for direct long-range morphogen activity of sonic hedgehog in the neural tube. Mol Cell 7:1279-1291.

Briscoe J, Pierani A, Jessell TM, Ericson J (2000) A homeodomain protein code specifies progenitor cell identity and neuronal fate in the ventral neural tube. Cell 101:435-445.
Briscoe J, Sussel L, Serup P, Hartigan-O'Connor D, Jessell TM, Rubenstein JL, Ericson J (1999) Homeobox gene Nkx2.2 and specification of neuronal identity by graded Sonic hedgehog signalling. Nature 398:622-627.
Brown CM, Hebert B, Kolin DL, Zareno J, Whitmore L, Horwitz AR, Wiseman PW (2006) Probing the integrin-actin linkage using high-resolution protein velocity mapping. J Cell Sci 119:5204-5214.
Buck KB, Zheng JQ (2002) Growth cone turning induced by direct local modification of microtubule dynamics. J Neurosci 22:9358-9367.
Burke R, Nellen D, Bellotto M, Hafen E, Senti KA, Dickson BJ, Basler K (1999) Dispatched, a novel sterol-sensing domain protein dedicated to the release of cholesterol-modified hedgehog from signaling cells. Cell 99:803-815.
Burnette DT, Schaefer AW, Ji L, Danuser G, Forscher P (2007) Filopodial actin bundles are not necessary for microtubule advance into the peripheral domain of Aplysia neuronal growth cones. Nat Cell Biol 9:1360-1369.
Butler SJ, Dodd J (2003) A role for BMP heterodimers in roof plate-mediated repulsion of commissural axons. Neuron 38:389-401.
Cajal SR (1892) La rétine des vertébrés. La Cellule 9:121-133.
Callejo A, Bilioni A, Mollica E, Gorfinkiel N, Andres G, Ibanez C, Torroja C, Doglio L, Sierra J, Guerrero I (2011) Dispatched mediates Hedgehog basolateral release to form the long-range morphogenetic gradient in the Drosophila wing disk epithelium. Proceedings of the National Academy of Sciences of the United States of America 108:12591-12598.
Camp D, Haitian He B, Li S, Althaus IW, Holtz AM, Allen BL, Charron F, van Meyel DJ (2014) Ihog and Boi elicit Hh signaling via Ptc but do not aid Ptc in sequestering the Hh ligand. Development 141:3879-3888.
Cao X, Shoichet MS (2003) Investigating the synergistic effect of combined neurotrophic factor concentration gradients to guide axonal growth. Neuroscience 122:381-389.
Capretto L, Cheng W, Hill M, Zhang X (2011) Micromixing within microfluidic devices. Top Curr Chem 304:27-68.
Cassimeris LU, Walker RA, Pryer NK, Salmon ED (1987) Dynamic instability of microtubules. Bioessays 7:149-154.
Chamberlain CE, Jeong J, Guo C, Allen BL, McMahon AP (2008) Notochord-derived Shh concentrates in close association with the apically positioned basal body in neural target cells and forms a dynamic gradient during neural patterning. Development 135:1097-1106.
Chamley JH, Dowel JJ (1975) Specificity of nerve fibre 'attraction' to autonomic effector organs in tissue culture. Exp Cell Res 90:1-7.
Charoy C, Nawabi H, Reynaud F, Derrington E, Bozon M, Wright K, Falk J, Helmbacher F, Kindbeiter K, Castellani V (2012) gdnf activates midline repulsion by Semaphorin3B via NCAM during commissural axon guidance. Neuron 75:1051-1066.
Charron F, Stein E, Jeong J, McMahon AP, Tessier-Lavigne M (2003) The morphogen sonic hedgehog is an axonal chemoattractant that collaborates with netrin-1 in midline axon guidance. Cell 113:11-23.
Chen MH, Li YJ, Kawakami T, Xu SM, Chuang PT (2004) Palmitoylation is required for the production of a soluble multimeric Hedgehog protein complex and long-range signaling in vertebrates. Genes Dev 18:641-659.
Ciepla P, Konitsiotis AD, Serwa RA, Masumoto N, Leong WP, Dallman MJ, Magee AI, Tate EW (2014) New chemical probes targeting cholesterylation of Sonic Hedgehog in human cells and zebrafish. Chem Sci 5:4249-4259.

Cohen M, Kicheva A, Ribeiro A, Blassberg R, Page KM, Barnes CP, Briscoe J (2015) Ptch1 and Gli regulate Shh signalling dynamics via multiple mechanisms. Nat Commun 6:6709.
Creanga A, Glenn TD, Mann RK, Saunders AM, Talbot WS, Beachy PA (2012) Scube/You activity mediates release of dually lipid-modified Hedgehog signal in soluble form. Genes Dev 26:1312-1325.
Dudanova I, Gatto G, Klein R (2010) GDNF acts as a chemoattractant to support ephrinA-induced repulsion of limb motor axons. Curr Biol 20:2150-2156.
Dudanova I, Klein R (2013) Integration of guidance cues: parallel signaling and crosstalk. Trends Neurosci 36:295-304.
Ebendal T, Jacobson CO (1977a) Tests of possible role of NGF in neurite outgrowth stimulation exerted by glial cells and heart explants in culture. Brain Res 131:373-378.
Ebendal T, Jacobson CO (1977b) Tissue explants affecting extension and orientation of axons in cultured chick embryo ganglia. Exp Cell Res 105:379-387.
Einstein A (1905) On the movements of small particles suspended in stationary liquids required by the molecular-kinetic theory of heat. Annalen der Physik 17:549-560.
Ensslen-Craig SE, Brady-Kalnay SM (2004) Receptor protein tyrosine phosphatases regulate neural development and axon guidance. Dev Biol 275:12-22.
Ericson J, Briscoe J, Rashbass P, van Heyningen V, Jessell TM (1997a) Graded sonic hedgehog signaling and the specification of cell fate in the ventral neural tube. Cold Spring Harb Symp Quant Biol 62:451-466.
Ericson J, Morton S, Kawakami A, Roelink H, Jessell TM (1996) Two critical periods of Sonic Hedgehog signaling required for the specification of motor neuron identity. Cell 87:661-673.
Ericson J, Muhr J, Jessell TM, Edlund T (1995a) Sonic hedgehog: a common signal for ventral patterning along the rostrocaudal axis of the neural tube. Int J Dev Biol 39:809-816.
Ericson J, Muhr J, Placzek M, Lints T, Jessell TM, Edlund T (1995b) Sonic hedgehog induces the differentiation of ventral forebrain neurons: a common signal for ventral patterning within the neural tube. Cell 81:747-756.
Ericson J, Rashbass P, Schedl A, Brenner-Morton S, Kawakami A, van Heyningen V, Jessell TM, Briscoe J (1997b) Pax6 controls progenitor cell identity and neuronal fate in response to graded Shh signaling. Cell 90:169-180.
Fazeli A, Dickinson SL, Hermiston ML, Tighe RV, Steen RG, Small CG, Stoeckli ET, Keino-Masu K, Masu M, Rayburn H, Simons J, Bronson RT, Gordon JI, Tessier-Lavigne M, Weinberg RA (1997) Phenotype of mice lacking functional Deleted in colorectal cancer (Dcc) gene. Nature 386:796-804.
Fick A (1855) V. On liquid diffusion. Philosophical Magazine Series 4 10:30-39.
Fisher PR, Merkl R, Gerisch G (1989) Quantitative analysis of cell motility and chemotaxis in Dictyostelium discoideum by using an image processing system and a novel chemotaxis chamber providing stationary chemical gradients. The Journal of cell biology 108:973-984.
Fuller D, Chen W, Adler M, Groisman A, Levine H, Rappel WJ, Loomis WF (2010) External and internal constraints on eukaryotic chemotaxis. Proceedings of the National Academy of Sciences of the United States of America 107:9656-9659.
Galko MJ, Tessier-Lavigne M (2000) Biochemical characterization of netrin-synergizing activity. J Biol Chem 275:7832-7838.
Gallet A, Ruel L, Staccini-Lavenant L, Therond PP (2006) Cholesterol modification is necessary for controlled planar long-range activity of Hedgehog in Drosophila epithelia. Development 133:407-418.
Gao X, Metzger U, Panza P, Mahalwar P, Alsheimer S, Geiger H, Maischein HM, Levesque MP, Templin M, Sollner C (2015) A Floor-Plate Extracellular Protein-Protein Interaction Screen Identifies Draxin as a Secreted Netrin-1 Antagonist. Cell Rep 12:694-708.

Giannone G, Mege RM, Thoumine O (2009) Multi-level molecular clutches in motile cell processes. Trends Cell Biol 19:475-486.
Gomez TM, Zheng JQ (2006) The molecular basis for calcium-dependent axon pathfinding. Nat Rev Neurosci 7:115-125.
Goodhill GJ (1997) Diffusion in axon guidance. Eur J Neurosci 9:1414-1421.
Goodhill GJ, Urbach JS (1999) Theoretical analysis of gradient detection by growth cones. J Neurobiol 41:230-241.
Gore BB, Wong KG, Tessier-Lavigne M (2008) Stem cell factor functions as an outgrowth-promoting factor to enable axon exit from the midline intermediate target. Neuron 57:501-510.
Govek EE, Newey SE, Van Aelst L (2005) The role of the Rho GTPases in neuronal development. Genes Dev 19:1-49.
Gundersen RW, Barrett JN (1979) Neuronal chemotaxis: chick dorsal-root axons turn toward high concentrations of nerve growth factor. Science 206:1079-1080.
Gundersen RW, Barrett JN (1980) Characterization of the turning response of dorsal root neurites toward nerve growth factor. The Journal of cell biology 87:546-554.
Gursky VV, Panok L, Myasnikova EM, Manu, Samsonova MG, Reinitz J, Samsonov AM (2011) Mechanisms of gap gene expression canalization in the Drosophila blastoderm. BMC Syst Biol 5:118.
Harrison RG (1910) The outgrowth of the nerve fiber as a mode of protoplasmic movement. The journal experimental zoology 9.
Hedgecock EM, Culotti JG, Hall DH (1990) The unc-5, unc-6, and unc-40 genes guide circumferential migrations of pioneer axons and mesodermal cells on the epidermis in C. elegans. Neuron 4:61-85.
Herzmark P, Campbell K, Wang F, Wong K, El-Samad H, Groisman A, Bourne HR (2007) Bound attractant at the leading vs. the trailing edge determines chemotactic prowess. Proceedings of the National Academy of Sciences of the United States of America 104:13349-13354.
Holley JA (1982) Early development of the circumferential axonal pathway in mouse and chick spinal cord. J Comp Neurol 205:371-382.
Iglesias PA (2012) Chemoattractant signaling in dictyostelium: adaptation and amplification. Sci Signal 5:pe8.
Isbister CM, Mackenzie PJ, To KC, O'Connor TP (2003) Gradient steepness influences the pathfinding decisions of neuronal growth cones in vivo. J Neurosci 23:193-202.
Ishii N, Wadsworth WG, Stern BD, Culotti JG, Hedgecock EM (1992) UNC-6, a laminin-related protein, guides cell and pioneer axon migrations in C. elegans. Neuron 9:873-881.
Islam SM, Shinmyo Y, Okafuji T, Su Y, Naser IB, Ahmed G, Zhang S, Chen S, Ohta K, Kiyonari H, Abe T, Tanaka S, Nishinakamura R, Terashima T, Kitamura T, Tanaka H (2009) Draxin, a repulsive guidance protein for spinal cord and forebrain commissures. Science 323:388-393.
Jay DG (2001) A Src-astic response to mounting tension. The Journal of cell biology 155:327-330.
Jeon NL, Stephan KW, Dertringer DT, Choi IS, Stroock AD, Whitesides G (2000) Generation of Solution and Surface Gradients Using Microfluidic Systems. Langmuir 16:8311-8316.
Jessell TM (2000) Neuronal specification in the spinal cord: inductive signals and transcriptional codes. Nat Rev Genet 1:20-29.
Jin T (2013) Gradient sensing during chemotaxis. Curr Opin Cell Biol 25:532-537.
Joanne Wang C, Li X, Lin B, Shim S, Ming GL, Levchenko A (2008) A microfluidics-based turning assay reveals complex growth cone responses to integrated gradients of substrate-bound ECM molecules and diffusible guidance cues. Lab Chip 8:227-237.
Keino-Masu K, Masu M, Hinck L, Leonardo ED, Chan SS, Culotti JG, Tessier-Lavigne M (1996) Deleted in Colorectal Cancer (DCC) encodes a netrin receptor. Cell 87:175-185.

Kennedy TE, Serafini T, de la Torre JR, Tessier-Lavigne M (1994) Netrins are diffusible chemotropic factors for commissural axons in the embryonic spinal cord. Cell 78:425-435.
Kennedy TE, Wang H, Marshall W, Tessier-Lavigne M (2006) Axon guidance by diffusible chemoattractants: a gradient of netrin protein in the developing spinal cord. J Neurosci 26:8866-8874.
Kent CB, Shimada T, Ferraro GB, Ritter B, Yam PT, McPherson PS, Charron F, Kennedy TE, Fournier AE (2010) 14-3-3 proteins regulate protein kinase a activity to modulate growth cone turning responses. J Neurosci 30:14059-14067.
Koh CG (2006) Rho GTPases and their regulators in neuronal functions and development. Neurosignals 15:228-237.
Kothapalli CR, van Veen E, de Valence S, Chung S, Zervantonakis IK, Gertler FB, Kamm RD (2011) A high-throughput microfluidic assay to study neurite response to growth factor gradients. Lab Chip 11:497-507.
Kundu A, Micholt L, Friedrich S, Rand DR, Bartic C, Braeken D, Levchenko A (2013) Superimposed topographic and chemical cues synergistically guide neurite outgrowth. Lab Chip 13:3070-3081.
Lander AD (2013) How cells know where they are. Science 339:923-927.
Langlois SD, Morin S, Yam PT, Charron F (2010) Dissection and culture of commissural neurons from embryonic spinal cord. J Vis Exp.
Lemons ML, Abanto ML, Dambrouskas N, Clements CC, Deloughery Z, Garozzo J, Condic ML (2013) Integrins and cAMP mediate netrin-induced growth cone collapse. Brain research 1537:46-58.
Letourneau PC (1983) Differences in the organization of actin in the growth cones compared with the neurites of cultured neurons from chick embryos. The Journal of cell biology 97:963-973.
Levchenko A, Iglesias PA (2002) Models of eukaryotic gradient sensing: application to chemotaxis of amoebae and neutrophils. Biophysical journal 82:50-63.
Li W, Lee J, Vikis HG, Lee SH, Liu G, Aurandt J, Shen TL, Fearon ER, Guan JL, Han M, Rao Y, Hong K, Guan KL (2004) Activation of FAK and Src are receptor-proximal events required for netrin signaling. Nat Neurosci 7:1213-1221.
Li X, Gao X, Liu G, Xiong W, Wu J, Rao Y (2008) Netrin signal transduction and the guanine nucleotide exchange factor DOCK180 in attractive signaling. Nat Neurosci 11:28-35.
Li X, Meriane M, Triki I, Shekarabi M, Kennedy TE, Larose L, Lamarche-Vane N (2002a) The adaptor protein Nck-1 couples the netrin-1 receptor DCC (deleted in colorectal cancer) to the activation of the small GTPase Rac1 through an atypical mechanism. J Biol Chem 277:37788-37797.
Li X, Saint-Cyr-Proulx E, Aktories K, Lamarche-Vane N (2002b) Rac1 and Cdc42 but not RhoA or Rho kinase activities are required for neurite outgrowth induced by the Netrin-1 receptor DCC (deleted in colorectal cancer) in N1E-115 neuroblastoma cells. The Journal of biological chemistry 277:15207-15214.
Liu G, Beggs H, Jurgensen C, Park HT, Tang H, Gorski J, Jones KR, Reichardt LF, Wu J, Rao Y (2004) Netrin requires focal adhesion kinase and Src family kinases for axon outgrowth and attraction. Nat Neurosci 7:1222-1232.
Long H, Sabatier C, Ma L, Plump A, Yuan W, Ornitz DM, Tamada A, Murakami F, Goodman CS, Tessier-Lavigne M (2004) Conserved roles for Slit and Robo proteins in midline commissural axon guidance. Neuron 42:213-223.
Lowery LA, Van Vactor D (2009) The trip of the tip: understanding the growth cone machinery. Nat Rev Mol Cell Biol 10:332-343.
Lumsden AG, Davies AM (1983) Earliest sensory nerve fibres are guided to peripheral targets by attractants other than nerve growth factor. Nature 306:786-788.
Lumsden AG, Davies AM (1986) Chemotropic effect of specific target epithelium in the developing mammalian nervous system. Nature 323:538-539.

Lyuksyutova AI, Lu CC, Milanesio N, King LA, Guo N, Wang Y, Nathans J, Tessier-Lavigne M, Zou Y (2003) Anterior-posterior guidance of commissural axons by Wnt-frizzled signaling. Science 302:1984-1988.
Maden M, Keen G, Jones GE (1998) Retinoic acid as a chemotactic molecule in neuronal development. Int J Dev Neurosci 16:317-322.
Mai J, Fok L, Gao H, Zhang X, Poo MM (2009) Axon initiation and growth cone turning on bound protein gradients. J Neurosci 29:7450-7458.
Medeiros NA, Burnette DT, Forscher P (2006) Myosin II functions in actin-bundle turnover in neuronal growth cones. Nat Cell Biol 8:215-226.
Meriane M, Tcherkezian J, Webber CA, Danek EI, Triki I, McFarlane S, Bloch-Gallego E, Lamarche-Vane N (2004) Phosphorylation of DCC by Fyn mediates Netrin-1 signaling in growth cone guidance. The Journal of cell biology 167:687-698.
Mitchison T, Kirschner M (1988) Cytoskeletal dynamics and nerve growth. Neuron 1:761-772.
Morel M, Shynkar V, Galas JC, Dupin I, Bouzigues C, Studer V, Dahan M (2012) Amplification and temporal filtering during gradient sensing by nerve growth cones probed with a microfluidic assay. Biophysical journal 103:1648-1656.
Morishita Y, Iwasa Y (2009) Accuracy of positional information provided by multiple morphogen gradients with correlated noise. Phys Rev E Stat Nonlin Soft Matter Phys 79:061905.
Mortimer D, Dayan P, Burrage K, Goodhill GJ (2011) Bayes-optimal chemotaxis. Neural Comput 23:336-373.
Mortimer D, Feldner J, Vaughan T, Vetter I, Pujic Z, Rosoff WJ, Burrage K, Dayan P, Richards LJ, Goodhill GJ (2009) Bayesian model predicts the response of axons to molecular gradients. Proceedings of the National Academy of Sciences of the United States of America 106:10296-10301.
Mortimer D, Fothergill T, Pujic Z, Richards LJ, Goodhill GJ (2008) Growth cone chemotaxis. Trends Neurosci 31:90-98.
Mortimer D, Pujic Z, Vaughan T, Thompson AW, Feldner J, Vetter I, Goodhill GJ (2010) Axon guidance by growth-rate modulation. Proceedings of the National Academy of Sciences of the United States of America 107:5202-5207.
Nawabi H, Briancon-Marjollet A, Clark C, Sanyas I, Takamatsu H, Okuno T, Kumanogoh A, Bozon M, Takeshima K, Yoshida Y, Moret F, Abouzid K, Castellani V (2010) A midline switch of receptor processing regulates commissural axon guidance in vertebrates. Genes Dev 24:396-410.
O'Connor MB, Umulis D, Othmer HG, Blair SS (2006) Shaping BMP morphogen gradients in the Drosophila embryo and pupal wing. Development 133:183-193.
Okada A, Charron F, Morin S, Shin DS, Wong K, Fabre PJ, Tessier-Lavigne M, McConnell SK (2006) Boc is a receptor for sonic hedgehog in the guidance of commissural axons. Nature 444:369-373.
Parra LM, Zou Y (2010) Sonic hedgehog induces response of commissural axons to Semaphorin repulsion during midline crossing. Nat Neurosci 13:29-35.
Perron JC, Dodd J (2011) Inductive specification and axonal orientation of spinal neurons mediated by divergent bone morphogenetic protein signaling pathways. Neural Dev 6:36.
Peters C, Wolf A, Wagner M, Kuhlmann J, Waldmann H (2004) The cholesterol membrane anchor of the Hedgehog protein confers stable membrane association to lipid-modified proteins. Proceedings of the National Academy of Sciences of the United States of America 101:8531-8536.
Phan KD, Hazen VM, Frendo M, Jia Z, Butler SJ (2010) The bone morphogenetic protein roof plate chemorepellent regulates the rate of commissural axonal growth. J Neurosci 30:15430-15440.
Poliak S, Morales D, Croteau LP, Krawchuk D, Palmesino E, Morton S, Jean-Francois C, Charron F, Dalva MB, Ackerman SL, Kao TJ, Kania A (2015) Synergistic integration of Netrin and ephrin axon guidance signals by spinal motor neurons. eLife 4.

Pujic Z, Giacomantonio CE, Unni D, Rosoff WJ, Goodhill GJ (2008) Analysis of the growth cone turning assay for studying axon guidance. J Neurosci Methods 170:220-228.
Ren XR, Ming GL, Xie Y, Hong Y, Sun DM, Zhao ZQ, Feng Z, Wang Q, Shim S, Chen ZF, Song HJ, Mei L, Xiong WC (2004) Focal adhesion kinase in netrin-1 signaling. Nat Neurosci 7:1204-1212.
Reversade B, De Robertis EM (2005) Regulation of ADMP and BMP2/4/7 at opposite embryonic poles generates a self-regulating morphogenetic field. Cell 123:1147-1160.
Robles E, Woo S, Gomez TM (2005) Src-dependent tyrosine phosphorylation at the tips of growth cone filopodia promotes extension. J Neurosci 25:7669-7681.
Roelink H, Porter JA, Chiang C, Tanabe Y, Chang DT, Beachy PA, Jessell TM (1995) Floor plate and motor neuron induction by different concentrations of the amino-terminal cleavage product of sonic hedgehog autoproteolysis. Cell 81:445-455.
Rosoff WJ, Urbach JS, Esrick MA, McAllister RG, Richards LJ, Goodhill GJ (2004) A new chemotaxis assay shows the extreme sensitivity of axons to molecular gradients. Nat Neurosci 7:678-682.
Ruiz de Almodovar C, Fabre PJ, Knevels E, Coulon C, Segura I, Haddick PC, Aerts L, Delattin N, Strasser G, Oh WJ, Lange C, Vinckier S, Haigh J, Fouquet C, Gu C, Alitalo K, Castellani V, Tessier-Lavigne M, Chedotal A, Charron F, Carmeliet P (2011) VEGF mediates commissural axon chemoattraction through its receptor Flk1. Neuron 70:966-978.
Schilling TF (2008) Anterior-posterior patterning and segmentation of the vertebrate head. Integr Comp Biol 48:658-667.
Schwank G, Dalessi S, Yang SF, Yagi R, de Lachapelle AM, Affolter M, Bergmann S, Basler K (2011) Formation of the long range Dpp morphogen gradient. PLoS Biol 9:e1001111.
Segal RA (2003) Selectivity in neurotrophin signaling: theme and variations. Annu Rev Neurosci 26:299-330.
Serafini T, Colamarino SA, Leonardo ED, Wang H, Beddington R, Skarnes WC, Tessier-Lavigne M (1996) Netrin-1 is required for commissural axon guidance in the developing vertebrate nervous system. Cell 87:1001-1014.
Serafini T, Kennedy TE, Galko MJ, Mirzayan C, Jessell TM, Tessier-Lavigne M (1994) The netrins define a family of axon outgrowth-promoting proteins homologous to C. elegans UNC-6. Cell 78:409-424.
Servant G, Weiner OD, Neptune ER, Sedat JW, Bourne HR (1999) Dynamics of a chemoattractant receptor in living neutrophils during chemotaxis. Mol Biol Cell 10:1163-1178.
Shekarabi M, Kennedy TE (2002) The netrin-1 receptor DCC promotes filopodia formation and cell spreading by activating Cdc42 and Rac1. Mol Cell Neurosci 19:1-17.
Shekarabi M, Moore SW, Tritsch NX, Morris SJ, Bouchard JF, Kennedy TE (2005) Deleted in colorectal cancer binding netrin-1 mediates cell substrate adhesion and recruits Cdc42, Rac1, Pak1, and N-WASP into an intracellular signaling complex that promotes growth cone expansion. J Neurosci 25:3132-3141.
Sloan TF, Qasaimeh MA, Juncker D, Yam PT, Charron F (2015) Integration of shallow gradients of shh and netrin-1 guides commissural axons. PLoS Biol 13:e1002119.
Sperry RW (1963) CHEMOAFFINITY IN THE ORDERLY GROWTH OF NERVE FIBER PATTERNS AND CONNECTIONS. Proceedings of the National Academy of Sciences of the United States of America 50:703-710.
Stein E, Tessier-Lavigne M (2001) Hierarchical organization of guidance receptors: silencing of netrin attraction by slit through a Robo/DCC receptor complex. Science 291:1928-1938.
Suter DM, Forscher P (2000) Substrate-cytoskeletal coupling as a mechanism for the regulation of growth cone motility and guidance. J Neurobiol 44:97-113.
Suter DM, Forscher P (2001) Transmission of growth cone traction force through apCAM-cytoskeletal linkages is regulated by Src family tyrosine kinase activity. The Journal of cell biology 155:427-438.

Suter DM, Schaefer AW, Forscher P (2004) Microtubule dynamics are necessary for SRC family kinase-dependent growth cone steering. Curr Biol 14:1194-1199.
Takei Y, Ozawa Y, Sato M, Watanabe A, Tabata T (2004) Three Drosophila EXT genes shape morphogen gradients through synthesis of heparan sulfate proteoglycans. Development 131:73-82.
Taylor AM, Menon S, Gupton SL (2015) Passive microfluidic chamber for long-term imaging of axon guidance in response to soluble gradients. Lab Chip 15:2781-2789.
Tessier-Lavigne M, Placzek M (1991) Target attraction: are developing axons guided by chemotropism? Trends Neurosci 14:303-310.
Tessier-Lavigne M, Placzek M, Lumsden AG, Dodd J, Jessell TM (1988) Chemotropic guidance of developing axons in the mammalian central nervous system. Nature 336:775-778.
Tian H, Callahan CA, DuPree KJ, Darbonne WC, Ahn CP, Scales SJ, de Sauvage FJ (2009) Hedgehog signaling is restricted to the stromal compartment during pancreatic carcinogenesis. Proceedings of the National Academy of Sciences of the United States of America 106:4254-4259.
Tukachinsky H, Kuzmickas RP, Jao CY, Liu J, Salic A (2012) Dispatched and scube mediate the efficient secretion of the cholesterol-modified hedgehog ligand. Cell Rep 2:308-320.
van Haastert PJ, Postma M (2007) Biased random walk by stochastic fluctuations of chemoattractant-receptor interactions at the lower limit of detection. Biophysical journal 93:1787-1796.
Vitriol EA, Zheng JQ (2012) Growth cone travel in space and time: the cellular ensemble of cytoskeleton, adhesion, and membrane. Neuron 73:1068-1081.
von Philipsborn AC, Lang S, Bernard A, Loeschinger J, David C, Lehnert D, Bastmeyer M, Bonhoeffer F (2006) Microcontact printing of axon guidance molecules for generation of graded patterns. Nat Protoc 1:1322-1328.
Wolf AM, Lyuksyutova AI, Fenstermaker AG, Shafer B, Lo CG, Zou Y (2008) Phosphatidylinositol-3-kinase-atypical protein kinase C signaling is required for Wnt attraction and anterior-posterior axon guidance. J Neurosci 28:3456-3467.
Xiao RR, Wang L, Zhang L, Liu YN, Yu XL, Huang WH (2014) Quantifying biased response of axon to chemical gradient steepness in a microfluidic device. Anal Chem 86:11649-11656.
Xiao RR, Zeng WJ, Li YT, Zou W, Wang L, Pei XF, Xie M, Huang WH (2013) Simultaneous generation of gradients with gradually changed slope in a microfluidic device for quantifying axon response. Anal Chem 85:7842-7850.
Xiong F, Tentner AR, Huang P, Gelas A, Mosaliganti KR, Souhait L, Rannou N, Swinburne IA, Obholzer ND, Cowgill PD, Schier AF, Megason SG (2013) Specified neural progenitors sort to form sharp domains after noisy Shh signaling. Cell 153:550-561.
Xu J, Rosoff WJ, Urbach JS, Goodhill GJ (2005) Adaptation is not required to explain the long-term response of axons to molecular gradients. Development 132:4545-4552.
Xu K, Wu Z, Renier N, Antipenko A, Tzvetkova-Robev D, Xu Y, Minchenko M, Nardi-Dei V, Rajashankar KR, Himanen J, Tessier-Lavigne M, Nikolov DB (2014) Neural migration. Structures of netrin-1 bound to two receptors provide insight into its axon guidance mechanism. Science 344:1275-1279.
Yam PT, Charron F (2013) Signaling mechanisms of non-conventional axon guidance cues: the Shh, BMP and Wnt morphogens. Curr Opin Neurobiol 23:965-973.
Yam PT, Kent CB, Morin S, Farmer WT, Alchini R, Lepelletier L, Colman DR, Tessier-Lavigne M, Fournier AE, Charron F (2012) 14-3-3 proteins regulate a cell-intrinsic switch from sonic hedgehog-mediated commissural axon attraction to repulsion after midline crossing. Neuron 76:735-749.
Yam PT, Langlois SD, Morin S, Charron F (2009) Sonic hedgehog guides axons through a noncanonical, Src-family-kinase-dependent signaling pathway. Neuron 62:349-362.
Yamauchi K, Varadarajan SG, Li JE, Butler SJ (2013) Type Ib BMP receptors mediate the rate of commissural axon extension through inhibition of cofilin activity. Development 140:333-342.

Yan D, Wu Y, Yang Y, Belenkaya TY, Tang X, Lin X (2010) The cell-surface proteins Dally-like and Ihog differentially regulate Hedgehog signaling strength and range during development. Development 137:2033-2044.
Yuan J, Chan S, Mortimer D, Nguyen H, Goodhill GJ (2013) Optimality and saturation in axonal chemotaxis. Neural Comput 25:833-853.
Zhou FQ, Cohan CS (2004) How actin filaments and microtubules steer growth cones to their targets. J Neurobiol 58:84-91.
Zhou S, Lo WC, Suhalim JL, Digman MA, Gratton E, Nie Q, Lander AD (2012) Free extracellular diffusion creates the Dpp morphogen gradient of the Drosophila wing disc. Curr Biol 22:668-675.
Zicha D, Dunn GA, Brown AF (1991) A new direct-viewing chemotaxis chamber. J Cell Sci 99 (Pt 4):769-775.
Zigmond SH (1981) Consequences of chemotactic peptide receptor modulation for leukocyte orientation. The Journal of cell biology 88:644-647.
Zigmond SH (1988) Orientation chamber in chemotaxis. Methods Enzymol 162:65-72.
Zou Y, Stoeckli E, Chen H, Tessier-Lavigne M (2000) Squeezing axons out of the gray matter: a role for slit and semaphorin proteins from midline and ventral spinal cord. Cell 102:363-375.

Appendix

Appendix.1. Detailed Experimental Protocol for *le Massif* assay

Appendix.1.i. Preparation of microfluidic devices and commissural neuron culture

During the week prior to commissural neuron dissection and dissociation:

1. Acid wash the glass microscopy slides in Nitric Acid for 24-36h, followed by 12 washes in *Milli-Q* water and heating at 225°C for 4-6h.
2. Mix PDMS polymer base and curing agent at a ratio of 10:1. *Use the mass rather than the volume to be more precise in the measurements. For one batch of devices (to cover one wafer), approximately 70 ml of solution is needed*. Stir thoroughly for 3-5 minutes, otherwise there is a risk of incomplete crosslinking.
3. Pour the uncured PDMS onto the silicone master wafer (in a pie plate) and allow the solution to cover the entire area. *The solution will be full of bubbles.* Place the plate with uncured PDMS into a vacuum desiccator, and allow 10-15 minutes for all bubbles to be removed from the uncured PDMS. *At this point it should be entirely transparent.*
4. Place the plate on a level shelf inside an oven and keep for at least 3 days at 60°C (Appendix Fig. 1A). *If left for too short a period of time, there will remain un-crosslinked PDMS that will decrease the viability of the neurons at a later step.*
5. Once cured, cut around the wafer with a blade, and use a metal spatula to carefully lift the cured PDMS away from the silicon wafer (Appendix Fig. 1B). *Be patient and delicate, the wafer can crack and break with excess pressure, and are expensive to replace.*
6. Place the cut-out piece of cured PDMS on a cutting board with the features facing up (Appendix Fig. 1C). Position your head at an angle with respect to the PDMS and a light source that allows you to see the fine details of the replicated features. *This step takes some getting used to, but it is possible to be quite accurate without any magnification*. Cut along the lines that demarcate each device, to result in rectangular PDMS chips (Appendix Fig. 2A).

7. Using a 4mm diameter biopsy punch, punch holes at the outlet and both inlets (Appendix Fig. 1D). Avoid punching the inlet holes too close to one another or to the edges of the chip – both of which could result in leakage (Appendix Fig. 2B).

<u>On the day prior to commissural neuron dissection and dissociation:</u>

8. Craft culture media reservoirs by cutting the 2-3 mm from the bottom of PCR tubes, and then cut the plastic piece that connects the sets of 8 tubes (Appendix Fig. 2C). Cut and store them in a 50 ml falcon tube within the culture hood within to maintain their sterility. *Plan accordingly so as to have 2 reservoirs for each device to be fabricated, and several extras to replace any faulty ones.*
9. Prepare a 0.1 µg/ml solution of Poly-D-Lysine by diluting the stock concentration in sterile *Milli-Q* water. Keep the solution cold while transporting.
10. Place two PDMS chips (features facing up) and two acid washed glass slides into a large petri dish, and label the glass slide close to the short edge with a fine-tipped sharpie marker.
11. Remove the top of the petri dish and expose samples to a gas plasma for 1 minute (Appendix Fig. 1E). Observe the plasma chamber through the observation window to confirm that a purple haze is generated within the chamber.
12. Replace lid carefully and remove samples from the plasma chamber. Be sure not to allow the Petri dish lid to touch the surface of the PDMS chips. Carefully, transport them to a tissue culture hood for bonding.
13. To bond the surfaces, carefully align the rectangular-shaped PDMS chip (features face-down) with the glass slide, ensuring that the punched holes are not too close to the edges of the glass slide (Appendix Fig. 1F). Bring the two surfaces into contact, and then press lightly on the area of the PDMS chip not containing features to remove any trapped air bubbles from between the glass and PDMS (Appendix Fig. 1G). Let the devices sit in the culture hood until all devices from this batch have been assembled.

14. After all devices have been assembled, use a 3ml syringe with a needle and syringe filter to fill the punched hole at the outlet with PDL solution (Appendix Fig. 1H). Repeat for all devices in this batch.
15. Check each device for bubbles trapped in the gradient chamber. If there are air bubbles, then proceed to fill both punched holes at the inlets with PDL solution. Remove the needle and filter from the syringe and place the luer tip firmly within the hole punched at the outlet (should be a perfect fit). Dislodge bubbles by pulling up on the plunger to aspirate PDL solution through the microfluidic device.
16. Once all devices have been loaded and cleared of bubbles, start timer for 1h PDL surface treatment.
17. After 1h, return the devices to a culture hood and remove the PDL solution from the inlets and outlets. Place 50 µl of sterile *Milli-Q* water into each inlet and outlet to rinse the residual PDL. Repeat 3x.
18. Install the PCR-tube reservoirs into the punched holes of the inlets for each device. *Be gentle and try to avoid twisting too much as this may cause the area around the punch to come unbound, which may cause leaks.* Remove any remaining water from within the punched holes by aspiration.
19. Place 200 µl of culture media containing heat-inactivated fetal bovine serum into each of the inlet reservoirs, and then place the devices into the 5% CO2 incubator overnight (Appendix Fig. 1I).

<u>On the day of commissural dissection and dissociation:</u>

20. The following morning, check each of the devices for leaks. If media has spilled from the device to the petri dish, or if one of the reservoirs appears emptier than the others, then dispose of this device entirely. *It is highly likely that this device will fail to generate a gradient.*
21. Remove the plating media from the inlet reservoirs and the punched hole at the outlet for each device, and replace with fresh serum-containing media (Appendix Fig. 1J). *It is*

not necessary to remove and replace the media of one device before moving on to the next. For efficiency, it is preferable to remove the media from all devices before adding media to each.

22. Return the devices to the incubator until the commissural preparation is ready. At this point, dissect and dissociate the commissural neurons of e13.5 rat embryos (Langlois et al., 2012).
23. After counting the neurons to determine the dissociation yield, concentrate the cell suspension to a density of 3,500,000 to 5,000,000 cells/ml. You will need ~ 40 µl for each device. Centrifuge the neuron suspension for 5 min at 1000 rpm, then remove the supernatant and add the appropriate amount of plating media to give the final concentration.
24. Retrieve the devices from the incubator and bring them to the culture hood. Remove most of the media from each of the inlet reservoirs, leaving ~50 µl in each. Remove one of the reservoirs for each device, and set it nearby in the Petri dish. Remove entirely the media that has accumulated in the punched hole at the outlet for each device.
25. Add 40 µl of concentrated cell suspension to the outlet of the device (Appendix Fig. 1K). Observe the chamber of the device with a 10x or 20x objective, and firmly position a 3-5 ml syringe at the punched hole at the inlet where the reservoir has been removed. Withdraw the plunger of a syringe to induce a flow within the microfluidic device, and observe the influx of neurons being pulled into the gradient chamber of the device (Appendix Fig. 1L). Once the cells have filled the gradient chamber, remove the syringe from the punched inlet hole, and return the device to the incubator. *This step can be long if you process one device at a time. I recommend processing a large petri dish with maximum of 5 devices simultaneously to avoid delays imposed by switching tools.*
26. Allow 4-6 hours for the neurons to adhere to the PDL-glass substrate (Appendix Fig. 1M). Once the neurons have attached, remove the remaining media from the inlet reservoirs and punched hole at the outlet and replace the reservoirs in the punched holes at the inlets. If performing a 45h assay, skip directly to step 29. Otherwise, fill the

reservoirs with fresh serum-containing media return the devices to the incubator overnight.

On the day after plating commissural neurons within the devices:

27. Observe each the chamber of each device with a 20x objective to judge the state of the neuron health and maturity. *Often at this time you will see several long axons and growth cones, but if not then it is not necessarily a cause for concern, as there is variability between the age of neurons from commissural preparation to the next.*
28. Remove the plating media from the inlet reservoirs and the punched hole at the outlet for each device, and replace the media with culture media without serum, supplemented with B27. *Again, it is not necessary to remove and replace the media of one device before moving onto the next. For efficiency, it is preferable to remove the media from all devices before adding media to each. There is enough residual media in the device that there is negligible risk to the neurons.*

Appendix.1.ii. *le Massif* microfluidic guidance assay

29. Prepare the reagents for use in the guidance assay in Eppendorf tubes*. Each experiment will consume 200 µl of guidance cue solution and 200 µl of culture media. Be sure to have the some volume of guidance cue solution and culture media without guidance cue readily available, preferably each in Eppendorf tubes.*
30. Begin the guidance assay by removing the growth media from the inlet reservoirs and the punched hole at the outlet, and adding the culture media and guidance cue solution to the reservoirs (Appendix Fig. 1N).

    Note*: The order is important: The culture media without guidance cue must be added first; if you add the guidance cue solution before adding the media without cue, all neurons will be briefly exposed to a bath application of high-concentration ligand.*

    Note: *Precisely when the guidance assay is started depends on the assay length. For 45h assays, the gradients are applied on the same day as the dissection and dissociation,*

using media containing serum. The following morning, gradients are replaced with the same concentration of guidance cue in media without serum, supplemented with B27. For a 24 h assay, gradients are applied the day after dissection/dissociation, in which case the guidance cue is diluted directly in media without serum, supplemented with B27.

31. After the guidance cue has been added, ensure that the fluid height in each pair of reservoirs is approximately equal. Return the devices carefully to the incubator and ensure that the petri dish containing them are level. *Do not stack petri dishes on top of one another, as this could lead to disruptions of the gradient profile.*
32. Before leaving the lab in the evening, bring the devices to the culture hood, and remove the media that has accumulated in the punched hole of the outlet. *This will delay the eventual change in gradient shape that will occur as the outlet begins to fill with media, and the flow rate through the device slows down proportionally.*
33. The following morning, repeat the last step to remove the media that has accumulated in the punched hole at the outlet. Return the devices to the incubator for the remainder of the assay (24h or 45h from the time the assay started).
34. Prepare 4% PFA and heating it to 37°C in a water bath. *Since the volumes required are quite small, it is preferable to have several 1.5 ml aliquots of 4% PFA available.*
35. To end the assay, remove the media from the punched hole at the outlet, and from both inlet reservoirs, respectively. Transfer one of the inlet reservoirs to the outlet, and insert it carefully, as done previously when installing them in the inlet. Transfer the devices from the culture hood to a bench, and add 100 µl of 4% PFA to the outlet reservoir of each device (Appendix Fig. 1O). *Never use PFA in the culture hood or incubator.*
36. Allow 15 min at room temperature for the fixative to act on the neurons, then remove the PFA from each outlet reservoir and replace with 200 µl of PBS.
37. If you are going to perform immunocytochemistry on these samples, now would be the time to block with PBST + 10% serum for 30 mins. Otherwise, proceed to next step.

38. Prepare the staining buffer with Rhodamine-Phalloidin (1/250) and Dapi (1/10,000) in PBS. If performing immunocytochemistry, prepare instead the 1° antibody buffer solution and add Dapi to this. Add 100 µl of the staining buffer solution to the outlet reservoir of each device (Appendix Fig. 1P), and return the devices to the large petri dish that was used to transport them to and from the incubator. Add one damp Kimwipe to each petri dish (5 devices), and seal the top and bottom lids of the petri dish with Parafilm to avoid evaporation. Stack all petri dishes used in the current experiment and wrap them in aluminum foil to minimize light exposure. Store overnight at 4°C.
39. Image the samples on an inverted fluorescent microscope (Appendix Fig. 1Q). If possible, use an automated high-content screening microscope to image chambers with speed and consistency. As an alternative, an inverted epi-fluorescent microscope with an automated stage would be sufficient, so long as the stage coordinates are stored in the image metadata.

Appendix Fig. 1. Microfluidic device fabrication and experimental paradigm**. A)** PDMS is poured onto a silicon wafer and cured > 3 days at 60°C. **B)** Cured PDMS is removed from the wafer and **C)** inverted such that the features are always facing up. **D)** The PDMS replica is cut into individual units, and holes are punched at the position of the inlets and outlet. See Figure 2 for specific details. **E)** PDMS chips (features facing up) and acid-washed glass slides are exposed to a gas plasma for 1 min. **F)** Plasma activated surfaces are brought into contact (features facing down) to form an irreversible bond **(G)** which has the added benefit of making the PDMS hydrophilic. **H)** 100 µl of Poly-D-Lysine solution is added to the outlet, such that the liquid fills the microfluidic channels by capillary forces. The solution is allowed to coat the substrate for 1h, is then removed and the devices are rinsed with *Milli-Q* water. **I)** PCR tube reservoirs are added and filled with culture media to drive a forward flow. Devices are left in an incubator overnight to continue to rinse. **J)** Culture media is replaced 2h prior to completion of the commissural neuron dissection. **K)** Dissociated neurons are re-suspended to a very high concentration, and the cell suspension is added to the outlet. **L)** A rubber hose attached to a syringe is placed into one of the punched holes at the inlet (or alternatively the syringe is pressed firmly against the PDMS) and the plunger is withdrawn to pull the cells into the gradient chamber. **M)** Neurons are allowed 4-6h to adhere to the PDL-coated glass substrate. **N)** A forward flow is generated by adding 200 µl of fresh serum-containing media to both reservoirs. The guidance assay can be started at this point (for a 45 hour assay), or alternatively the devices can be left in culture media in the incubator overnight and the assay started the following day (for a 24 hour assay). To begin the guidance assay, the guidance cue is diluted in 200 µl of culture media. The same volume of culture media with no guidance cue is added to one reservoir while the other is filled with the guidance cue solution, in this order. **O)** After 24 or 45h, the fluid is removed from inlets and outlet, and one of the reservoirs is placed in the outlet. 100 µl of 4% PFA diluted in PBS is added to the outlet reservoir for 15 min. **P)** The PFA is removed from the outlet reservoir and replaced with a staining buffer containing Dapi to stain cell nuclei and Rhodamine-conjugated Phalloidin to stain F-actin. **Q)** After staining overnight, the buffer is replaced with PBS, and the chambers are imaged on an inverted fluorescent microscope. In all panels, the arrows represent the direction of fluid flow.

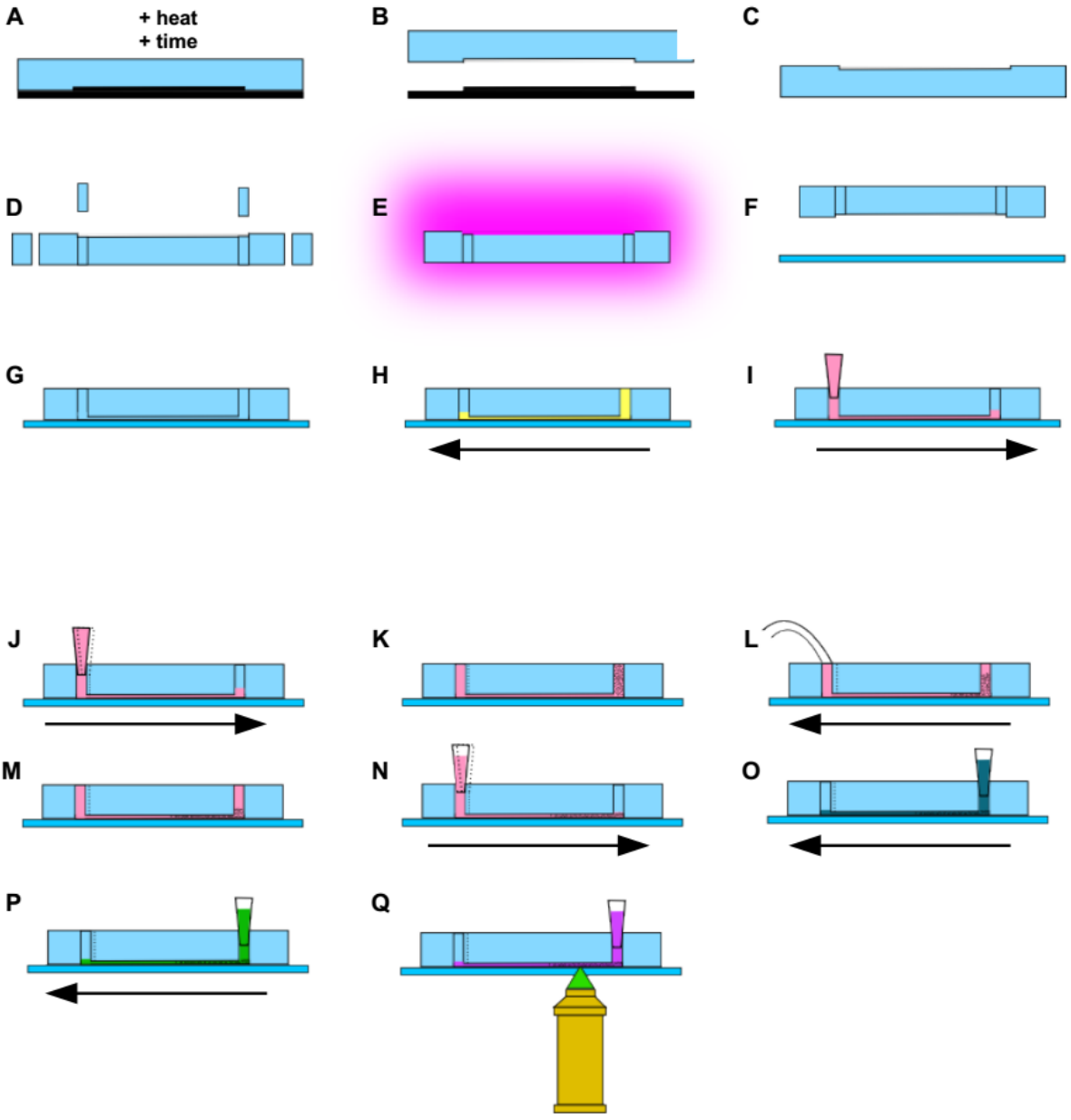
A
+ heat
+ time
B
C
D
E
F
G
H
I
J
K
L
M
N
O
P
Q

Appendix Fig. 2. Preparation of PDMS microfluidic gradient generators. **A)** Each silicon wafer contains 5 copies of the *le Massif* gradient generator, separated by rectangular bounding boxes which indicate the size of a standard glass microscopy slide (2.5cm x 7.5cm). Each individual gradient device is cut out along these lines. **B)** A 4 mm diameter biopsy punch is used to create through-holes for the inlets and the outlet. Holes are punched as indicated by the dashed red circles. Special attention must be made to avoid punching the two holes too close to one another, or too close to either long edge of the PDMS chip. The blue arrows indicate the critical areas where to be cautious to avoid a higher risk of the device leaking, negatively influencing the gradient profile. **C)** PCR tubes are used to craft fluid reservoirs, which allow for a hydrostatic, pressure-driven flow to keep the liquid moving through the microfluidic channels. The dashed red lines indicate where the tubes are cut to separate them from one another, and to allow the solution to flow into the fluidic network.

A

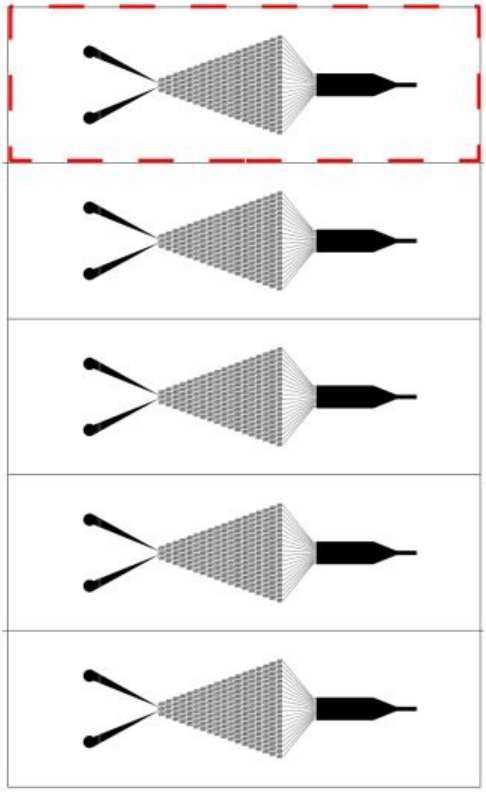

B

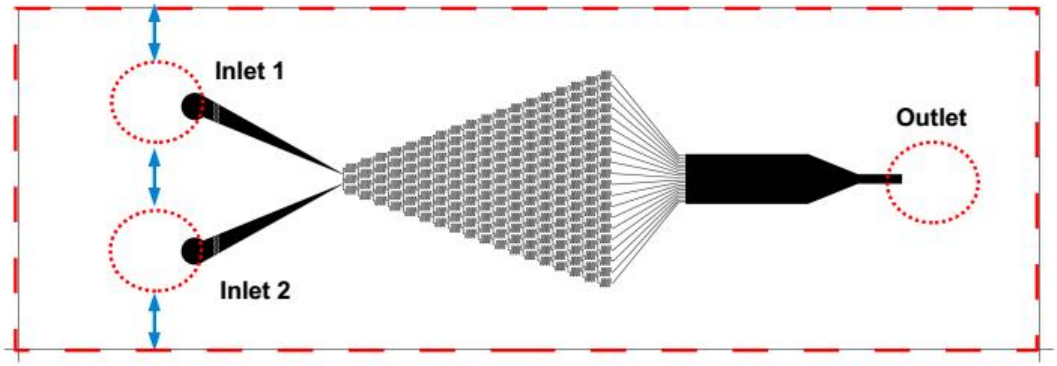

C

Appendix.2. Quantitative analysis of microscopy images

This section provides a detailed description of the process flow for the quantitative analyses described superficially in Chapter II. I will first outline a brief account of the overall process, followed by a more detailed account of each step of the analysis. For a copy of the complete file in its original format (*.ijm or *.m), please contact the author at: Tyler DOT Sloan AT mail DOT mcgill DOT ca.

Appendix.2.i. Measurement of turned angle and calculation of the concentration and ΔC/C

After imaging the gradient chambers with a high-content screening microscope, each chamber produced 275-300 individual photomicrographs, each with two fluorescent channels. The first channel contains Dapi signal, used to indicate the location of the cell body (Appendix Fig. 3A), while the second channel contains Rhodamine-Phalloidin signal, for axon tracing (Appendix Fig. 3B). The filenames contain no information regarding the experimental conditions, such that it is possible for the investigator to remain blind to the experimental conditions until all chambers have been analyzed. The images are acquired in such a manner that the first image always contains the upper-left hand corner of the gradient chamber, so that the relative offsets can be calculated for each individual gradient chamber, to account for inter-experimental variability.

Briefly, the investigator uses the Dapi staining to identify the center of the cell body of a neuron with an isolated axon. He then draws a line along the axon, from the cell body to the axon tip. Measurements are recorded into an imageJ results file for each neuron in the experiment. After all of the images from the related gradient chamber have been analyzed in this way, another imageJ macro is used to condense the imageJ results into an easily-accessible format, where the data for each neuron occupy a single row of the text file. This data includes the length of the axon, the position of the cell body and the growth cone, as well as the axon base and axon tip angles.

The offset of the gradient chamber in the first image and the angle it is rotated as compared with a horizontal line is recorded for each gradient chamber (Shown in Appendix Fig.4B). After all of the axons in each of the gradient chambers within a given experiment have been

analyzed, and the offset measurements have been made for each individual gradient chamber, then a MATLAB script is used to calculate the turned angle for each axon, and to calculate the position of each neuron within the gradient, in order to calculate the concentration and fractional change in concentration for each neuron.

Appendix.2.i.a. Axon tracing macro for ImageJ (Fiji)

A script containing a macro set was written by the author to measure turned angles in a semi-automated manner. The amount of user input required is minimized, while the decision of which neurons to include is maintained. However, steps have been included to keep the investigator blind to the experimental condition, and the direction of the concentration gradient, in order to avoid potential biases that could result from subjective appraisal which neurons are to be considered.

Upon loading the first image of the folder, the investigator uses the ***'initialize'*** macro (shown below), which first provides the program with file path information for the folder being analyzed. From the filename, the macro determines the image number (out of 275 or 300). The macro then enhances the Phalloidin and Dapi contrast so the axons can be clearly seen. The two channels are then merged so that the Dapi staining of the cell nucleus is overlaid on the Phalloidin-stained neuron. The image then has a 50% chance of being flipped vertically, such that the investigator cannot know what direction the gradient is facing while making the measurement. The intensity of the image is then inverted such that the axon appears black or grey on a white background with the nucleus overlaid in magenta, and the image is sharpened (Appendix Fig. 3C). These steps are performed for purely esthetic reasons, as it reduces the strain on the eyes of the investigator, making the analysis procedure more comfortable over the long periods of time required.

```
macro "initialize [i]" { // Does the merge and image modification
    path = getDirectory("image");
    // Flip the analyzed image back to it's original orientation
    if (vertInverted == 1){
        run("Flip Vertically");
    }
    selectImage(1); // Selects current image
```

```
    fileNamePhallo = getInfo("image.filename");
    fileName = getInfo("image.filename");
    path = getDirectory("image");

// Extract the image number from the filename. Must use substrings for cases where there
// are less than three digits
    imageN=substring(fileName,(lengthOf(fileName)-10),(lengthOf(fileName)-7));
    if (startsWith(imageN,"s")){
        newString=substring(imageN,1,3);
        imageN=newString;
    } else {
        if (startsWith(imageN,"_")){
            newString=substring(imageN,2,3);
            imageN=newString;
         }
    }

    // Change Phalloidin contrast
    run("Enhance Contrast", "saturated=0.35");

    selectImage(2); // Selects second image
    fileNameDapi = getInfo("image.filename");

    //Change Dapi Contrast
    setMinAndMax(400,800);

    //Merge channels

    run("Merge Channels...","c4=["+fileNamePhallo+"] c2=["+fileNameDapi+"]  keep
ignore");

    //Randomly flip the image

    //Flip image vertically
    rand = random;
    if (rand > 0.5) {
    run("Flip Vertically");
    vertInverted = 1;
     } else {
    vertInverted = 0;
     }

    rename(imageN);
    run("Invert");
    run("Sharpen");
    run("Sharpen");
    setLocation(0, 0, 1300, 1300);
} // End of macro initialize
```

Axons are considered for inclusion if the axon and its growth cone are separate enough from their neighbors to be traced. This involves subjective judgement that results in a distance of ~25 µm separation between neighboring axons, growth cones or cell bodies. When an admissible axon has been located, the investigator uses the point tool to identify and measure the center of the Dapi-stained nuclei. The position of the cell body is extracted, and the investigator then traces along the axon, from the cell body to the axon tip, using the ‘freeline’ tool. The shape of the traced axon is saved as a sequence of coordinates that is exported to a text file for further analysis in MATLAB.

After all of the acceptable axons within a given image have been traced as described above, the investigator moves on to the next image in the folder, at which point the macro reverts the image to its original orientation and corrects the measurements (if the image was flipped), saves a copy of the analyzed images with the measurements made, advances to the next image in the folder, performing the same steps as outlined for the ***'inialization'*** macro. In some cases, these above axon tracing steps (and only these steps) were sub-contracted to Flatworld Solutions. The raw images and ImageJ macros were supplied along with detailed explanatory figures instructions. The tracing results were closely monitored to ensure high-quality output.

Appendix.2.i.b. Guidance assay analysis in MATLAB

A script was written to load condensed results from any number of individual gradient chambers, pools the data together, performs calculations of the turned angle, concentration and fractional change. The investigator selects the experiments to be considered in the present analysis. The script loads an excel file containing the chamber-specific measurements and values, including: the experiment name, the concentration of guidance cue added to either well, the offset of the chamber top-left hand corner in the initial image, and the angle at which the upper boundary of the gradient chamber deviates from a horizontal line (discussed in detail below).

This data is loaded into MATLAB, and the script proceeds to loop through each of the experiments included in the list of chambers to be analyzed. For each gradient chamber, the condensed summary file is loaded, containing the image number, the position of the cell body and growth cone within the image, the base and tip angles as well as the axon length. For each axon, it is then determined whether the turn is toward or away from the gradient, based on the ImageJ angle measurements, and the initial and resulting Cartesian quadrants. For each neuron in each of the listed chambers, the set of Cartesian coordinates representing the axon are loaded into MATLAB, and the script calculates the unit vectors representing the base angle and tip angle. The turned angle is then calculated as the dot product of the base and tip angles, and the sign is determined by whether the axon turned up or down the gradient.

```
%% Calculate the turned angle using the traced XY coordinates of the axon.


% Point i: initiation point of axon
axonXi=currNeuronXdata(1); % vector of x values from imageJ
axonYi=currNeuronYdata(1); % vector of y values from imageJ

% Point ii: end of base segment
sumLength=0;
i=1;
dsqrd=0;
while sumLength<axonHillockLength
    if i<numel(currNeuronXdata)
           dsqrd =(currNeuronXdata(i+1)-currNeuronXdata(i))^2 ...
            + (currNeuronYdata(i+1)- currNeuronYdata(i))^2;
           sumLength=sumLength+sqrt(dsqrd);
    end
    i=i+1;

end
axonXii=currNeuronXdata(i);
axonYii=currNeuronYdata(i);

% Point iii: beginning of tip segment
sumLength=0;
j=numel(currNeuronXdata);
dsqrd=0;
while  sumLength<axonFinalLength
    if j>0
           dsqrd =(currNeuronXdata(j-1)-currNeuronXdata(j))^2 ...
           + (currNeuronYdata(j-1)-currNeuronYdata(j))^2;
           sumLength=sumLength+sqrt(dsqrd);
    end
    j=j-1;
end

axonXiii=currNeuronXdata(j);
axonYiii=currNeuronYdata(j);

% Point iv: end-point of axon
axonXiv=currNeuronXdata(numel(currNeuronXdata));
axonYiv=currNeuronYdata(numel(currNeuronXdata));

% Make calculations for base, tip and turned angles.
% Use gradient direction as reference point

% Create unit vector for initial angle, beginning at (0,0).
unitAxonXi=axonXii-axonXi;
unitAxonYi=axonYii-axonYi;
unitVectorInitial=[unitAxonXi unitAxonYi];

% Find base angle with respect to gradient
di=sqrt(unitAxonXi^2+unitAxonYi^2);
gradVectorInitial=[0 -di];

% Create unit vector for tip angle, beginning at (0,0).
unitAxonXf=axonXiv-axonXiii;
unitAxonYf=axonYiv-axonYiii;
unitVectorFinal=[unitAxonXf unitAxonYf];

% Find tip angle with respect to gradient, '-' because Y
% axis inverted from image
df=sqrt(unitAxonXf^2+unitAxonYf^2);
gradVectorFinal=[0 -df];
```

```
% Calculate base, tip and turned angles
dotInitial=acosd(dot(gradVectorInitial,unitVectorInitial)/sqrt(sum(gradVectorInitial.^2)…
           *sum(unitVectorInitial.^2)));
dotFinal=acosd(dot(gradVectorFinal,unitVectorFinal)/sqrt(sum(gradVectorFinal.^2)...
      *sum(unitVectorFinal.^2)));
dotTurned=acosd(dot(unitVectorInitial,unitVectorFinal)/sqrt(sum(unitVectorInitial.^2)...
       * sum(unitVectorFinal.^2)))*turnTwdGrad(neuronIndex);
```

For each image, the image number is used to determine the position of the field of view with respect to the matrix of acquired images, which is always 25 images wide (Appendix Fig. 4A). For each gradient chamber, the positions are then corrected to compensate for the variability in the offset of the upper-left hand corner of the gradient chamber in the initial image (Appendix Fig. 4B). For each neuron, the Cartesian coordinates of the cell nucleus with respect to the image coordinate system (Appendix Fig. 4C) is used with the position of the image with respect to the image matrix to determine the position of the neuron with respect to the gradient chamber (Appendix Fig. 4D), which is converted from pixels into microns. Each neurons position is then adjusted according to the rotation of the chamber relative to horizontal.

Since the concentration at the inlet and outlet are user defined, and the width of the gradient chamber is constant (3650 µm), then the position along the dimension of the increasing gradient determines the absolute concentration experienced by each neuron (Appendix Fig. 4D). This is calculated as the neurons position as a fraction of the width of the chamber, multiplied by the difference between the investigator-defined minimum and maximum concentrations. The minimum concentration (usually zero) is then added to the calculated concentration, to compensate specifically in experiments involving a non-zero low end of the gradient. Using the growth cones position within the gradient, in microns, the fractional change is calculated as the difference in concentration of a point 5 µm above and 5 µm below the neurons position, divided by the concentration calculated at the neurons position.

```
%% Calculate neuron position, concentration, FC and correct pixel lengths

% Image position relative to image matrix
imageXrelImageMatrix=(imageColumnNumber-1)*imageWidthMicrons;
imageYrelImageMatrix=(imageRowNumber-1)*imageHeightMicrons;
% Neuron position relative to image matric
neuronXrelImageMatrix=imageXrelImageMatrix + centroidXimage*micronsPerPixel;
neuronYrelImageMatrix=imageYrelImageMatrix + centroidYimage*micronsPerPixel;
% Neuron position relative to chamber, before rotating
neuronXrelChamberUnrot=neuronXrelImageMatrix-xOffsetMicrons;
```

```
neuronYrelChamberUnrot=neuronYrelImageMatrix-yOffsetMicrons;
% Final position of Neuron relative to chamber
neuronXposition=neuronXrelChamberUnrot*cosd(rotationDeg)...
   -neuronYrelChamberUnrot*sind(rotationDeg);
neuronYposition=neuronXrelChamberUnrot*sind(rotationDeg)...
    +neuronYrelChamberUnrot*cosd(rotationDeg);

% Calculation of concentration and fractional change at neurons position
    concentrationNgMl=((3650-neuronYposition)/3650)*(concentrationMaxNgMl ...
    - concentrationMinNgMl)+concentrationMinNgMl;
% Easier to separate fractional change calculation into several seperate
    concentrationAbove=((3650-neuronYposition-5)/3650) ...
      *(concentrationMaxNgMl-…concentrationMinNgMl)+concentrationMinNgMl;
    concentrationBelow=((3650-neuronYposition+5)/3650) ...
      *(concentrationMaxNgMl-concentrationMinNgMl)+concentrationMinNgMl;
    fractionalChange=abs(concentrationAbove-concentrationBelow) ...
      ./concentrationNgMl.*100;
```

Since the position of the axon tip reflects the resultant migration of the growth cone over the course of the 24-45h assay, while the cell body reflects the position of the neuron at the time of plating, it is impossible to know the precise position of any individual growth cone when the gradient was applied. The difference between the values of the fractional change in concentration calculated either at the growth cone or the cell body are slight, but show more variability in regions of higher fractional change (Appendix Fig. 5A). In the range of the gradient where synergy was observed, the average difference between ΔC/C measurements at the growth cone or the cell body is quite low, ~0.1% (Appendix Fig. 5B). While there are several axons for which the difference between ΔC/C measurements is > 0.2%, these tend to be abnormally long axons (Appendix Fig. 5C), which have quite possibly grown a substantial distance away from the cell body before the gradient was applied.

The length of the axon in pixels is then converted to microns. After an array containing the values for each of the neurons has been generated, the exclusion criteria are applied, such that only axons meeting these criteria are added to a new array. Axons are included if:

- The axon length is greater than 20 µm
- The axon is facing toward the flow
- The axon is not within ~450 µm of either boundary (the exact number used is $1/8^{th}$ of chamber), which corresponds to regions of the chamber where the gradient flattens.

Appendix.2.ii. Measurement of the fractional change in pSFK activity across a growth cone

The measurements for pSFK asymmetry at the growth cones were made in a similar manner as described for the turned angle above, with the addition of further steps to trace the outline of the growth cone, make relevant intensity measurements, and subtract the appropriate background values. All measurements of the turned angle and fractional change are calculated in the same way as described above. Therefore, what follows is a detailed description of the macros and scripts used to calculate the asymmetry of pSFK in the growth cone (Appendix Fig. 6A), with a focus on the features that distinguish these scripts from those mentioned previously.

Appendix.2.ii.a. Growth cone tracing macro for ImageJ (Fiji)

Images are loaded and growth cones are located manually, similar to the previously described guidance assay. After identifying the nucleus with the point tool, and tracing the axon with the 'freeline' tool, the investigator traces around the growth cone using the 'freeline' tool, which is selected automatically by the macro for efficiency. When the shape has been traced to satisfaction, the investigator runs a command which causes a series of measurements to be made, using the traced shape.

The midpoint of the growth cone in the dimension perpendicular to the gradient is defined as half of the width of the bounding rectangle that fits the traced growth cone (Appendix Fig. 6B). The ***'measureProfile()'*** function is run (shown below), which draws a line between the two points of the growth cone that are located at the midpoint of the growth cone width. The intensity profile is measured along this line, and the line is then shifted leftward and rightward to make a total of 5 measurements of independent pixels in close proximity to the original line (Appendix Fig. 6C). For each growth cone, the 5 independent measurements of the fluorescence profile are exported as an array to a text file, along with other growth-cone specific variables for later use in MATLAB, including: the background intensity (on the coverslip) and the average fluorescence intensity of the growth cone.

```
function measureProfile() {

        gcxMidpoint = floor(gcxMidpoint);
        for (i=0; i<xCoordinates.length; i++){
            if (xCoordinates[i]==gcxMidpoint){
                if (yPointOne == 0){
                    yPointOne = yCoordinates[i];
                    i=i+2;
                } else if (yPointTwo ==0){
                    yPointTwo = yCoordinates[i];
                }
            }
        }
        // Make sure that the gradient is measured low to high
        if (yPointOne < yPointTwo) {
            var tempYpoint = yPointOne;
            yPointOne = yPointTwo;
            yPointTwo = tempYpoint;
        }
      // Make the lines and measure the gradient
      makeLine(gcxMidpoint, yPointOne, gcxMidpoint, yPointTwo);
      tempProfileArray1=getProfile();
      wait(50);
      makeLine(gcxMidpoint-1, yPointOne, gcxMidpoint-1, yPointTwo);
      tempProfileArray2=getProfile();
      wait(50);
      makeLine(gcxMidpoint+1, yPointOne, gcxMidpoint+1, yPointTwo);
      tempProfileArray3=getProfile();
      wait(50);
      makeLine(gcxMidpoint+2, yPointOne, gcxMidpoint+2, yPointTwo);
      tempProfileArray4=getProfile();
      wait(50);
      makeLine(gcxMidpoint-2, yPointOne, gcxMidpoint-2, yPointTwo);
      tempProfileArray5=getProfile();

      // Export the values to the log window
      for(j=0; j<tempProfileArray1.length;j++){
            print(tempProfileArray1[j],tempProfileArray2[j], tempProfileArray3[j], ...
            tempProfileArray4[j],tempProfileArray5[j]); // Continued from last line.
      }
      // Save log file as Text file and clear.
      selectWindow("Log");
      saveAs("Text", path+"gcIntensitiesVertical-" + n);
      print("\\Clear");

} // End of function measureProfile
```

Appendix.2.ii.b. Growth cone pSFK fluorescence asymmetry measurement in MATLAB

This scripts works similarly to the turning assay script, however it loads additional text files that contain the traced growth cone coordinates and the intensity measurements made in ImageJ. The background intensity staining is determined for the set of experiments as the mean intensity of the staining on the coverslip. For each neuron, the script loads the neuron-specific file containing the 5 intensity profile measurements exported from ImageJ, and finds the mean value of the 5 lines. The mean intensity profile is then divided into 3 bins (Appendix Fig. 6D-E),

which are determined by the number of pixels in the measurement, and is proportional to the growth cone width in the dimension parallel to the gradient. The mean intensity is then calculated for each of the three bins (Appendix Fig. 6F). The background intensity value is subtracted from each bin, and from the mean intensity value of the entire growth cone (also imported from ImageJ). The absolute difference in pSFK activity across the growth cone Δ_{GC} was calculated as the difference between the upper third and lower third of the mean gradient profile (with respect to the high-end and low-end of the gradient, respectively) and the fractional change in pSFK activity across the growth cone (δ_{GC}) was calculated by dividing the absolute change in pSFK activity (Δ_{GC}) by the mean intensity of the growth cone (Appendix Fig. 6F). There is a strong consistency between the δ_{GC} measurements resulting from an average profile of 5 parallel lines as compared with 4 lines (Appendix Fig. 6G) or 3 lines (Appendix Fig. 6H), and whether the growth cone is divided into 2, 3 or 4 bins (Appendix Fig. 6 I-J).

```
% Load relevant intensity measure
GcIntensityMean=gcIntensity(neuronIndex)-bgIntensity;

% Make string variables before writing
fileNameCommonBegin='gcIntensitiesVertical-';
currGCFilename=strcat(fileNameCommonBegin,nNeuronString,fileNameCommonEnd);
% Use currNeuronFilename with dlmread to load the Intensity profiles of n
 currGcVerticalData = dlmread(currGCFilename);
 % Find the mean of the 5 lines
 currGcVerticalMean = mean(currGcVerticalData');

 % Divide the growth cone into a constant number of bins
 binSize = numel(currGcVerticalMean)/gcBinNumber; % gcBinNumber = 3
 binSize = round(binSize);
 distalBinBoundary = binSize;
 proximalBinBoundary = numel(currGcVerticalMean) - binSize;

 % Calculate mean distal and proximal-most bins of
 % intensity profile, absolute and fractional change
 distalBinMean=mean(currGcVerticalMean(1:distalBinBoundary))-bgIntensity;
 proximalBinMean=mean(currGcVerticalMean(proximalBinBoundary:numel(currGcVerticalMean)))…
   - bgIntensity; % Continued from last line
 GcDeltaC=proximalBinMean-distalBinMean;
 GcFractionalChange=GcDeltaC/GcIntensityMean*100; % Expressed as a percent
```

Since the fractional change of the gradient was calculated in a manner identical to the turning assay above, then each growth cone has an associated estimate of the local fractional change. This was used to assess the asymmetrical pSFK distribution (δ_{GC}) in growth cones in the same range of the gradient where synergy was observed for axon turning ($1.4 < \delta < 1.8\%$).

Appendix.2.iii. Measuring concentration gradients *in vivo*

Briefly, the analysis involved processing immuno-stained spinal cord sections by rotating the image so the dorsal-ventral axis of the spinal cord is vertical, and selecting a point within the floorplate on each side of the spinal cord as a reference. An ImageJ macro then measures the intensity profile along a line of a defined distance from the selected point at several angles with respect to vertical. The intensity measurements are then exported as text files, which are then loaded by a MATLAB script for calculating the average profile, and pooling the results from multiple sections for each embryo.

Appendix.2.iii.a. Quantitative analysis of spinal cord sections using ImageJ (Fiji)

The investigator opens and image and draws a line from the floor plate to the roof plate of the spinal cord, and rotates the image such that the spinal cord is vertical in the image. Using the point tool the investigator selects the reference points: by selecting a point on the left side of the floorplate. Using the reference point, the macro measures a series of angles emanating from the selected point, and returns this to the log window. Next, the same procedure is performed on the right side of the spinal cord, using the ***'autoMeasureRadialRight'*** macro command, shown below (equivalent operations are performed on either side of the spinal cord, only the angles values are different).

```
macro "autoMeasureRadialRight" {

        theta = 95;
        while(theta < 130){
            // Polar to Cartesian conversion
            Xn = Xr + r*cos(-theta*PI/180);
            Yn = Yr + r*sin(-theta*PI/180);
            // Make a line and print out its values to the log dialogue box
            makeLine(Xn,Yn,Xr,Yr);
            tempProfileArray=getProfile();
            for(j=0; j<tempProfileArray.length;j++){
                print(tempProfileArray[j]);
            }
            theta=theta+angleIncrement;
            wait(25);
        }
    } // End of autoMeasureRadialRight macro
```

The investigator then exports the current data in text format to be read by MATLAB, the next image in the folder is loaded, and the procedure is repeated until all images have been

analyzed.

Appendix.2.iii.b. Processing and pooling spinal cord gradient measurements in MATLAB

A list of the sections to be included are defined in a variable of the MATLAB script for each embryo to be examined independently. Background values are measured from control tissue on the same slides, or slides processed identically, in parallel.

For each of the sections, each angle for which the profile was measured is loaded into a data array. The background intensity level is subtracted for each profile. The maximum value of fluorescence intensity is calculated for the entire dataset, and the intensity levels are normalized to this value. To account for variability in the spinal cord height between sections or embryos, each gradient profile was interpolated to occupy a vector of 1000 linearly-spaced values.

```
% Interpolate

xVect=linspace(0,numel(newVect_s1),numel(newVect_s1));
xq=linspace(0,numel(newVect_s1),interpLength);
interpData_s1(sectionIndex,angleIndex,:)=interp1(xVect,newVect_s1,xq);
```

For each section, the mean value at this relative position is calculated across 5 of the measured angles, providing an overall mean value for each section. For each normalized position value, the mean value of all sections is then calculated, providing a mean intensity profile for each embryo.

```
% Calculate the mean profile per section (mean across angles)
for nSection=1:numel(sectionList)
    for nPos=1:interpLength
       meanPerSection_s1(nSection,nPos)=mean(interpData_s1(nSection,[1:5 19:23],nPos));
    end

    % Also calculate the mean length of the segment used across the same
    % selection of rows - used for calculating spinal cord height in microns
    meanHeightPixels(nSection)=mean(scHeights(nSection,[1:5 19:23]));
end

% Calculate the overall mean profile
for nPos=1:interpLength
```

```
    % Average the mean per section
    overallMeanProfile_s1(nPos)=mean(meanPerSection_s1(:,nPos));
end
```

The mean value is then calculated across angles and sections, providing an averaged measure that is sufficiently sensitive to detect subtle changes in gradient steepness, in a quantitative manner.

Appendix Fig. 3. Calculation of the turned angle from a traced axon. Images are acquired with fluorescence channels for **(A)** Dapi and **(B)** Phalloidin. The images are merged **(C)** and processed such that the axons can be traced easily and rapidly. For each neuron with an isolated axon, the investigator traces along the axon, from the cell body to the tip of the growth cone. This generates a series of Cartesian coordinates. **D)** The base angle is defined as a line between the first point and the point at which the sum of the distance between coordinates is at its maximum value that is no greater than 30 pixels, corresponding to a length of ~20 µm. This is performed algorithmically by calculating the cumulative length of the sequential segments of the axon, moving away from the cell body, until this value is reached. **E)** The tip angle is calculated analogously, beginning with the last point in the series of coordinates, and iterating backwards through the list until the cumulative length of the distance between coordinates is at its maximum value that is no greater than 30 pixels. The turned angle is then calculated as the dot product of the vectors representing the base angle and the tip angle. In D-E, each subsequent segment of the axon used to calculate the cumulative length is plotted in different color.

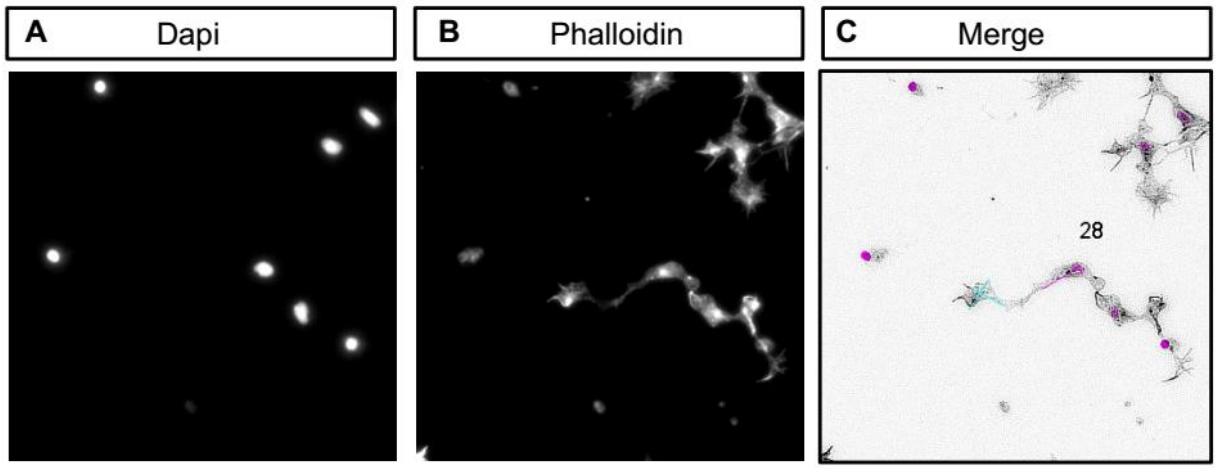
A
Dapi
B
Phalloidin
C
Merge
28

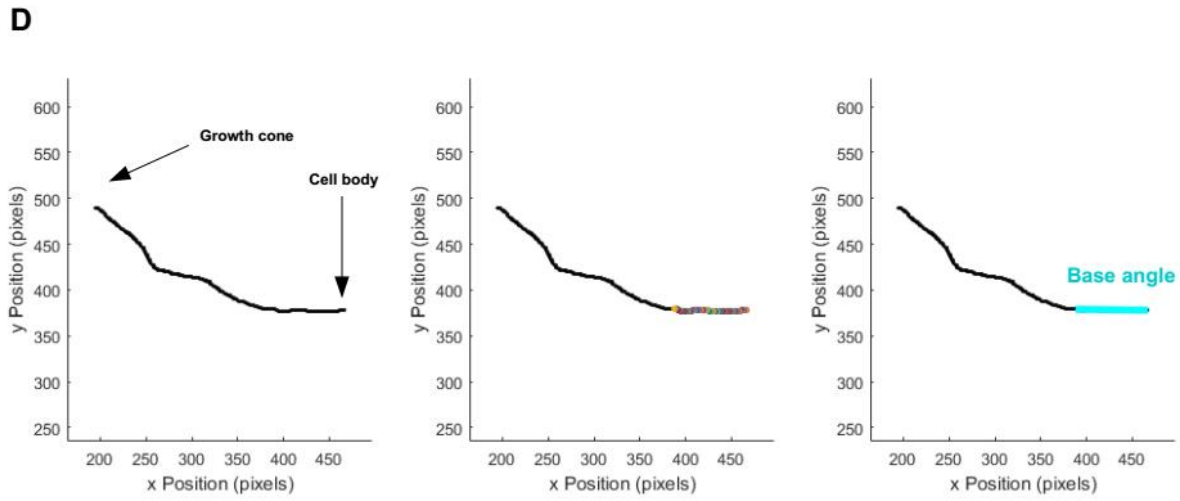
D
Growth cone
Cell body
Base angle
y Position (pixels)
x Position (pixels)

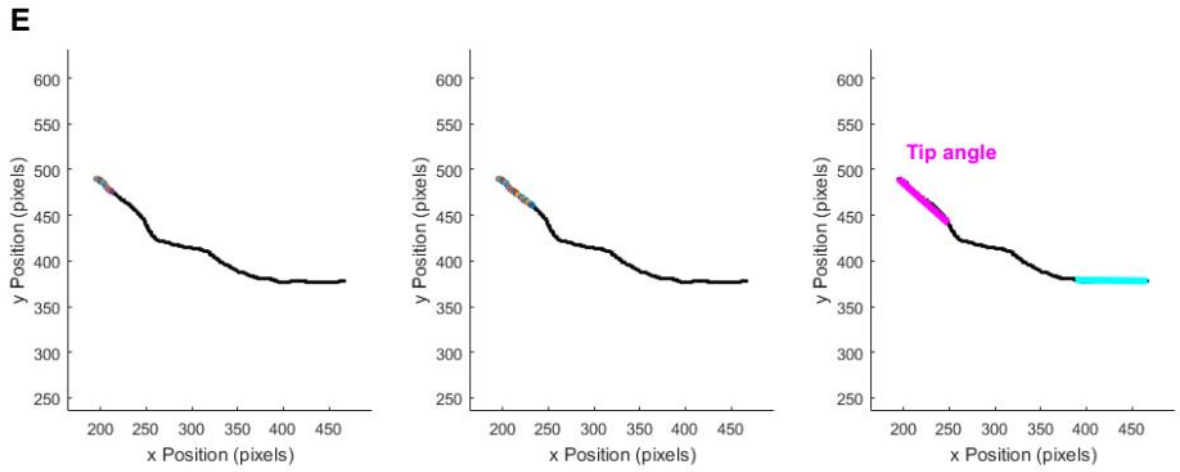
E
Tip angle
y Position (pixels)
x Position (pixels)

Appendix Fig. 4. Estimating the absolute concentration for each neuron based on its position. **A)** For each gradient generator, neurons were imaged with a 20x objective, which required 275 individual fields of view in order to cover the entire area of the gradient. As there are a defined number of columns (25) in the image matrix, for any arbitrary image (filled blue square), the number of the image in the sequence is sufficient to determine the position with respect to the image matrix. Each gradient chamber was imaged such that the first image contained the upstream upper boundary of the gradient chamber (filled red square) such that experimental differences could be corrected. **B)** In the first image for each gradient chamber, measurements are made of the x-offset (green line) and the y-offset (purple line), as well as the angle at which the upper boundary of the gradient chamber deviates from a horizontal line (light blue line relative to dashed black line). These three parameters are used to correct for variability of the bonding of the microfluidic devices. **C)** The position of each neuron with respect to the image coordinate system are recorded, as well as the constant image width and height. These four parameters, along with the image number allow for the position of the neuron with respect to the gradient chamber to be calculated **(D)**. Using the vertical position of each neuron within the gradient chamber, with experimentally controlled minimum and maximum concentration of guidance cue, it is possible to calculate an estimate of the absolute guidance cue concentration at each neuron's position, and the related gradient steepness ($\Delta C/C$).

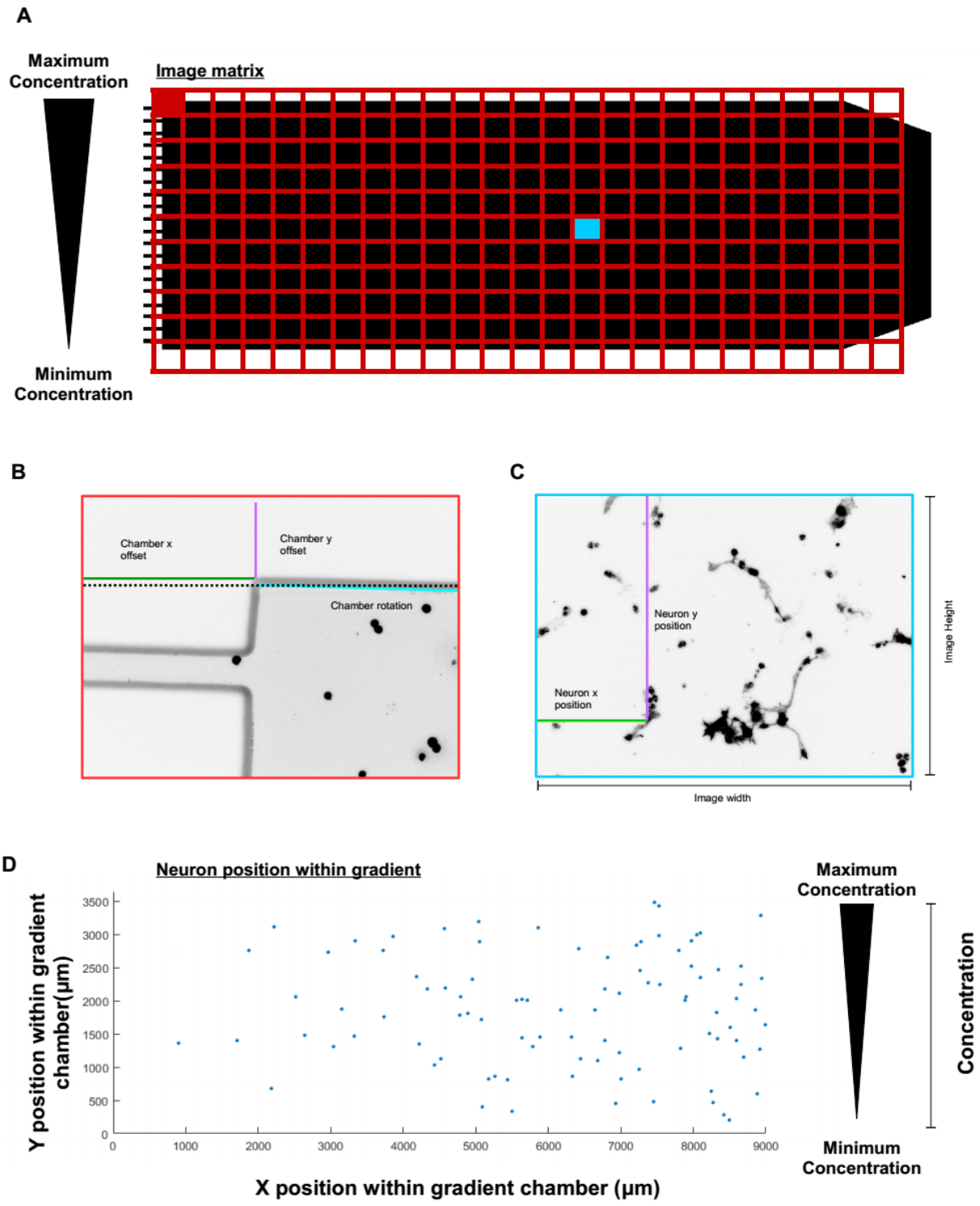
A
Maximum Concentration
Image matrix
Minimum Concentration
B
Chamber x offset
Chamber y offset
Chamber rotation
C
Neuron y position
Neuron x position
Image Height
Image width
D
Neuron position within gradient
Y position within gradient chamber(µm)
X position within gradient chamber (µm)
Maximum Concentration
Minimum Concentration
Concentration

Appendix Fig. 5. Estimation of the gradient steepness is not strongly influenced by whether the position of the growth cone or the cell body is used for the calculation. **A)** A sample dataset of 5557 axons is plotted to compare the calculated value of the fractional change in concentration at the growth cone versus at the cell body. Unsurprisingly, the two measures are strongly correlated (R^2=0.985), with larger deviations observed for higher fractional change values, resulting from the smaller area associated with high ΔC/C. **B)** The absolute difference between measurements of ΔC/C measured at the growth cone or cell body is plotted in a histogram specifically for neurons in the range of the gradient where we observed synergy, $1.4 < \delta < 1.8\%$. There is a clear peak around the mean value of 0.09%, while the maximum deviation between the measurements in the subset of 414 neurons is 0.36%. **C)** However, outliers such as this are largely a result of axons which have grown an abnormally large distance during the period in culture. Of the 28/414 neurons which have a difference between the ΔC/C measurements of > 0.2%, 19 of these axons have a length that is greater than 1 standard deviation above the mean axon length. Therefore, axons which show a strong disagreement between measures of the ΔC/C at the growth cone and the cell body are uncommon.

A

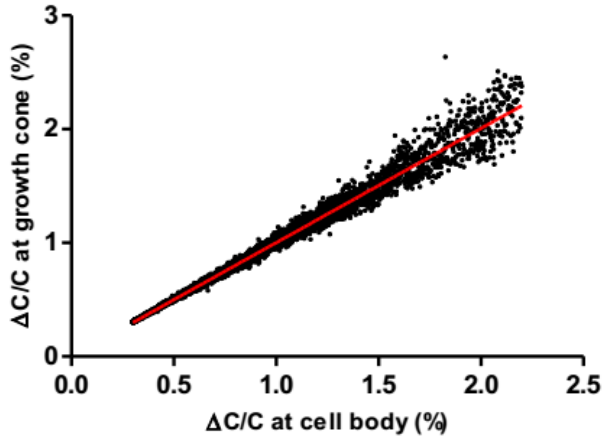
ΔC/C at growth cone (%)
ΔC/C at cell body (%)
0
1
2
3
0.0
0.5
1.0
1.5
2.0
2.5

B

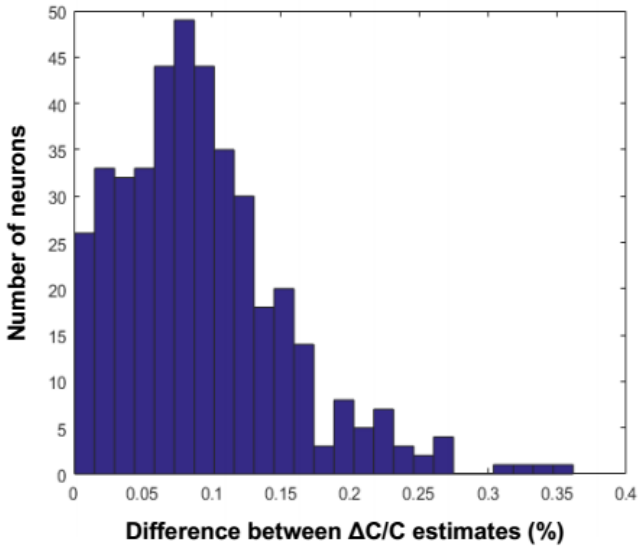
Number of neurons
Difference between ΔC/C estimates (%)
0
5
10
15
20
25
30
35
40
45
50
0
0.05
0.1
0.15
0.2
0.25
0.3
0.35
0.4

C

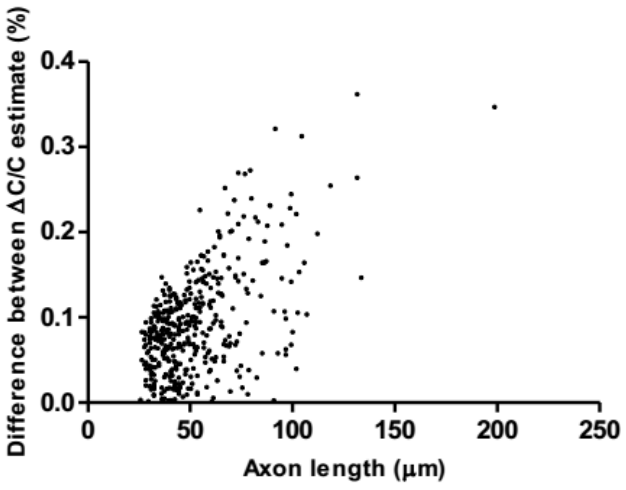
Difference between ΔC/C estimate (%)
Axon length (μm)
0.0
0.1
0.2
0.3
0.4
0
50
100
150
200
250

Appendix Fig. 6. Calculation of the fractional change in pSFK signal intensity across a growth cone, δ_{GC}. **A)** Growth cones were imaged such that the gradient is parallel with the y-dimension of the image coordinates. For each growth cone, the investigator traced around the perimeter using the freehand tool in ImageJ. **B)** The traced shape was stored as a series of Cartesian coordinates, and the midpoint of the shape in the x-dimension (perpendicular to the gradient) was determined as half the width of a bounding rectangle which entirely contains the traced shape. **C)** The algorithm then determined the pair of y-coordinates corresponding with the midpoint in the x-dimension. Once these points have been obtained, a line is drawn from the distal side of the growth cone to the proximal side (with respect to the concentration gradient). The line was then shifted leftward and rightward by one and two pixels, and intensity profile measurements are made along each line, measuring a distinct array of pixels for each measurement. **D)** Each measured profile was separated into 3 equally sized bins, each representing a third of the growth cone width (green line = proximal, red line= distal). **E)** The mean intensity profile was calculated across the 5 lines shown in C, and is plotted as a proportion of the width of the growth cone. **F)** The mean intensity in each of the bins is calculated. The fractional change in signal intensity (δ_{GC}) is calculated as the difference between the proximal and distal bins, divided by the mean intensity of the entire traced growth cone (dashed line). The sign and magnitude of the δ_{GC} measurement is maintained whether the mean intensity profile is calculated across 5 lines (as in Figure II.6) compared with 4 lines **(G)** or 3 lines **(H)**. The measurement is also robust to changes in the bins being considered, for example if instead half **(I)** or one quarter **(J)** of the growth cone width is used. In all panels, the triangular wedge indicates the direction of the concentration gradient.

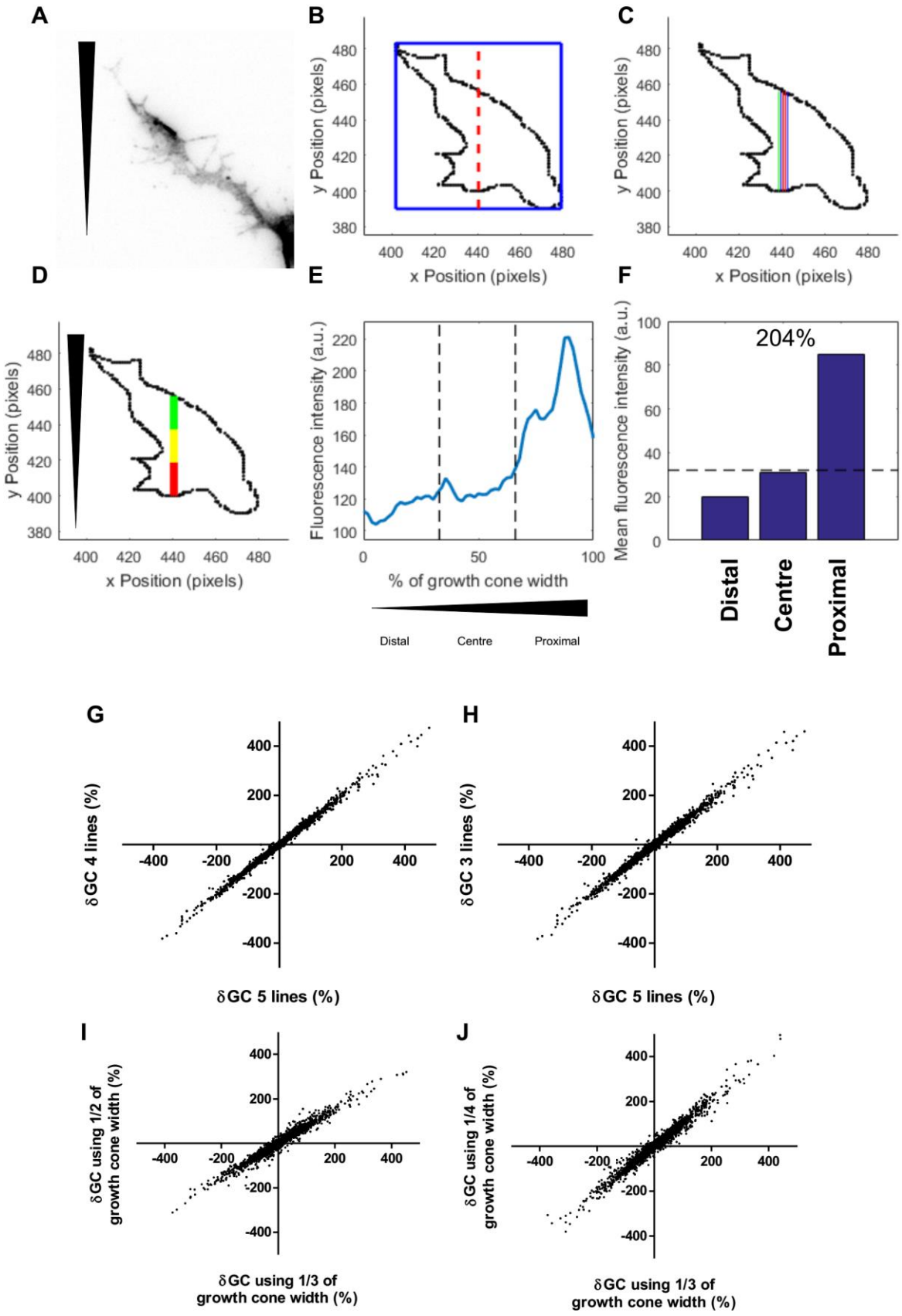
A
B
C
D
E
F
y Position (pixels)
x Position (pixels)
Fluorescence intensity (a.u.)
% of growth cone width
Distal
Centre
Proximal
Mean fluorescence intensity (a.u.)
204%
G
H
I
J
δGC 4 lines (%)
δGC 3 lines (%)
δGC 5 lines (%)
δGC using 1/2 of growth cone width (%)
δGC using 1/4 of growth cone width (%)
δGC using 1/3 of growth cone width (%)